MICROPHONE SUPPRESSION OF AIR-NOISE ON GEOPHONES

\-

A Thesis

Presented to

the Faculty of the Department of Earth and Atmospheric Sciences

University of Houston

\-

In Partial Fulfillment

of the Requirements for the Degree

Master of Science

\-

By

Nathanael Mark Babcock

August 2012

MICROPHONE SUPPRESSION OF AIR-NOISE ON GEOPHONES

_____

Nathanael Mark Babcock

APPROVED:

_____

Dr. Robert Stewart, Chairman

_____

Dr. Christopher Liner

_____

Dr. Stephen Danbom

_____

Dean, College of Natural Sciences and Mathematics

ACKNOWLEDGEMENTS

MICROPHONE SUPPRESSION OF AIR-NOISE ON GEOPHONES

An Abstract of a Thesis

Presented to

the Faculty of the Department of Earth and Atmospheric Sciences

University of Houston

In Partial Fulfillment

of the Requirements for the Degree

Master of Science

By

Nathanael Mark Babcock

August 2012

ABSTRACT

Air-noise in seismic records creates a loss in signal quality, reducing seismic image clarity. A microphone may be used to estimate and remove air-noise in seismic records. This thesis covers the characterization of air-noise on a prototype 4-Component geophone (3-C geophone plus microphone), as well as the development of two air-noise removal filters. Vibration-isolated, noise characterization experiments were performed to determine the 4-C geophone's directional and frequency dependent response to air-noise. Sensor placement within the geophone appeared to affect each geophone component's directional response; showing increased sensitivity to sounds from the same side the sensor was mounted. In addition, a walk-away seismic survey was performed to determine the effect of distance on geophone air-noise. Peak amplitude decay rates differed from the theoretical $1/R$, R representing total distance. The microphone and inline geophone decayed at $1/R^{1.4}$, the crossline component at $1/R^{1.15}$, and the vertical component at $1/R^{1.81}$. These results indicate a loss of energy to heat through air-ground interactions. Results from the noise characterization tests were used to develop two air-noise filters; a real-time filter, which could remove air-noise from geophone signals before they are recorded; and a post-acquisition filter, which could be used to more precisely remove air-noise. Both filters were effective at reducing air-noise, up to 21 dB reduction for near offsets. However, the real-time filter affected seismic data due to microphone recorded seismic events.

CONTENTS

LIST OF FIGURES

CHAPTER 1:   INTRODUCTION

Noise in seismic records can obscure desirable signals, cause a loss of detail, and even create spurious events; thus degrading the seismic image. Fortunately, some noises are removed relatively easily by stacking data or using filters (FK, frequency, etc.). However, not all noise is so easily removed. Air-noise is a significant source of noise in seismograms. The most obvious source of air-noise is from the seismic shot. Whether it is dynamite or vibroseis, all seismic sources generate air-pressure waves that travel past the geophones. As this noise travels across the geophone spread, it vibrates the geophones, creating noise in the seismic records. There are other ways for air-noise to affect a geophone. Since the near surface is porous, pressure waves from sound can more easily penetrate into the subsurface. This creates additional vibrations, which can be recorded by the geophone.

To remove air-noise from seismic records, its character and strength in the geophone signal must be estimated. A microphone can be used for this purpose. It will record the air-wave, and other air-noise that affects the geophone. There will not necessarily be a direct correlation between the microphone and geophone recorded air-noise. The purpose of this thesis was to characterize the relationship between microphone-recorded air-noise and geophone-recorded air-noise. The knowledge obtained in this process was used to create a real-time filter, which can

1

be applied in the field to remove air-noise from the geophone signal before it is recorded by the seismograph.

A series of experiments were undertaken to understand the microphone-geophone relationship. Controlled experiments were performed to determine the geophone's response to sound coming from different angles, as well as for sounds of varying frequencies. By recording these sounds using the microphone at the same time, a microphone-geophone transfer function was calculated, which was used in the development of the filter. An experiment was also performed to determine how the geophone-microphone pair reacts to sounds coming from different distances. This experiment was performed in the field because large source-receiver offsets are required to fully characterize the relationship.

After the relationship between microphone and geophone was well characterized, a filter was designed to work in real-time. The filter was tested on field data, in real-time and post-acquisition settings, to determine its effectiveness. This filter could be programmed to a digital signal processor, and built into a special 4-C geophone, to create a geophone that automatically removes air-noise before outputting clean signal. However, this implementation was not tested here, and is reserved for future work. Before analyzing the microphone-geophone relationship, an overview of the many ways air-noise can affect the geophone is presented.

1.1: Types of noise that affect a geophone

The operational portion of any geophone contains two main parts, a reference frame and oscillating proof mass. Analog geophones contain a coil that surrounds a moveable magnet (or a metal case surrounding moveable coils), while MEMS accelerometers contain two electrodes that sandwich a moveable mass acting as a capacitor. The reference frame being stationary is only relative. In reality, the reference frame moves about the mass, while the "moving" mass stays still. For geophones, it is this relative movement of the mass compared to the reference frame that creates the desired signal. In the analog geophone, the velocity of the moving magnet creates a voltage in the surrounding coil.   In the MEMS accelerometer, accelerations displace the mass (capacitor) changing the voltage detected in the reference frame (Hons and Stewart, 2007). The reference frame (referred to as the geophone element) attaches to a housing structure (the geophone case) that contains a spike for planting in the ground. Visual diagrams for analog and MEMS geophones can be seen in Figure 1.1.

In a seismic experiment, vibrations from seismic waves will move the spike and thus the entire geophone (except for the proof mass). These movements are recorded and analyzed later to create seismic images. Other, undesirable, vibrations can affect the geophone in two ways; spurious ground vibrations cause movement in the geophone through the spike embedded in the ground, or air vibrations directly move the geophone case without transferring through the spike first. All of these excess movements of the geophone create noise in the seismic record. Air

vibrations and ground vibrations caused by air vibrations are collectively called air-noise. Removal of air-noise helps to create sharp and accurate subsurface images.
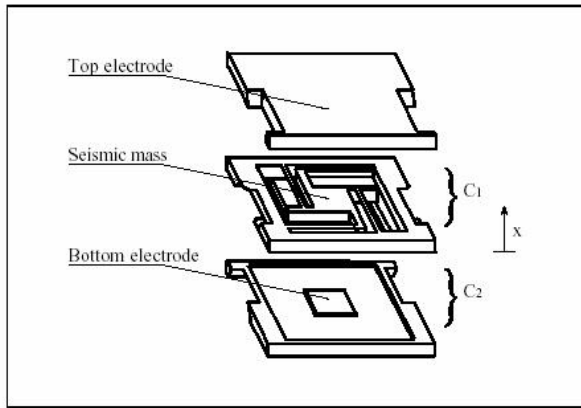
Figure 1.1: Left: Diagram of a MEMS accelerometer (Hons and Stewart, 2007). As ground accelerations displace the seismic mass there is a capacitance change at the top and bottom electrodes. Right: A cutout analog geophone. The geophone case moves about the seismic mass (copper coils) when subjected to ground motion. The voltage created by the coil is proportional to ground velocity.

1.1.1: Noise that affects the geophone case

The most common source of air-noise for any seismic survey is the air-blast or air-wave. This acoustic wave is produced, and defined, by the source used in the seismic experiment; air-wave is created by a seismic vibrator and air-blast by an impulsive source. These waves travel through the air at the speed of sound (346 m/s at 25° C) and strike the geophone case, causing it to shake. This creates noise in the seismic record.

Wind is another common phenomenon that creates noise in seismic records. This disturbance, which directly affects the geophone case, is created by turbulent eddies and vortices, referred to as turbules. These turbules, carried by the wind, vibrate the geophone case as they move past (Hedlin and Raspet, 2003). This type of wind noise is generally spatially coherent and can be followed across geophone traces. The correlation coefficient, for wind-induced noise, between seismic traces is estimated by

$$R_{downwind} = e^{-\alpha x} * \cos(k_1 x)$$

$$R_{crosswind} = e^{-\beta y} \, ,$$

where x and y are the downwind and crosswind geophone spacing, respectively (Shields, 2005). k_1 is the spatial wavenumber of the turbulent wind flow and is given by

$$k_1 = \frac{2\pi F}{v},$$

where v is the wind velocity and F is the frequency of the pressure fluctuations produced, i.e. the frequency of the noise present on the geophone. The remaining coefficients are given by

$$\alpha = 0.33 * k_1^{1.28} \text{ for } 0.5 < \frac{1}{k_1} < 50$$

$$\frac{1}{\beta} = 0.84 * \left(\frac{1}{\alpha}\right)^{0.74} \text{ for } 3 < \frac{1}{\alpha} < 500 .$$

Identification and reduction of wind noise is very important for infrasonic monitoring stations. These stations are used to detect sub-audible signal (<20 Hz), which can be used to identify nuclear blasts, battlefield noise, meteors entering the earth's atmosphere, even large storms and tornados. Infrasonic monitoring stations use either microbarometers or specially designed microphones capable of detecting sound down to, and below, 1 Hz (Kromer, 2000; Shields, 2005). These infrasonic microphones would be suitable for air-noise cancellation from seismic records.

The final sources of air-induced noise are transient sources. These sources of noise are finite in time and may or may not affect multiple geophones at a time. Examples of transient noises include vehicles, helicopter and other aircraft, oilfield equipment, and human/animal movement near geophones. Essentially, transient sources are any noise source not previously categorized.

1.1.2: Noise that affects the geophone elements

Air-noise does not solely affect geophones by directly striking their case. Air-noise may couple to the ground and directly vibrate the geophone elements to produce unwanted noise. This can happen in three separate ways. One of the more obvious is wind-noise coupling. Wind not only directly vibrates the geophone case but every structure that impedes its movement: trees, buildings, even grass become secondary sources of noise (Stewart, 1998). Wind may also directly couple to the ground without shaking any intermediary structure. Withers et al. (1996) performed wind noise experiments in a remote area in New Mexico, which had gentle topography and little surface vegetation. Even with the favorable conditions, there was still significant ground-coupled wind noise. A covered seismometer near the surface (30 cm burial) detected wind noise at speeds as low as 3 m/s (10.8 km/hr). Furthermore, a magnitude 1.6 event was barely detectable at a wind speed of 8 m/s (28.8 km/hr), as seen in Figure 1.2.

It has been recommended to bury geophones to decrease wind effects. Bland and Gallant (2001) measured a 3 dB increase in signal-to-noise ratio for every 10 cm of burial depth. The total depth to bury the geophone depends on desired noise reduction, but Withers et al. (1996) generally recommend a minimum burial depth of 43 m.
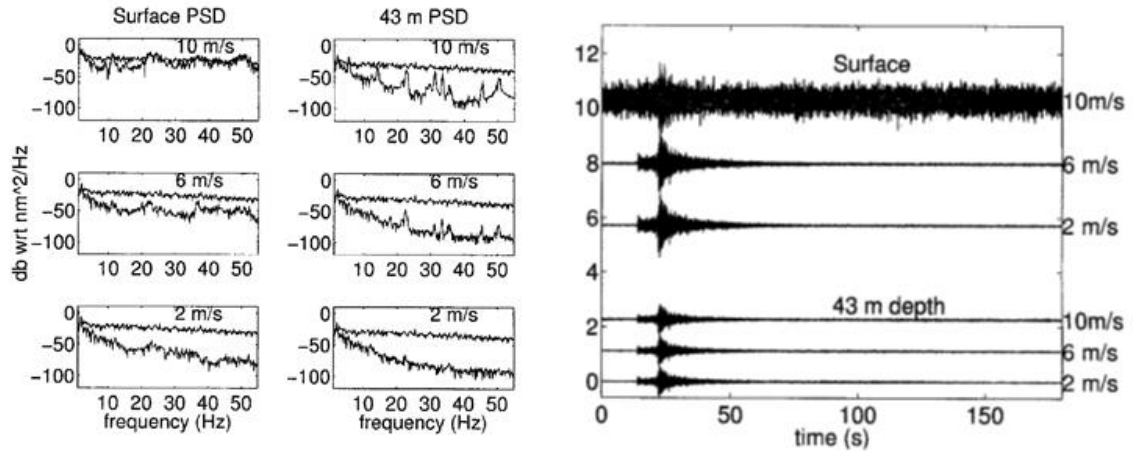
Figure 1.2: Left: Power spectral density (PSD) comparison of wind noise (lower line)

and M1.6 seismic event (upper line) at varying wind speeds for a geophone located on

the surface and at depth. Right: Superimposed M1.6 event on time records of wind

noise at varying wind speeds for a geophone located at the surface and at depth.

(Withers et al., 1996)

Since the acoustic impedance of air is not zero, there will be some transfer of energy from any compressional wave in the air, to the ground. However, the coupling of acoustic-to-seismic waves is 1000 times larger than would be calculated from direct transmission (Sabatier et al., 1986a). This increase in energy transfer occurs because the air-to-ground interface is not sharp. The upper few decimeters (or in some cases meters) of the earth are highly porous and permeable. Any sound that propagates in air will easily penetrate into this region. A Biot-Stall medium is a good model for this near-surface layer. A Biot-Stall medium is poroelestic, with fully interconnected pores saturated by fluid. Both the matrix and pore fluid are considered isotropic, homogeneous, and elastic. In the near-surface case, the matrix

8

is the unconsolidated sediments, and the pore fluid is air. A peculiar feature of a Biot-Stall medium is its ability to support the propagation of two compressional waves, one fast and one slow. The fast compressional wave is analogous to a P-wave and travels mainly through the matrix. The slow compressional wave, on the other hand, travels mostly through the pore fluid. This slow wave is rarely detected in seismic records because it is extremely attenuative. In the air-noise case, acoustic waves propagating in the air refract more easily to the slow wave than the fast wave in the poroelestic, near-surface layer. Energy is then transferred from the air-filled pores to the matrix creating seismic motion (Sabatier et al., 1986b). Because the slow wave in the ground is highly attenuative, the ground motion will only occur directly beneath the current location of the acoustic wave in the air (Sabatier et al., 1986a). In other words, an air-wave will not spawn a leading or lagging compressional seismic wave.

Lastly, air-waves may also couple to the ground through Rayleigh waves. This occurs when the air-wave velocity is similar to the phase velocity of the Rayleigh wave. Since surface waves are dispersive, only one frequency of the Rayleigh-wave's fundamental mode will have a phase velocity matching the air-wave. Thus, the ground roll created by the air-wave will oscillate at a singular frequency. Furthermore, the group velocity is typically one half that of the air-wave velocity (Press and Ewing, 1951). This means that the induced ground roll will lag behind the air-wave that created it. For any given point in the subsurface, the wave train that follows the air-wave arrival will last for the same duration as the original

travel time of the air-wave. An example for clarification, for an air-wave velocity of 345 m/s, the Rayleigh-wave with a matching phase velocity will have a group velocity of approximately 173 m/s. The air-wave will constantly couple to this Rayleigh-wave. However, due to the Rayleigh-wave's lower group velocity, all induced ground roll will lag behind. After one second, the air-wave will have travelled 345 m, but the first-coupled Rayleigh-wave will have only travelled 173 m. If a geophone were place at this point, it would detect the air-wave arrival at one second, which would be immediately followed by the monofrequency Rayleigh-wave. Due to the lagging velocity, the Rayleigh-wave train continues for one second after the air-wave arrival. An example cartoon of the expected geophone response to air-noise and seismic signal is shown in Figure 1.3. This air-to-ground roll coupling will occur for any air-wave, adding noise to seismic recordings.

Ground roll coupling is not a one-way transfer from air-to-ground, Rayleigh waves can also produce motion in the air. Ground-to-air coupling is the inverse of the air-to-ground process. The ground roll at the correct phase velocity will couple to the air and create a train of constant frequency air-waves that trail behind (Press and Ewing, 1951). Air-waves created by ground roll are an additional source of noise that affects the geophone case, and may be detectable by microphone. While the air-noise effects of ground roll can be actively cancelled, the concept cannot be extended to the cancellation of all ground roll from geophone records. This is due to the differing frequency content of the microphone-recorded ground-to-air-wave signal and the seismic ground roll recorded by the geophone. For every seismic

event (hammer shot, Vibroseis) there is a concurrent air event. Any receiving geophone will record signal from both events. To extract the seismic data, the air-noise signature must be determined and removed from the geophone record.
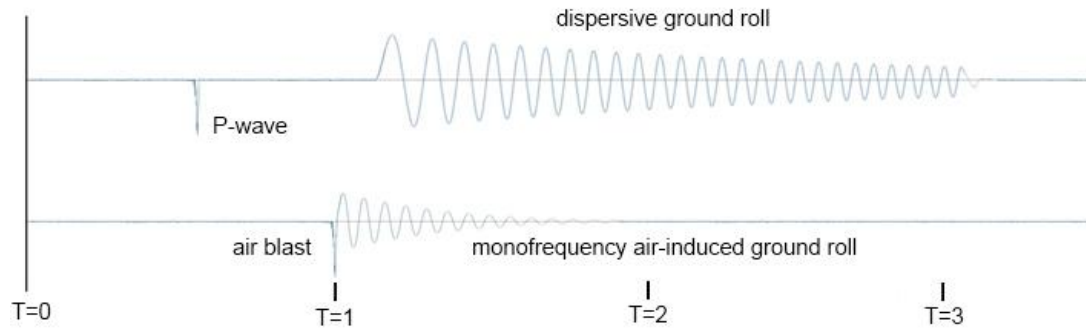
Figure 1.3: Synthetic seismic traces showing a vertical geophone's response to a theoretical impulse source, according to Press and Ewing (1951). The top trace shows the source generated ground motion only. The bottom trace shows the air-wave induced ground motion. The true geophone response will be the combination of these two traces. Time is to scale, however the amplitude response is not.

1.2: Prior work

The CREWES project, at the University of Calgary, has worked extensively in the area of geophone noise cancellation using microphones. The work performed here is the continuation and advancement of that performed by CREWES. The first experiment performed was during a hospital implosion in Calgary, Alberta in 1998. It was found that the microphone and geophone recordings of the blast showed distinct similarities. In fact, the air-blast recorded by the microphone appeared to be 180° out of phase with the blast recorded by the geophone. Thus, the sum of the microphone and geophone traces showed a reasonable reduction of air-blast. Stewart (1998) proposed two noise-reducing multi-sensors that could be used during seismic data acquisition to reduce the noise present in geophone records. One of the sensors was a multi-channel setup consisting of microphone data recorded simultaneously with geophone data. The microphone data could later be used to filter noise as necessary. The other sensor consisted of an integrated filtering circuit that would use the signal from a collocated microphone to suppress noise in the geophone signal. Noise cancellation was performed at geophone level and the resulting signal was output to the data acquisition system as an unfiltered geophone would. A comparison of these sensor types can be seen in Figure 1.4.
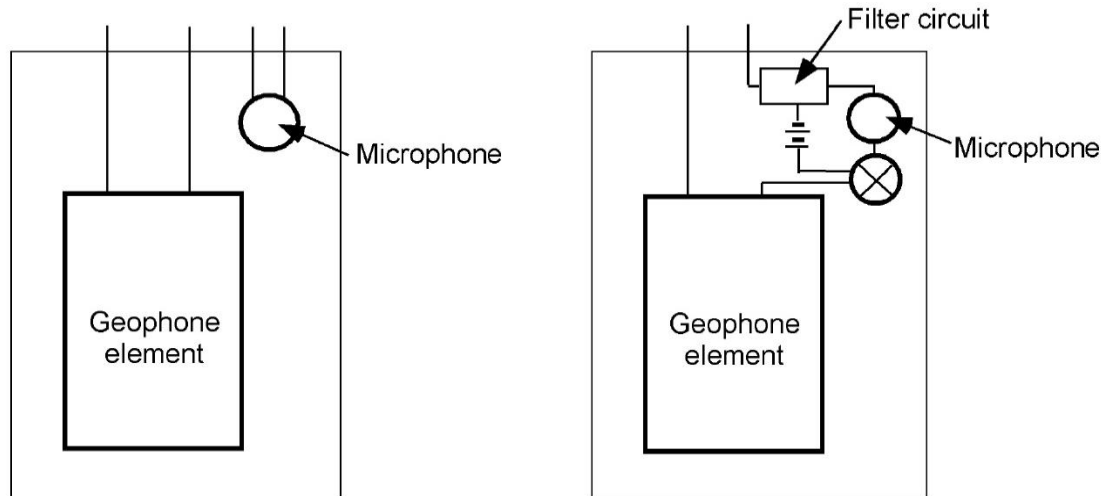
Figure 1.4: Schematic of noise cancelling geophones. Left: A multi-channel system, which would record geophone and microphone data separately to be processed after acquisition. Right: A single channel system, which would record and filter air-noise at the geophone. The data acquisition system would record "clean" data.

(Stewart, 1998)

Dey et al. (2000) used a multiline survey to analyze the capability of air-blast attenuation using microphones. A 3.8 km seismic survey was performed with microphones and vertical geophones placed every 20 m, 3-C geophones every 10 m, and vibroseis shot points every 20m. The data from each sensor type were compared for similarities in time and FK domains, which are shown in Figure 1.5. The microphone record contained not only the air-blast but also significant low frequency data, although it was spatially aliased.
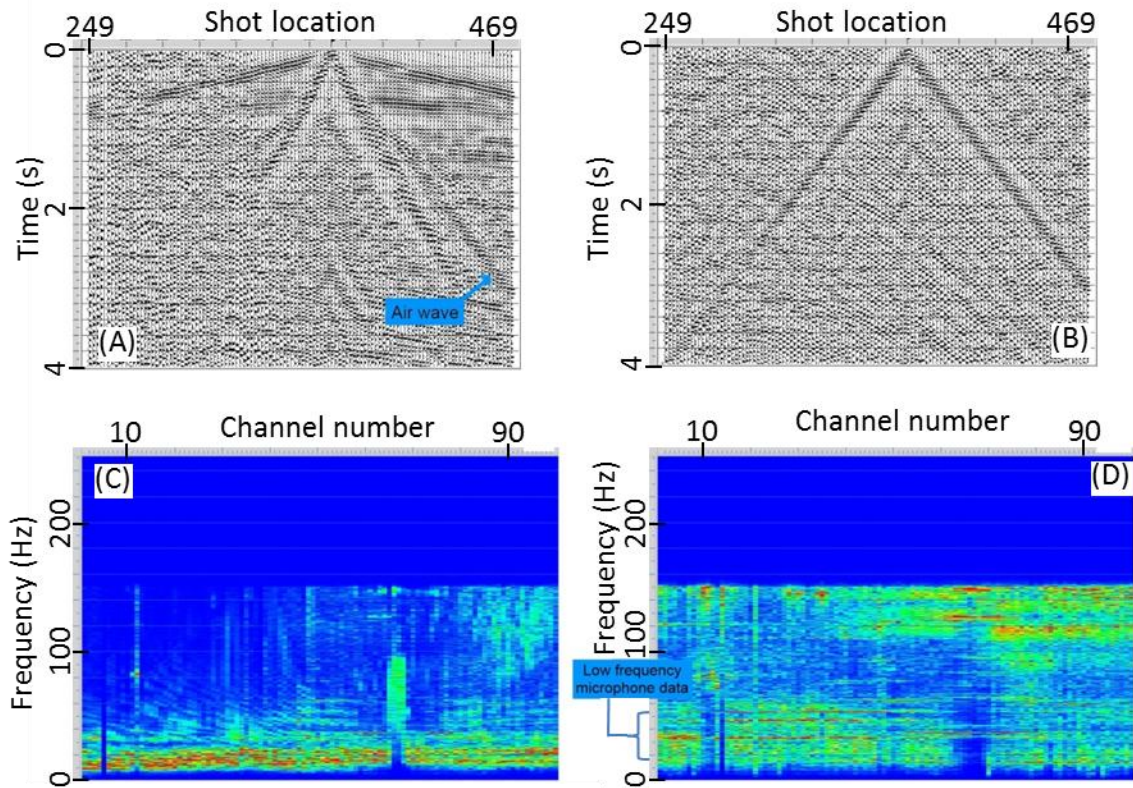
Figure 1.5: (A) Time record from vertical geophones. The air-wave is easily visible. (B) Time record from microphones. (C) FK spectrum of geophone data. (D) FK spectrum of microphone data. The low frequency seismic data is highlighted. (Dey et al., 2000)

Data cross correlation was also performed to indicate similarity. The largest correlation between microphone and vertical geophone records occurred at 6 ms offset, indicating a phase mismatch between the data. After phase analysis, the phase mismatch was determined to be $\pi/2$ as seen in Figure 1.6.
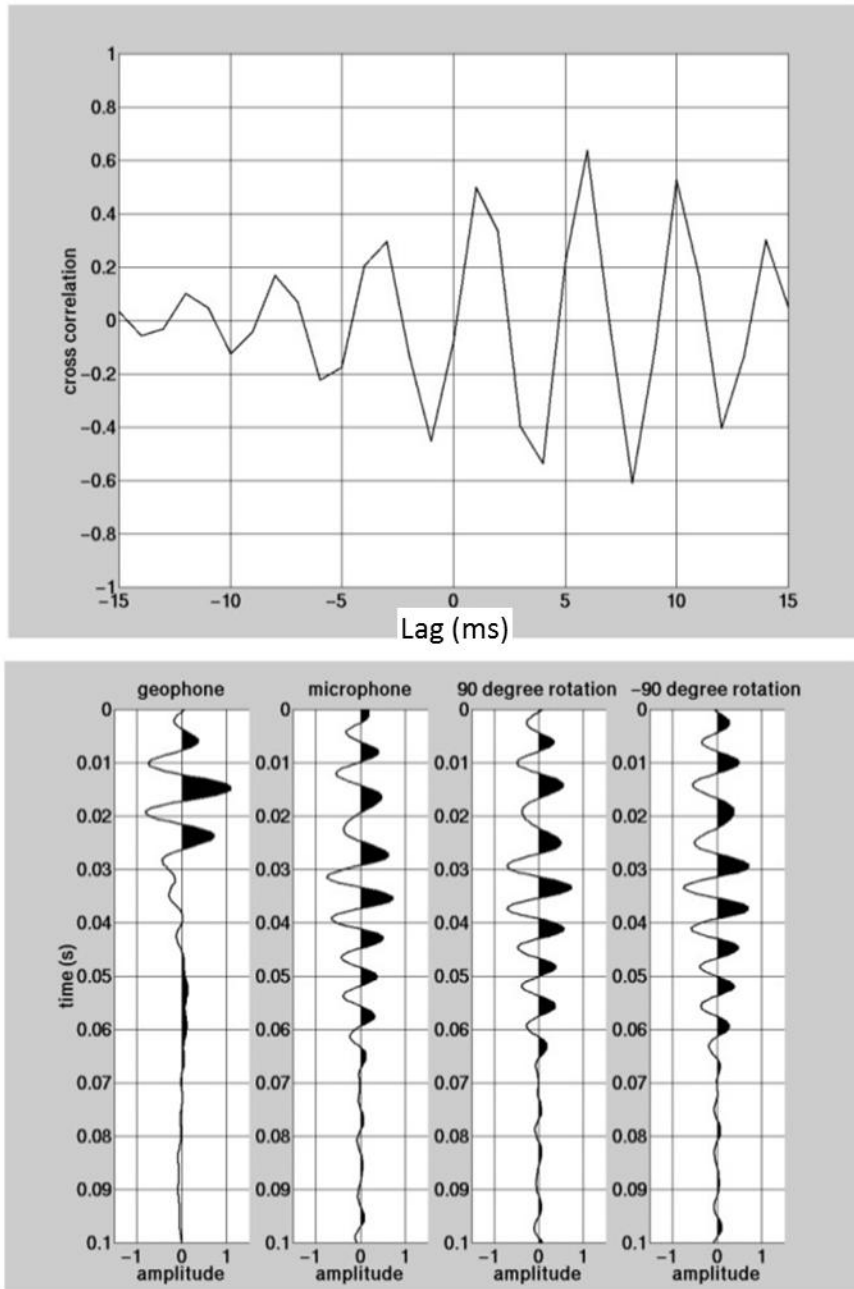
Figure 1.6: Top: cross correlation of the vertical geophone and microphone components, with lag in milliseconds. Bottom: Time record comparison of the geophone record and microphone record with phase rotations of plus and minus 90^0 (Dey et al., 2000)

Alcudia (2009) performed his master's thesis in the area of air-blast suppression. As part of his work, Alcudia utilized collocated microphones and geophones during data acquisition. The recorded data were transformed to the time-frequency domain using the Gabor transform. For each microphone channel, a null mask was created surrounding the microphone-recorded air-wave from the seismic source. This mask was multiplied by the geophone data (in time-frequency domain) to cancel the source induced air-noise. Sample data can be seen in Figure 1.7.
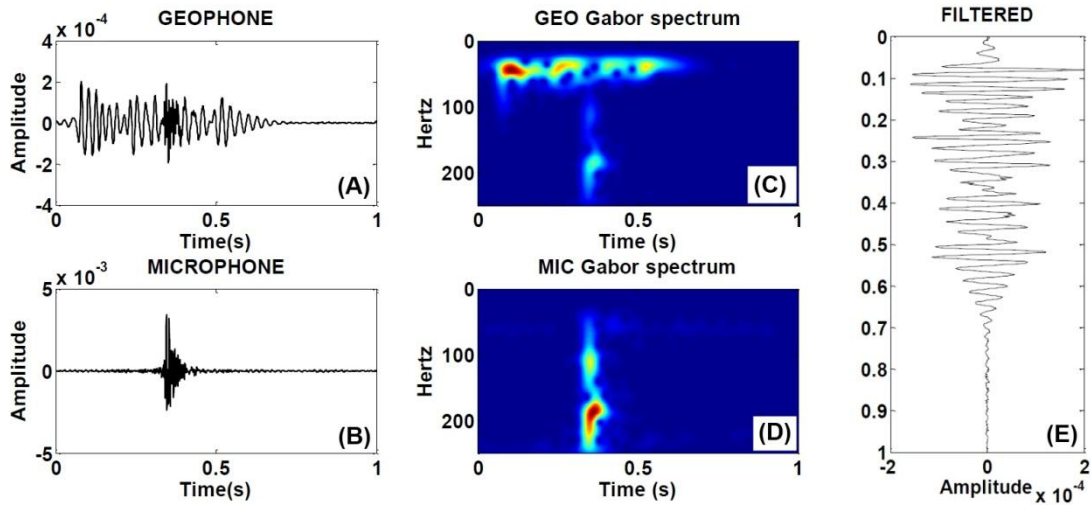
Figure 1.7: (A) Geophone trace showing air-blast at 0.35 seconds. (B) Microphone record showing the air-blast at the geophone location. (C) Gabor spectrum (frequency-time) of microphone record, showing air-blast at 0.35 seconds. (D) Gabor spectrum of microphone record. (E) Filtered geophone record after removing the air-blast using a null mask from the microphone record. (Alcudia, 2009)

CHAPTER 2:   NOISE CHARACTERIZATION STUDY

The basis of any noise-cancellation filter is the estimation and removal of noise present in an incoming signal. There are various classes of noise cancellation filters, including static and active. Static filters are ones that do not change over time; however, this does not mean they are simple. Active filters, on the other hand, change over time using input from any number of sources. Each class of filter has particular strengths and weaknesses. Static filters are typically smaller than active filters, in terms of resources used. They are also less flexible, requiring an accurate characterization of the noise present in the signal. Active filters are much more flexible since their parameters change over time. This means that the noise does not need to be perfectly characterized, as any discrepancies are updated in real-time. The goal of the noise characterization test is to determine how sound affects a 3C geophone, which will help determine which filtering method is best suited for removing air-noise.

2.1: Hardware design

A significant portion of the work presented here revolves around the design and use of a prototype 4-C geophone. The prototype consists of a 3-C geophone with an attached microphone. The overall design of the prototype has evolved through multiple iterations throughout the course of this thesis.

The first microphone design considered was an electret condenser microphone purchased from a local electronics store. This microphone produces a voltage when the electret film is vibrated by sound. This type of microphone is inexpensive and is used in many electronics, such as cell phones and webcams. The electret microphone was chosen as a test candidate for the 4-C geophone because design documentation is readily available. The basic design of an electret microphone consists of three parts: the microphone element, a power source, and a low-cut filter to isolate the microphone output from the power source. The microphone element is simple enough to find, purchased for less than $1 at any electronics supply store. The electret used in the microphone is a standard sized (1/4" or 6mm wide) element. The power source is also very simple, consisting of either a 9V or AA batteries. The battery is used to power an internal amplifier in the microphone element. This is where battery choice becomes important. The higher voltage 9V battery will power a higher amplification by the microphone, increasing sensitivity, but a low power density means the device will have a short battery life. AA batteries, on the other hand provide a lower voltage, reducing the power of the internal amplifier and decreasing sensitivity. The tradeoff is a much longer battery life. The choice of battery thus becomes a balance between microphone sensitivity, battery life, and size. AA batteries were chosen after a few quick tests determined the voltage they supplied the amplifier produced suitable results for field work. The final part of the microphone design is the low-cut filter. The filter serves two purposes, removing low frequency noise and isolating the signal output from the

battery. Typical low-cut filters could be 60 Hz or higher, depending on use. The desired microphone for the 4-C geophone cannot use a standard design; it requires lower frequency content to pass through to the recording system. A corner frequency of about 1 Hz was chosen to keep the signal output isolated while still allowing sound in the seismic band to pass.

The next design considered was a pressure capsule-based microphone. It is constructed using two piezoelectric transducers, consisting of a piezoelectric ceramic atop a brass disc, using a method similar to Shields (2005). These discs are cemented to a metal ring, creating a small air pocket in between. The discs are attached facing opposite directions, ensuring the piezoelectric surfaces facing inward have the same polarity. The two elements are then wired in series, doubling voltage produced by any pressure changes. Because this microphone creates a sealed cavity, it can theoretically detect atmospheric variations down to 0 Hz. In practice, however, the rigidity of the elements, and imperfect sealing restrict response to a few Hz or more. One great benefit to the piezoelectric design is that it requires no power, or supporting filtering circuit. Thus, it can be permanently mounted on a geophone without the need for future maintenance. One weakness of the piezoelectric transducer design is its potential susceptibility to motion-induced noise. When the piezoelectric element is shaken, bent, or otherwise moved, the resulting flexing of the element will produce a voltage. Since the two elements are mounted in opposing directions, any motion that creates a positive voltage in one element will create a negative voltage in the other element, cancelling out. This

process is not perfect, so small left-over charges can remain to be detected by the recording system. To prevent motion-induced noise, the piezoelectric pressure capsule can be mounted in a vibration-damping housing.

After considering each microphone proof of concept, the piezoelectric pressure capsule was chosen for use in the 4-C geophone prototype. It was chosen because it has a better low frequency response than the electret microphone, and does not require a power source. The issue with motion sensitivity may be avoided by making sure the microphone is properly damped in the geophone design. The first piezoelectric microphone was built from two, 15 mm buzzer elements from an electronics supply store. The elements were mounted to a hard butyl ring and connected in series. This unit was only used to evaluate the piezoelectric pressure capsule concept. A second, sturdier microphone was built using 25 mm professional piezoelectric elements, which were mounted on a 1" steel ring (the brass disc that holds the piezoelectric element is a few mm wider than the actual piezo-disc). The larger element size, and stiffer mounting ring give this microphone a more consistent low-frequency response. A secondary benefit of piezoelectric transducers is their low cost; the total cost for materials was under $5. This microphone element was used during all experiments in this thesis, and can be seen in Figure 2.1.
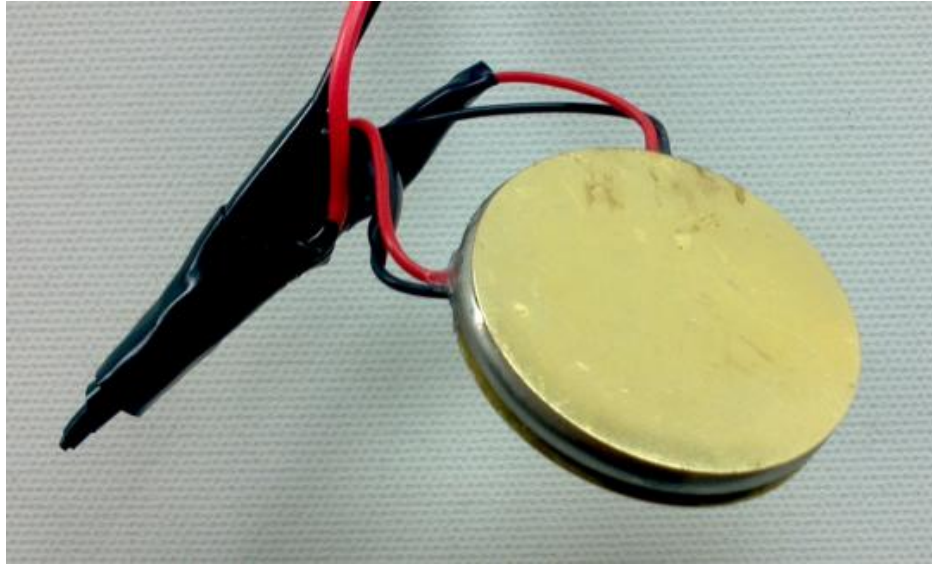
Figure 2.1: Final piezoelectric microphone. A brass disc contains a piezoelectric ceramic on one side. This is glued, facing inward, to a steel ring. A similar element is glued on the opposite side of the ring. The two pairs of wires coming from the microphone are from each piezo-element. They are wired in series to double the voltage produced by pressure changes on the microphone.

2.2: Experimental setup

The noise characterization tests consist of playing a sound and recording the geophone's response, while in a controlled environment. A microphone is collocated with the geophone during the test to create a microphone-to-geophone transfer function. This function describes how a sound recorded by a microphone relates to the same sound recorded by a geophone. To conduct the test, all unnecessary sources of noise, both mechanical and air vibrations, need to be reduced or accounted for. This ensures the transfer function created by the

characterization tests only applies to sounds picked up by both microphone and geophone, and nothing else.

The chosen test site was a large room, in Science and Research Building 1 on the University of Houston campus, which has thick cinder-block walls. To ensure lower levels of background noise the characterization tests were run at night. The only significant source of noise was an industrial air conditioning system, located outside the test room approximately 20 m away. This system created noise from 10 Hz to 30 Hz, mostly within narrow bands at 15 Hz and 30 Hz. To isolate the test setup a vibration isolation platform was built (see Figure 2.2). The isolation system consists of a series of springs connected to a wooden frame, suspended from the ceiling. The springs slightly stretch and compress when subjected to vibration, damping motion for the suspended platform. Air-noise created by the air conditioner still affects the test setup, but this is an unexpected benefit, as it allows for the analysis of low-frequency sound.

There is also a small amount of 60 Hz noise from electrical interference. To reduce this noise, all lights were turned off during testing and ancillary electronic devices were unplugged from their outlets. Any record stored by the StrataVisor seismic recording system can be converted from amplitude to true voltage using a scaling factor, determined by the system recording gain. For the noise characterization tests, this scaling factor is 1.6985e-4 mV. To determine the
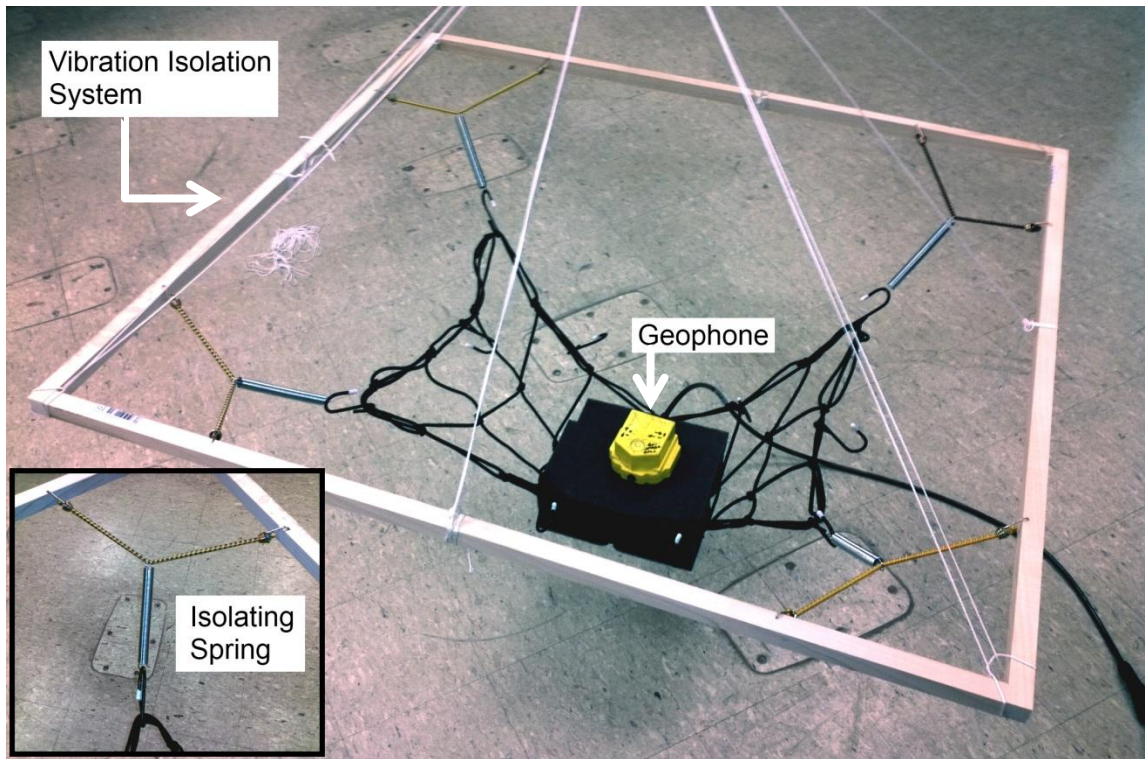
Figure 2.2: Picture of the noise isolation system. Inset shows a close-up of the isolating spring system.

background noise level in the room a 16-second recording was made with no sources present. Originally, the geophone was planted in a foam block, as if it were planted in the ground, and placed on the floor. The background noise level in the test room was 2850 or 0.48 mV RMS, and 9500 or 1.61 mV peak. With the isolation system, the background noise level dropped to 1500 or 0.25 mV RMS, and 5000 or 0.85 mV peak (see Figure 2.3, Figure 2.4, and Figure 2.5). The background noise level on the microphone is an order of magnitude smaller than on the geophone. The background noise level is 200 or 30 μV RMS. This is only 16.5 dB above the electrical noise floor, which is at an amplitude of 30 or 5 μV RMS.
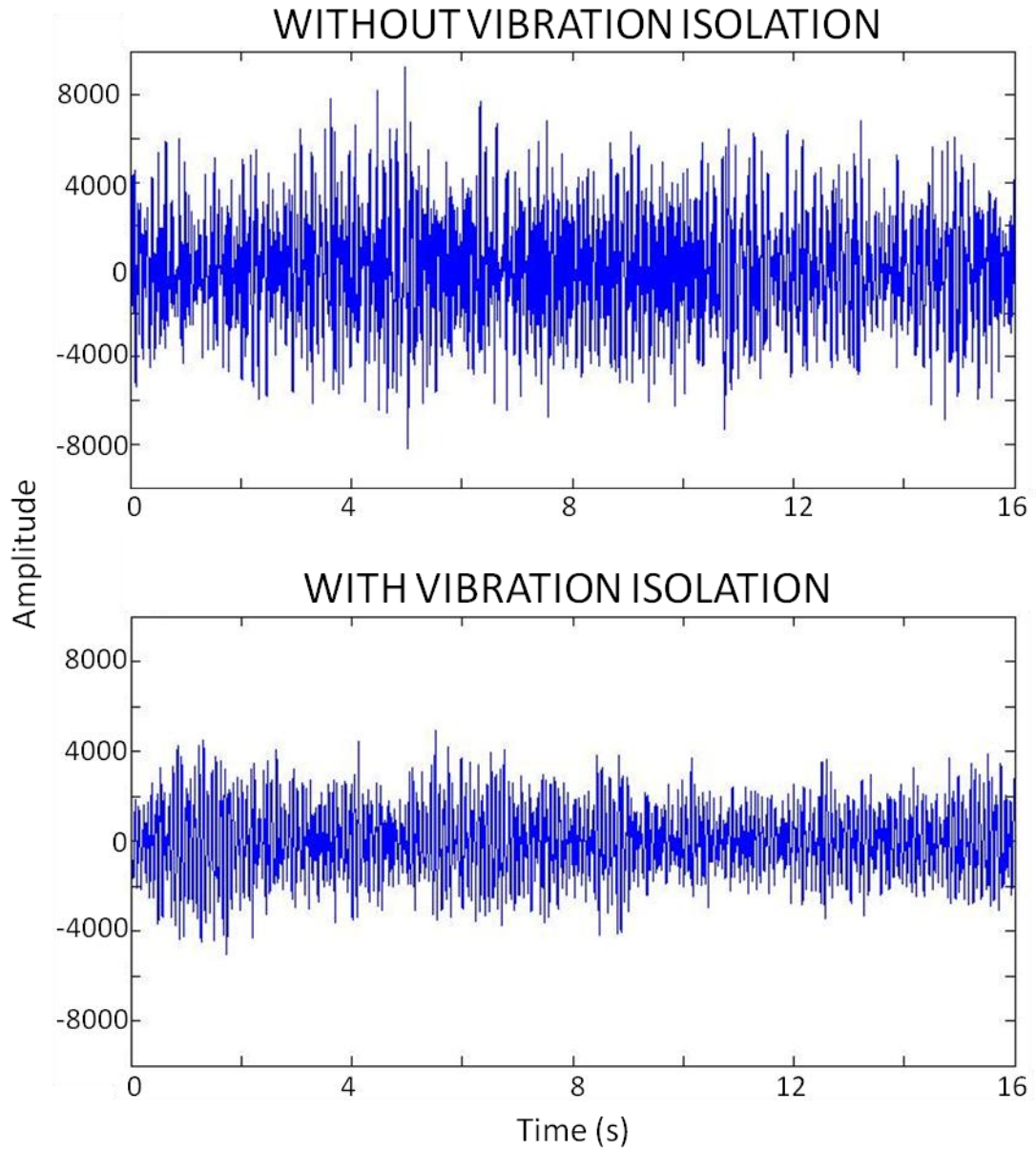
Figure 2.3: Time domain signal comparison of the isolation system used to decouple the test apparatus from background noise vibrations. The isolation system decreases background noise levels to less than half, compared to no isolation system.
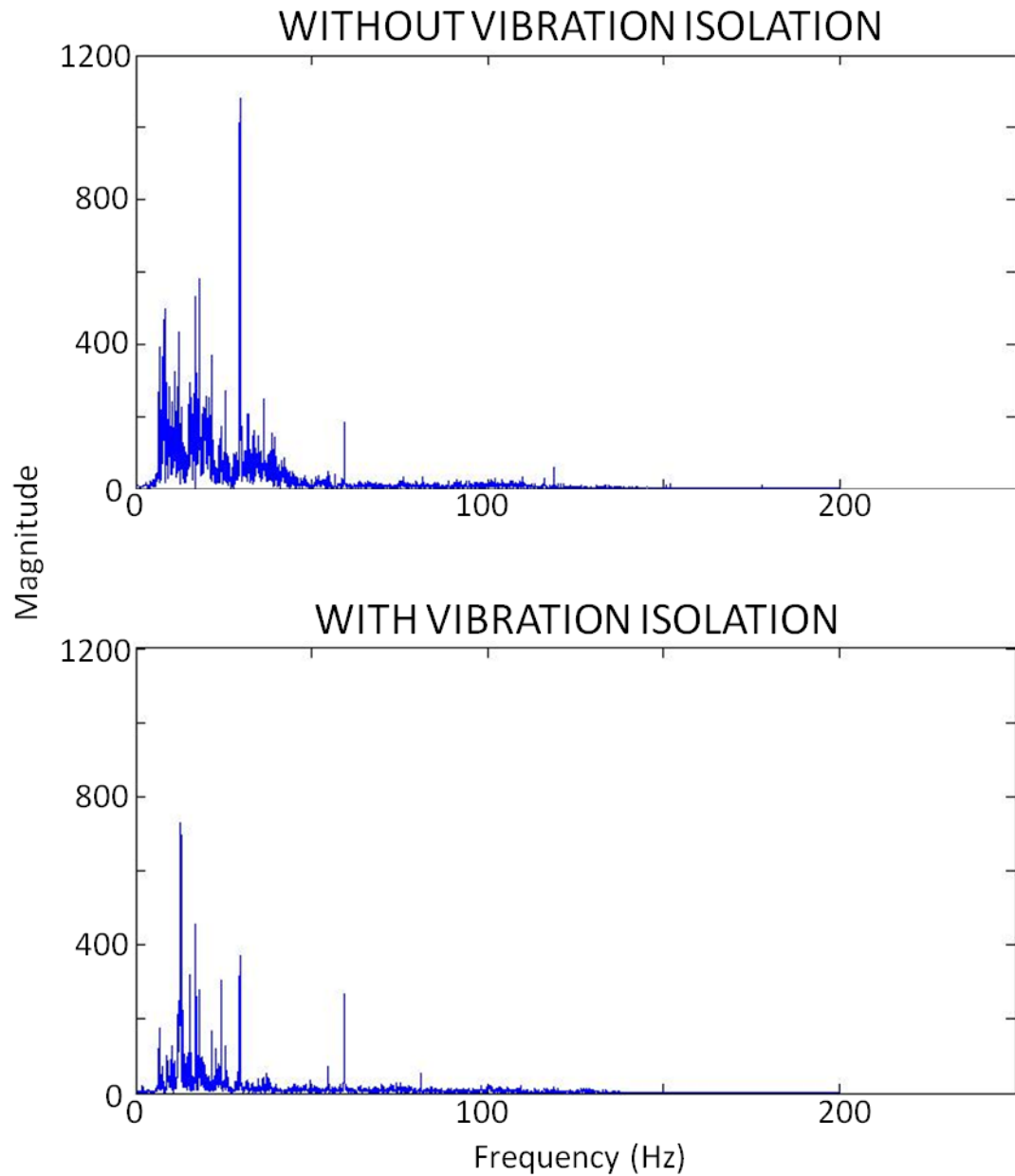
Figure 2.4: Frequency domain spectra comparison of the isolation system used to decouple the test apparatus from background noise vibrations. The isolation system significantly reduces background noise levels below 40 Hz. The remaining noise is in the 15 Hz, 30 Hz, and 60 Hz bands.
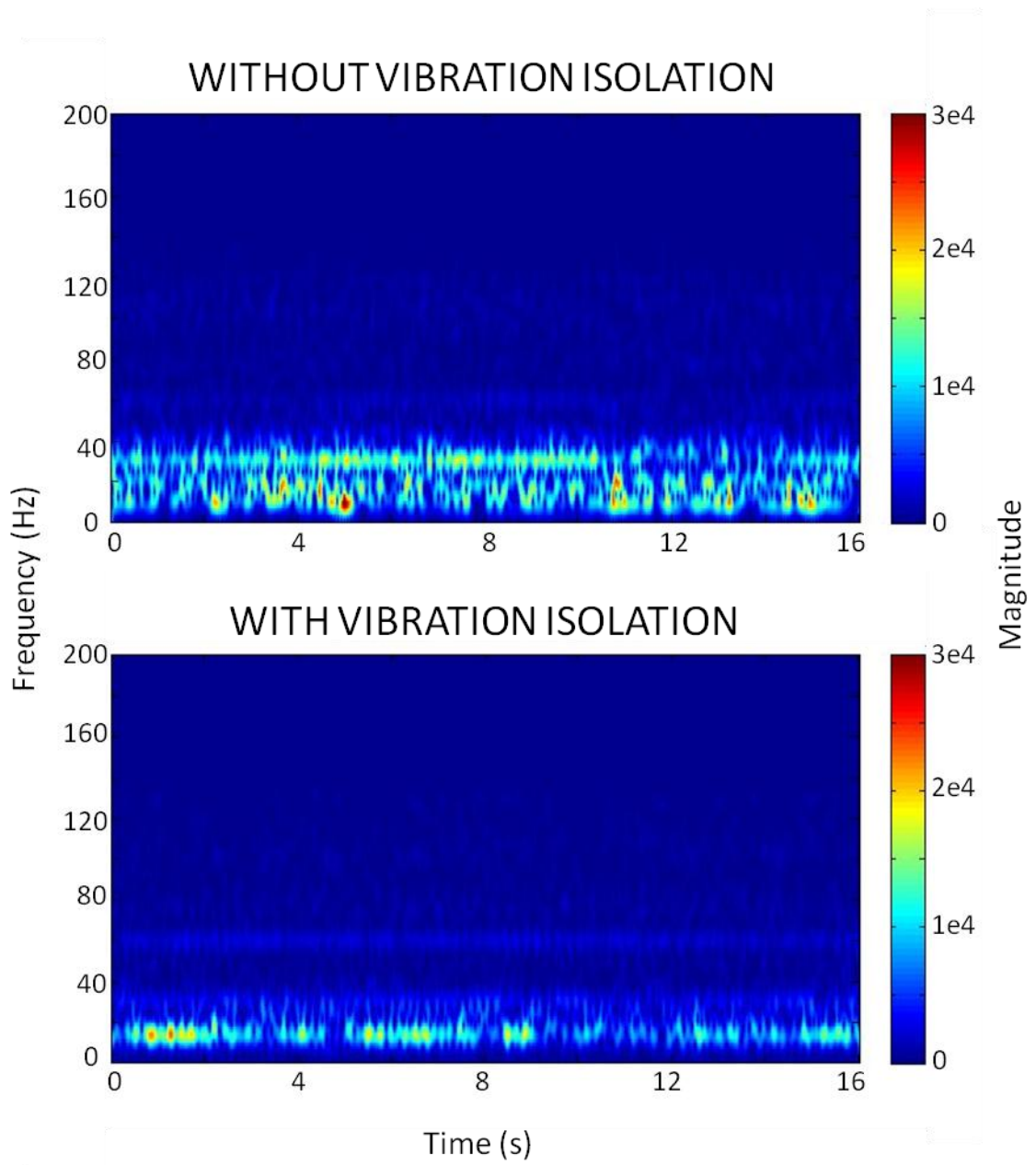
Figure 2.5: Time-frequency domain spectral comparison of the isolation system used to decouple the test apparatus from background noise vibrations. A large portion of the background noise below 40 Hz is reduced. Remaining noise occurs at 15 Hz, 30 Hz, and 60 Hz.

The test setup consisted of a geophone, microphone, recording system, and a sound source. The microphone is the piezoelectric pressure capsule, which allows for very low frequency operation. The geophone used was a 14 Hz, 3C unit from OYO GeoSpace. The recording system used was a Geometrics StrataVisor NZXP. Lastly, the speaker system was a 300 W, 12" subwoofer from Polk Audio. The microphone-geophone pair was placed on the vibration isolation platform, and the recording system and sound source were set up 8 m away. This distance is smaller than one wavelength for sounds up to 45 Hz, so care must be taken to avoid source geometry effects on the microphone-geophone pair. To minimize these effects, the microphone was placed on top of the geophone, separated by a piece of foam 1 cm thick.

The noise characterization test consisted of a sound sweep across the seismic band, from 15 Hz to 150 Hz. For the first test, the geophone was placed with the inline component pointed toward the subwoofer; this will be referred to as the starting position or 0° position. The microphone-geophone pair recorded the sweep, which was repeated two additional times to create one test. After each test, the microphone-geophone pair was rotated 30° counterclockwise, and the 3-sweep test was repeated until the pair completed one revolution (Figure 2.6). A picture of the recording location, without the microphone, can be seen in Figure 2.2. A picture of the subwoofer sweep location, and recording equipment can be seen in Figure 2.7. Noise characterization tests were performed at positions from 0° through 330°, for 12 total positions. One benefit is gained by keeping the subwoofer stationary.

Sound propagates from the subwoofer in all directions. These sounds may bounce off walls constructively or destructively interfering with the main wave. By keeping the subwoofer in one position, these interferences remain constant, and can be identified in the seismogram as frequencies with a consistently weak, or strong, response.

There are a few positions of note: at 90° the crossline component points at the source, at 180° the inline component points away from the source, and at 270° the crossline component points away from the source. The positions at 0°, 90°, 180° and 270° had additional 3-sweep tests performed, in which the microphone was aligned with the other two geophone components, inline and crossline. These tests were used to confirm the omnidirectional response of the microphone. After all noise characterization tests were acquired, a final test was conducted at the 0° position to determine test repeatability. A table describing each test position is seen in Figure 2.8.
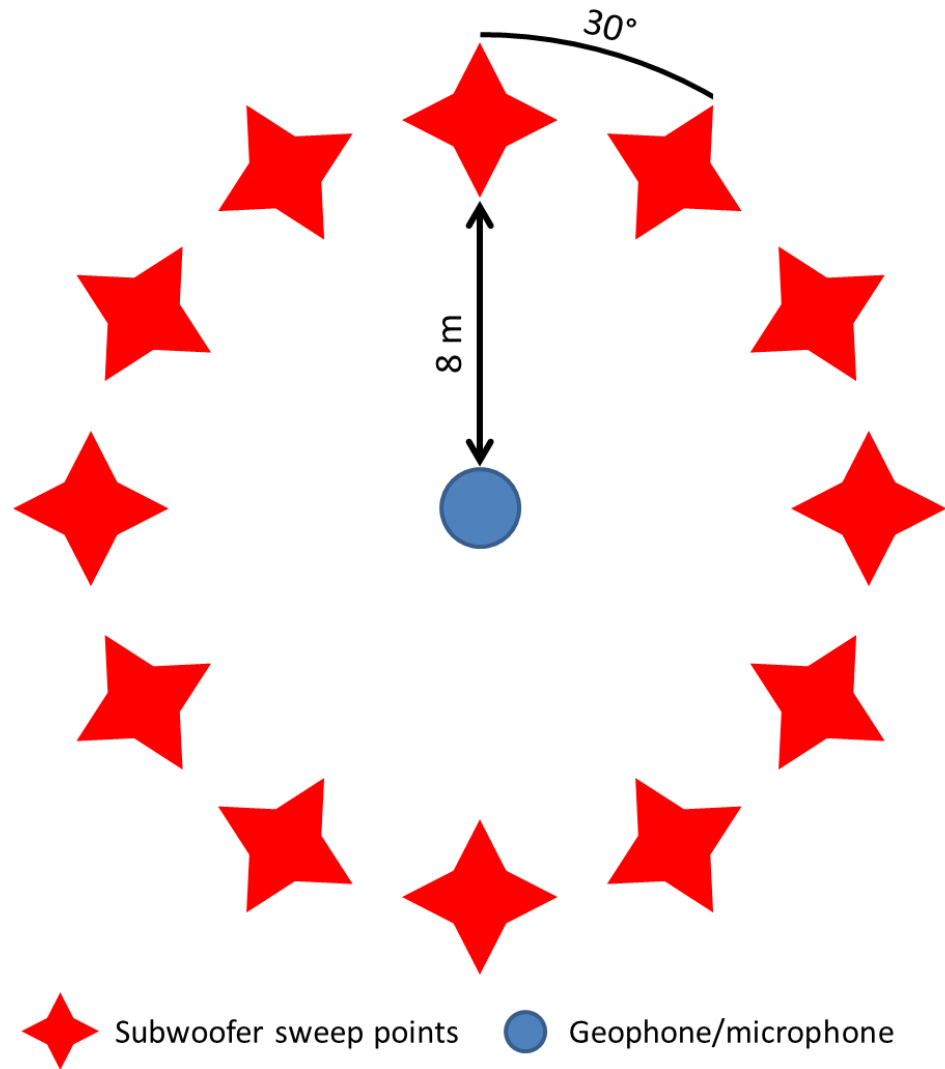
Figure 2.6: Apparent shot points, relative to the microphone/geophone setup. Subwoofer sweeps were performed three times at each position, which were 30° apart. Due to space constraints, it was actually the microphone/geophone pair that rotated, while the subwoofer remained in one position. The subwoofer was located eight meters from the test apparatus.
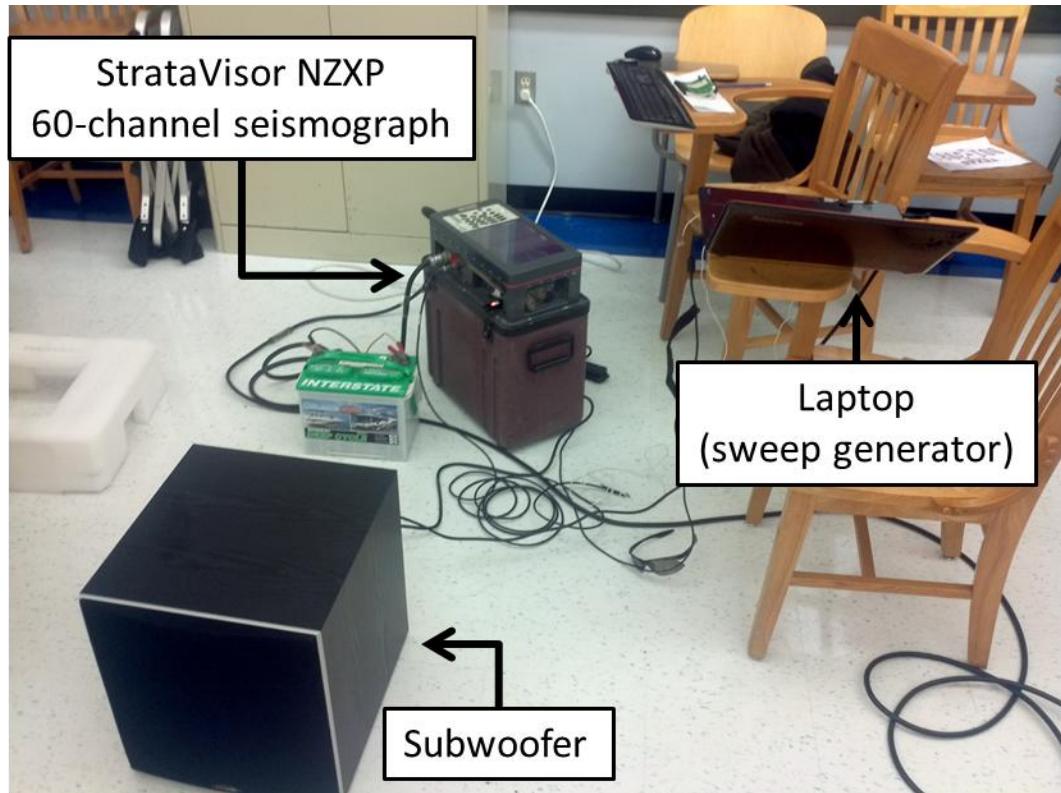
Figure 2.7: Subwoofer sweep location, and recording equipment. The laptop

generated a linear audio sweep from 15 Hz to 150 Hz, which was amplified and played

by the 12" subwoofer. The StrataVisor NZXP recorded the 3-C geophone/microphone

response to the sound sweep.

Position name	Geophone orientation	Microphone orientation	Number of tests at position	Type of test
1V	0°	Vertical	2	Background noise
1V	0°	Vertical	3	Sound sweep
1X	0°	Crossline	3	Sound sweep
1I	0°	Inline	3	Sound sweep
2V	30°	Vertical	3	Sound sweep
3V	60°	Vertical	3	Sound sweep
4V	90°	Vertical	3	Sound sweep
4X	90°	Crossline	3	Sound sweep
4I	90°	Inline	3	Sound sweep
5V	120°	Vertical	3	Sound sweep
6V	150°	Vertical	3	Sound sweep
7V	180°	Vertical	3	Sound sweep
7X	180°	Crossline	3	Sound sweep
7I	180°	Inline	3	Sound sweep
8V	210°	Vertical	3	Sound sweep
9V	240°	Vertical	3	Sound sweep
10V	270°	Vertical	3	Sound sweep
10X	270°	Crossline	3	Sound sweep
10I	270°	Inline	3	Sound sweep
11V	300°	Vertical	3	Sound sweep
12V	330°	Vertical	3	Sound sweep
1V	0°	Vertical	3	Sound sweep

Figure 2.8: Summary of acquired data for noise characterization tests.

2.3: Data analysis

The noise characterization study produced 65 data files from 22 tests. Given the amount of data, a standardized method was conceived to summarize and analyze the results. Before fully analyzing the noise characterization tests the data should be looked over, to become familiar with the sound sweep and expected response. Summaries of data from the first noise characterization test (geophone at 0°) are shown below for each component: microphone, vertical, inline, and crossline

(Figure 2.9, Figure 2.10, Figure 2.11, and Figure 2.12 respectively). The subplots within help characterize the sound recorded by each component. The time domain signal shows exactly what was recorded. The FFT chart displays the overall frequency content of the signal. The FFT cannot distinguish short sounds, of high amplitude from long sounds, of low amplitude. This means that the sound sweep cannot be distinguished from background noise from the nearby air conditioners. The only way to distinguish between these sounds is by converting to the time-frequency domain using the Gabor transform. The Gabor transform is a type of STFT that applies a Gaussian window. This type of window strikes a good balance between time localization and frequency localization, which is usually a trade off when converting to the time-frequency domain. The window length used for this analysis was 10 ms. In essence, this gives a windowed Fourier transform every 10 ms across the entire signal, showing exactly which signals are present at each point in time.
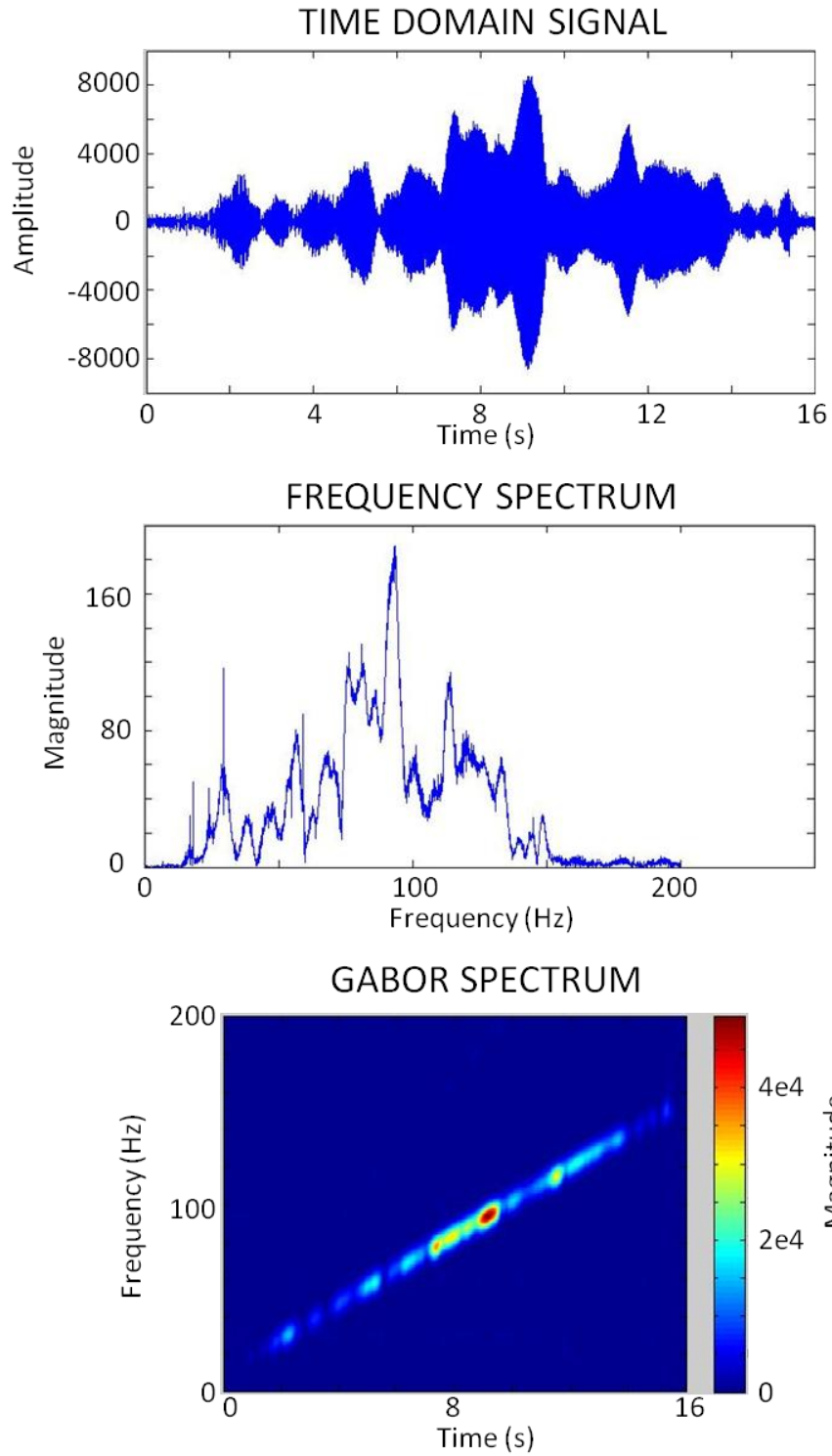
Figure 2.9: Data characterization of the microphone component. The recording is of a

16 s subwoofer sweep from 15 Hz to 150 Hz.

33
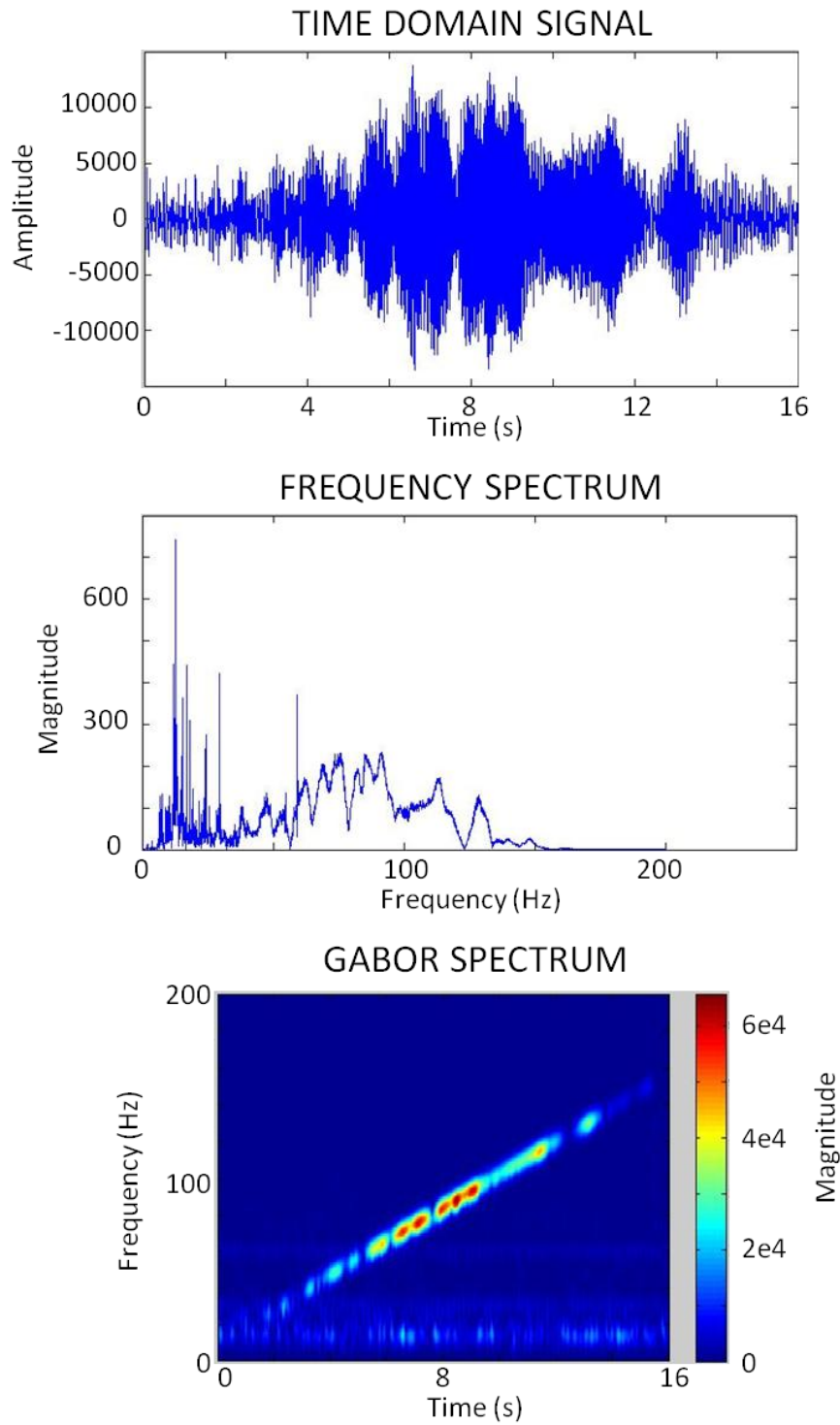
Figure 2.10: Data characterization of the vertical component. The recording is of a 16 s subwoofer sweep from 15 Hz to 150 Hz.

34
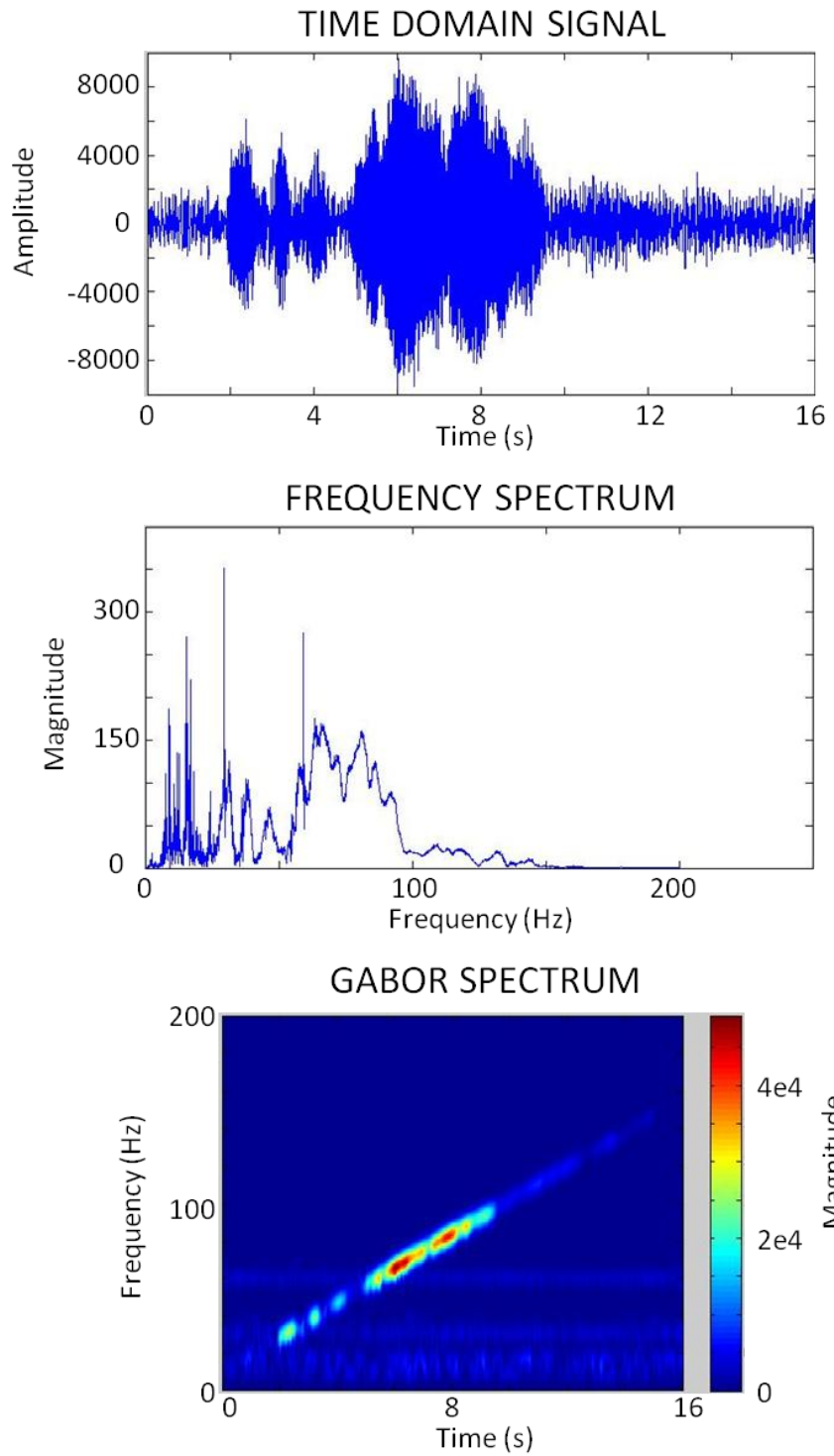
Figure 2.11: Data characterization of the inline component. The recording is of a 16 s

subwoofer sweep from 15 Hz to 150 Hz.

35
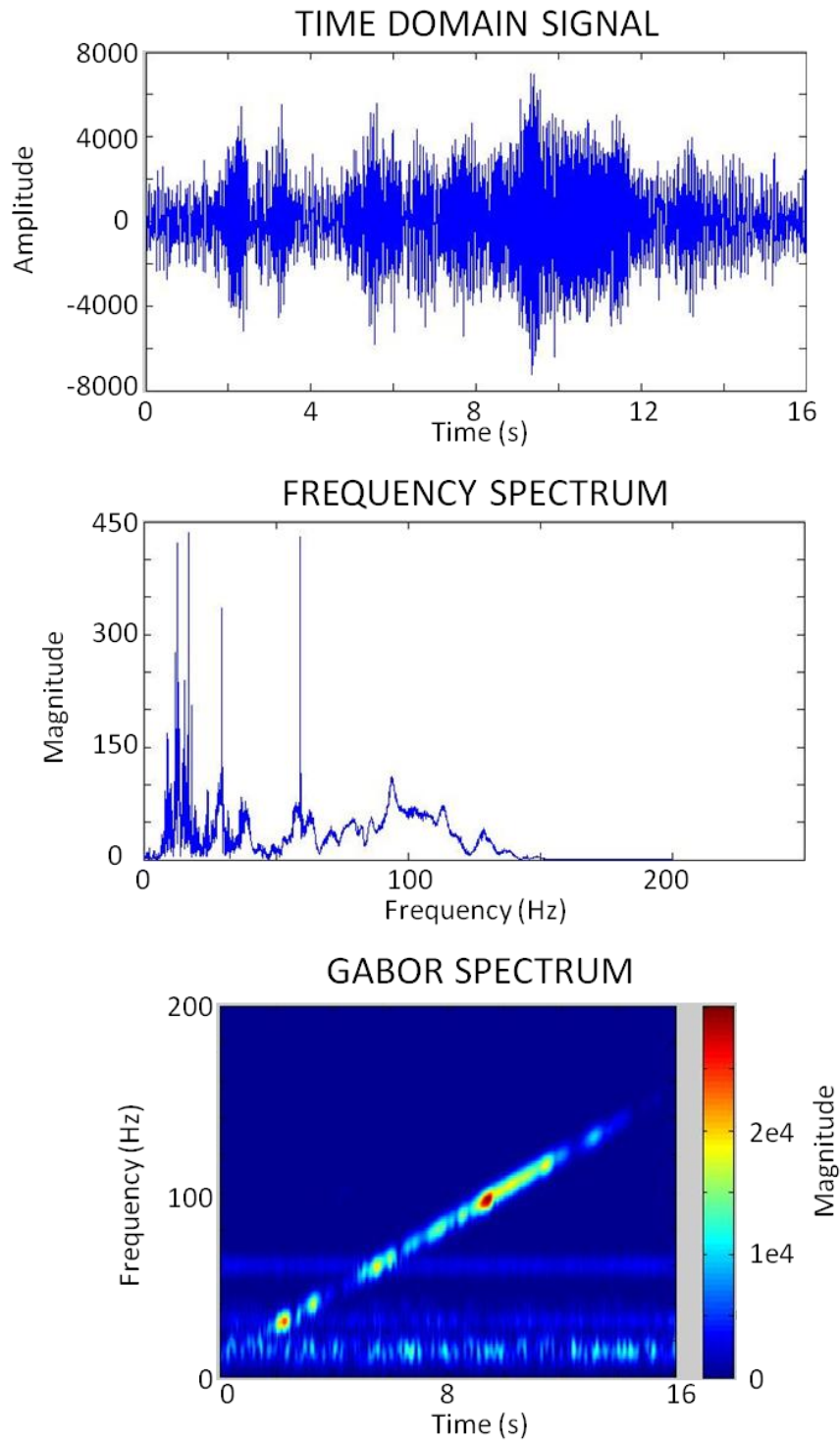
Figure 2.12: Data characterization of the crossline component. The recording is of a

16 s subwoofer sweep from 15 Hz to 150 Hz.

The noise characterization test was of a sound sweep from 15 Hz to 150 Hz over 15 s, with a total recording time of 16 s. This simulates an uncorrelated seismic trace from a field survey using a vibroseis source. The upper limit of the sweep is seen by the microphone FFT, but the range from 130 Hz to 150 Hz is much weaker. Because the subwoofer has an integrated high-cut filter of 120 Hz, any sound above this frequency is played at a reduced volume. The lower frequency limit is also unclear due to the subwoofer's resonant frequency, which is 23 Hz. Again, if any sound is below this frequency it will be played at a significantly reduced volume. While the true sound sweep was from 15 Hz to 150 Hz, the operational response is closer to 25 Hz to 130 Hz. From the time-domain signal of the microphone, the mid frequencies appear to be stronger (70 Hz to 100 Hz), compared to frequencies on the edges of the range (similarly indicated by the FFT). This means that the subwoofers output is not flat across the frequency range of the sound sweep. While the signal response of the subwoofer is important to keep in mind, it should not affect the characterization of sound between geophone and microphone. The important thing is that the microphone-geophone pair records the same sound, whatever it may be. Looking at the Gabor transform of a signal is a quick way to determine the presence of background noise. The Gabor transform for the microphone clearly shows the sweep, and shows very little background noise in the seismic band. This is confirmed by the time domain signal, which shows background noise levels of 500. The RMS amplitude for this trace is 2250 and the peak amplitude is 8400. This gives a RMS signal-to-noise ratio of 4.5:1, and a peak

signal-to-noise ratio of 16.8:1. Having a low background noise level on the microphone is important, because any noise present may be combined into the geophone record during noise cancellation.

The vertical geophone component has a similar story, compared to the microphone. From the FFT, the high frequency data weakens past 130 Hz and cuts off at 150 Hz, but the low frequency data are different. Below 30 Hz, the sound sweep entangles with background noise from nearby air conditioning units. This noise is low in amplitude, but constant throughout the entire test, creating a large response on the FFT. There is also 60 Hz power line noise, which manifests as a spike on the FFT. The Gabor transform shows the sweep down to near 20 Hz or 25 Hz. The spectrum does help separate the sweep from the air conditioning and power line noise. Since these noise sources are constant, they show up as lines of constant frequency in the Gabor transform. The air conditioning noise is contained below 30 Hz, with two distinct sources of noise at 15 Hz and 30 Hz. The power line noise is seen at 60 Hz. The RMS background noise is around 1000 with peak amplitudes of 2000, and the RMS of the signal is 3750 with peak amplitude near 14000. This gives a RMS signal-to-noise ratio of 3.75:1 and peak signal-to-noise ratio of 7:1.

The inline geophone component is quite different from the vertical component. The FFT of the inline component mostly recorded signal from 50 Hz to 100 Hz, with small additions at lower frequencies. The background seems stronger on this component, due to the sweep signal being weaker. There is general

background hum below 25 Hz; large noise spikes at 15 Hz and 30 Hz, from the air conditioner; and 60 Hz power-line noise. The Gabor transform confirms the signal bandwidth from the FFT, although it is able to separate the 30 Hz signal from the 30 Hz background noise. The background noise is clearer on the Gabor transform, compared to the vertical component. The background noise level remains the same as the vertical component, RMS amplitude of 1000 and peak amplitude of 2000. However, the signal is weaker, with a RMS amplitude of 2350 and a peak amplitude of 9500. This gives a RMS signal-to-noise ratio of 2.4:1 and peak signal-to-noise ratio of 4.8:1.

The crossline component is even weaker than the inline component because it is orthogonal to the sound source. The FFT shows a weak response across the entire frequency band. The background noise from the air conditioner and power line appear even stronger, dictating the scale of the FFT diagram. Even with the relatively stronger response of the noise, the Gabor transform is still able to distinguish the sweep. Again, the background noise has a RMS amplitude of 1000 and a peak amplitude of 2000, with a RMS signal level of 1700 and a peak amplitude of 8000. This gives a RMS signal-to-noise ratio of 1.7:1 and peak signal-to-noise ratio of 4:1.

Now that a general description of each component has been determined, full analysis of the geophone's response to noise coming from different angles can be performed. To determine the strength of each geophone component's response to sound, RMS and peak amplitude values are calculated. When plotted as a function of

incoming sound angle, these results show the directional response of that geophone component. Results are averaged from three consecutive noise tests to reduce variance. There are 13 total results, 12 from the test positions spaced 30° apart, and one repeat test at station 0° for control. The response charts indicate the geophone is directionally sensitive to air-noise and are shown in Figure 2.13.

Each component within the geophone exhibits a different directional sensitivity. The inline geophone component shows a bidirectional response to sound, with increased sensitivity to sound coming from 0° and 180°. The crossline geophone component shows a similar bidirectional sensitivity, with peaks at 90° and 270°, but with overall increased sensitivity to sound coming from the left. The increase sensitivity for left incoming sounds could be caused by the geophone element being attached to the left side of the case. This can be seen in the picture of the 3-C geophone construction in Figure 2.13. This bidirectional sensitivity of the inline and crossline components is expected; when these components are in line with the sound source their response should be stronger. The vertical geophone component remains pointing the same direction during all rotation tests, therefore it should not show any directional sensitivity to air-noise. Looking at the actual response for the vertical component shows a different story. The vertical geophone component exhibits a mild unidirectional response, weaker to sounds coming from 0° and stronger to sounds from 210°. Looking at the geophone construction, the vertical component is located at the back left of the geophone. This could explain the directional sensitivity.
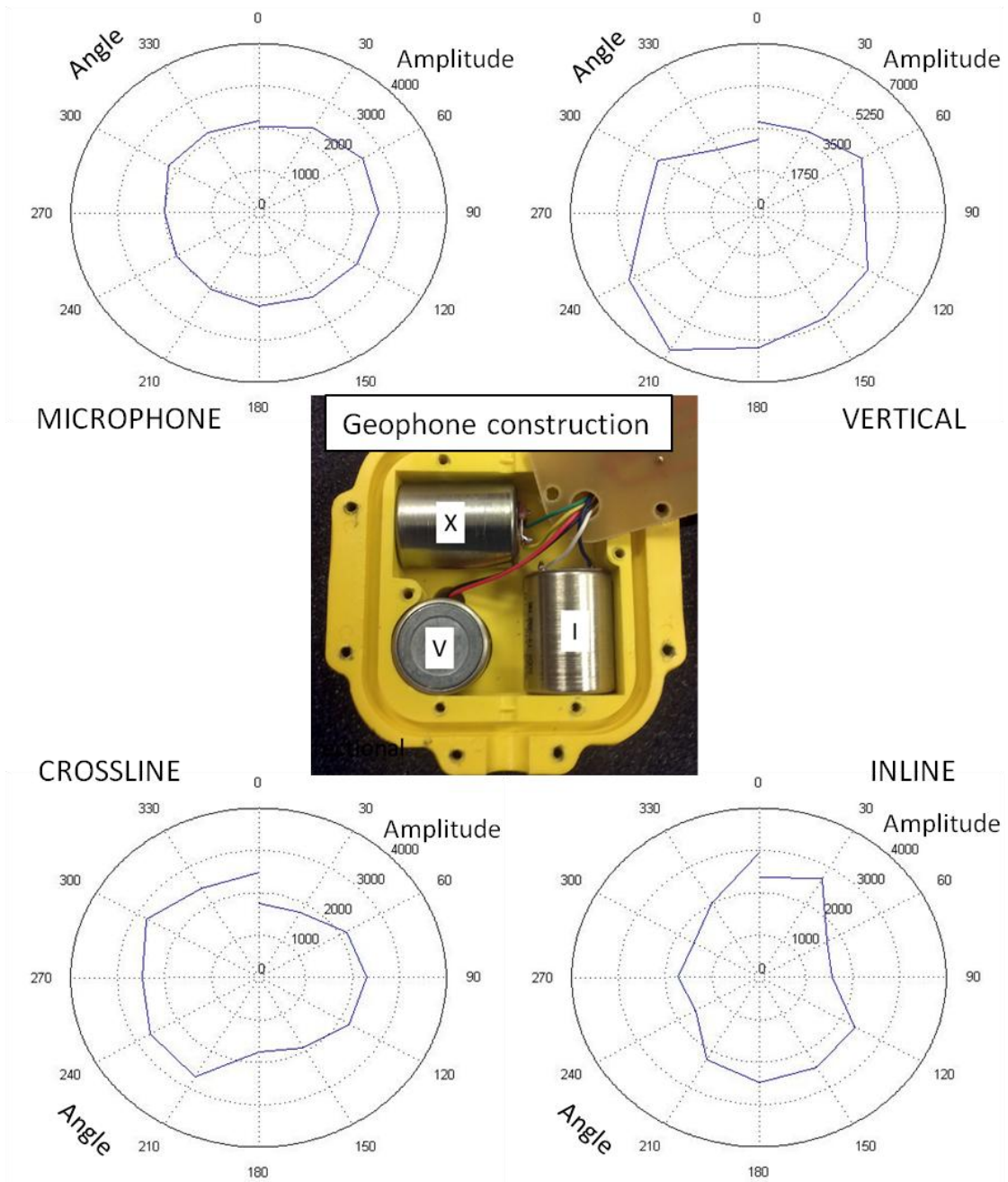
Figure 2.13: Directional sensitivity diagram for each component, showing RMS amplitudes for each directional test. The geophone picture at bottom shows how the construction might affect directional sensitivities. The components are as follows: V – vertical, X – crossline, I – inline.

41

The microphone used in these experiments was built to be omnidirectional. To confirm this, the microphone was tested at the same time, and in the same way, as the geophone. The directional response diagram is also in Figure 2.13. The diagram shows the microphone to be very nearly omnidirectional, producing an equal response to sounds from all directions.

2.4:   Microphone-to-geophone transfer function

To determine the microphone-to-geophone transfer function we must find how they relate in two ways, amplitude and phase. The amplitude comparison sounds simple enough; it is the difference in amplitude between the microphone and geophone records, but stopping here would be a gross approximation. In the characterization study, the geophone and microphone responded differently to sounds of different frequencies. Typically, the microphone has a stronger response to high frequency sounds while the geophone has a stronger response to lower frequency sounds. Thus, the amplitude relation must be determined at each frequency of interest. Phase shows similar frequency dependent response, so its transfer function will need to be determined for each frequency. Each geophone component has a different response to sound, so each component will have its own unique transfer function. A useful, first-order comparison between two signals is the cross-correlation. This operation calculates the similarity between two signals at various offsets. The higher the correlation value, the more similar the two signals

are to each other. If the correlation value is one, the two signals contain the same signal, but might still have differing amplitudes.

Figure 2.14 shows the comparison between the microphone and vertical geophone component for the first noise characterization test at 0° (position 1V). The cross-correlation shows a strong positive correlation, 0.58, but this value does not occur at the expected 0 ms offset. It instead occurs at -5 ms, indicating an overall phase mismatch between the microphone and geophone signals. Looking at the phase chart confirms this, the microphone record remains close to 180° out of phase with the geophone record, for the entire band of the sound sweep. One issue with using a simple correlation to determine signal similarity is that it does not consider these phase differences. A more effective correlation method would occur in the frequency domain, where phase differences arise as offsets in a cross-correlation. I call this type of correlation "frequency-band correlation," and it is done in the Gabor domain. The process is as follows. After performing the Gabor transform of the microphone and geophone data, the resulting spectra are divided into frequency slices. These are, essentially, spectrally decomposed signals. These spectrally decomposed signals can then cross-correlated in much the same manner as normal signal cross-correlation. Each frequency band from the microphone spectrum is cross-correlated with the corresponding frequency band from the geophone spectrum. After every frequency band correlation is calculated, they are all stacked atop each other to produce a frequency dependent similarity chart between the two signals. A cartoon of the process is shown in Figure 2.15, with the

results of this correlation shown in the data summary in the bottom frame of Figure 2.14.

The middle frame of Figure 2.14 shows the maximum frequency-band correlation value for each frequency level. This is a more accurate estimate of the similarity between the microphone and geophone records, compared to a standard signal cross-correlation. This chart indicates a similarity between microphone and vertical geophone component above 0.7, a very strong similarity, across much of the frequency band of the sound sweep. The main exception occurs at 60 Hz, where power line noise interferes with the signals. The other exceptions occur at 80 Hz, 120 Hz and from 135 Hz to 145 Hz. The weaker correlation at 80 Hz is persistent across many experiments and may be related to a dead spot in the room. A dead spot occurs when signals interfere destructively. In audio applications, this typically happens near walls and corners where a wave can bounce back and interfere with itself. This type of dead spot is located ¼ wavelength away from a wall, where a reflecting wave would be completely out of phase with an incident wave. For an 80 Hz sound, this dead spot would be 1.07 m away from the wall. This is approximately how far the microphone-geophone pair was from the wall. The weaker response between 135 Hz and 145 Hz may be related to the subwoofer output. Since this frequency band is above the subwoofer's low pass filter, it is output at a smaller volume. The final exception at 120 Hz is caused by a lack of signal on the geophone component. This notch in the frequency content is consistent across most characterization tests, but its explanation is unclear.
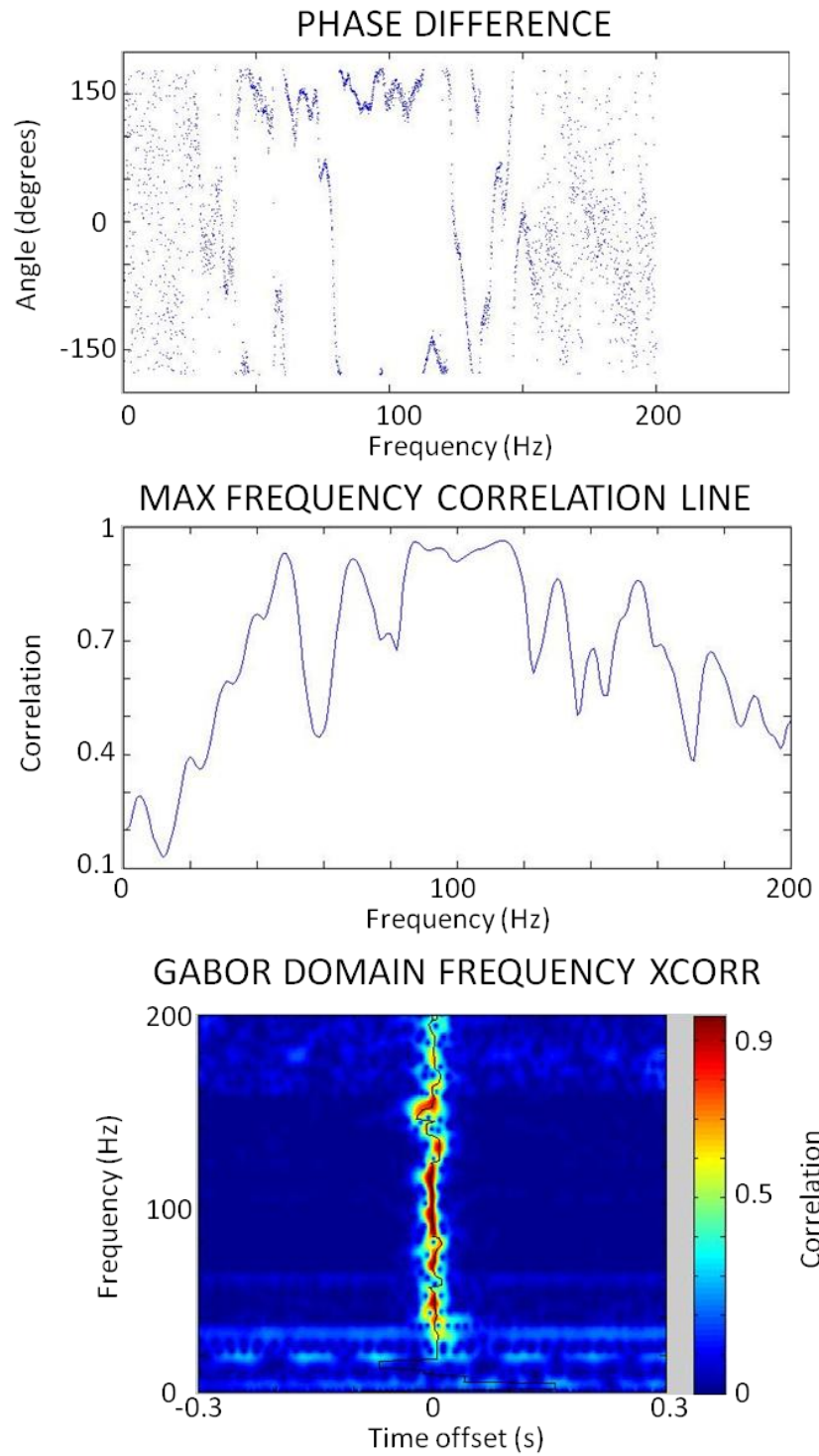
Figure 2.14: Correlation between the microphone and vertical geophone component.

Each plot contains unique information about the phase and amplitude relationship.
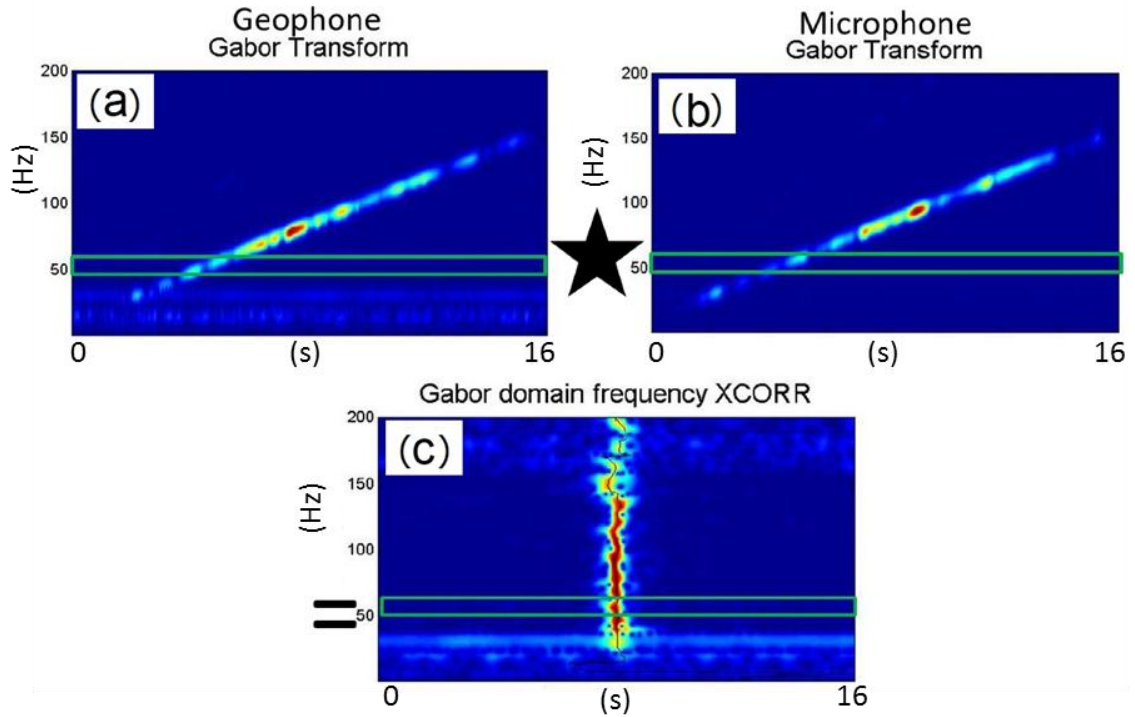
Figure 2.15: Cartoon process showing frequency-band correlation. Frequency slices are taken from the Gabor domain (a) and (b), then cross-correlated. The result is placed in the appropriate frequency slot in (c).

The summary of the microphone-to-inline comparison, for test location 0° (position 1V) is shown in Figure 2.16. For this test position, the inline component is most sensitive to the sound sweep. This is appropriately reflected by a high maximum cross-correlation value with the microphone, 0.59. Similar to the vertical geophone component, the inline also show evidence of phase shift in the cross-correlation, because the maximum correlation value occurs at 2 ms offset. Looking at the phase diagram, the difference between the microphone and inline geophone component remains near -90° for most of the sound sweep, only deviating at

frequencies above 110 Hz. The frequency band correlation shows a higher and more consistent correlation than the vertical geophone. The similarity is above 0.7 from 30 Hz to 130 Hz, and is above 0.9 for much of that frequency band as well. There is still a weak similarity notch at the 60 Hz power line. The notch from the dead spot has weakened, compared to the vertical component, and is now closer to 75 Hz.

The summary of the microphone-to-crossline comparison for test location 0° (position 1V) is shown in Figure 2.17. While the inline component is in its strongest position to detect sound from the subwoofer, the crossline geophone component is in its weakest. The maximum cross-correlation value between crossline and microphone components is only -0.37, which occurrs at 35 ms offset. This indicates a very inconsistent phase difference between the two records. Looking at the phase difference plot tells the whole story. For over half of the sound-sweep band, the phase difference is either rapidly progressing or regressing, as is indicated by the continual wrapping around the vertical axis. Only between 80 Hz and 120 Hz does the phase difference stay relatively constant. Even though the microphone and crossline component are significantly out of phase they still show good similarity in the frequency band correlation. Correlation values are above 0.7 from 25 Hz to 40 Hz, and are above 0.9 from 75 Hz to 135 Hz. The weak similarity between 45 Hz and 70 Hz is due to a weak response by the crossline geophone component to sounds in this frequency range, which is consistent across multiple test locations.
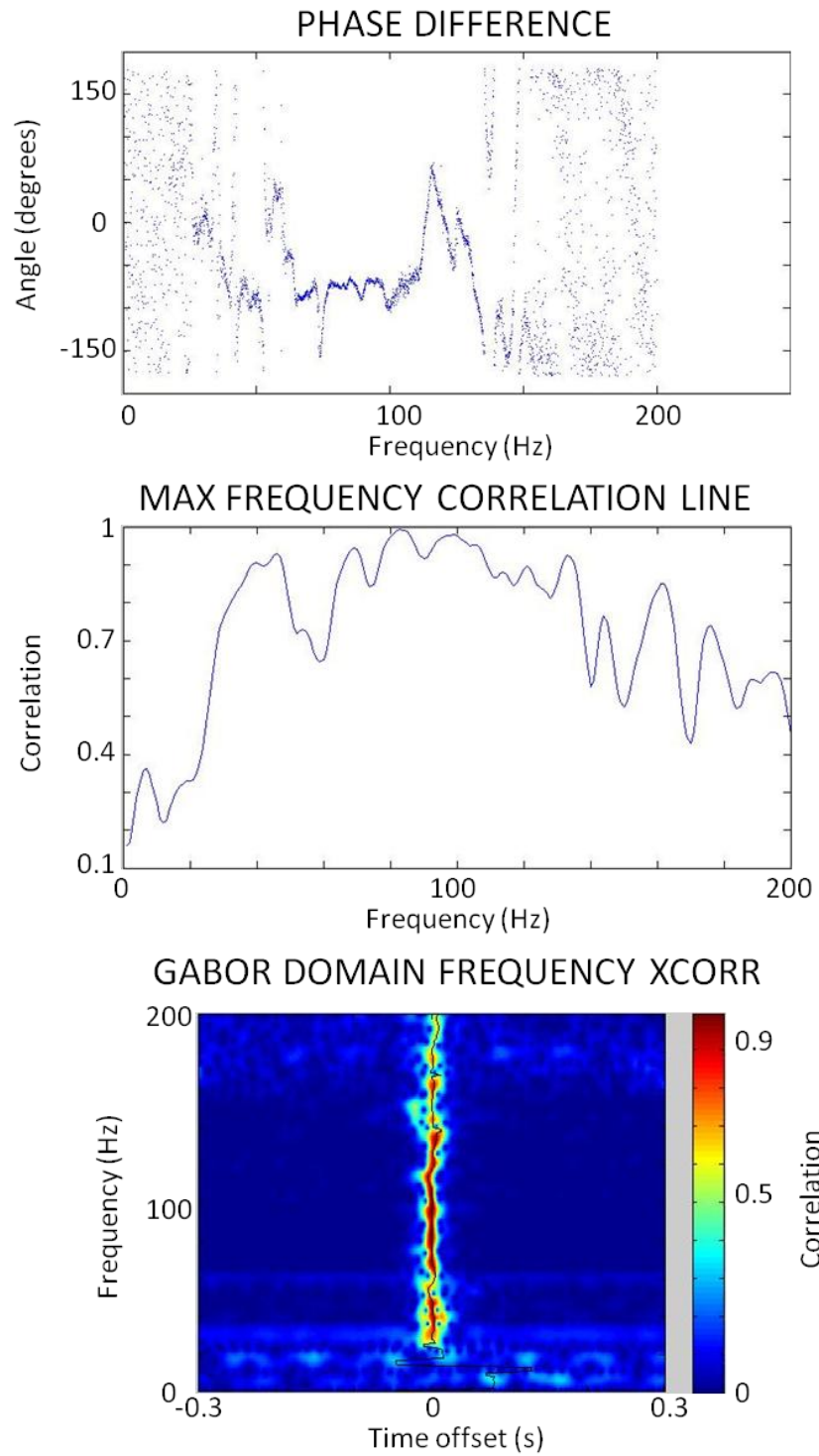
Figure 2.16: Correlation between the microphone and inline geophone component.

48
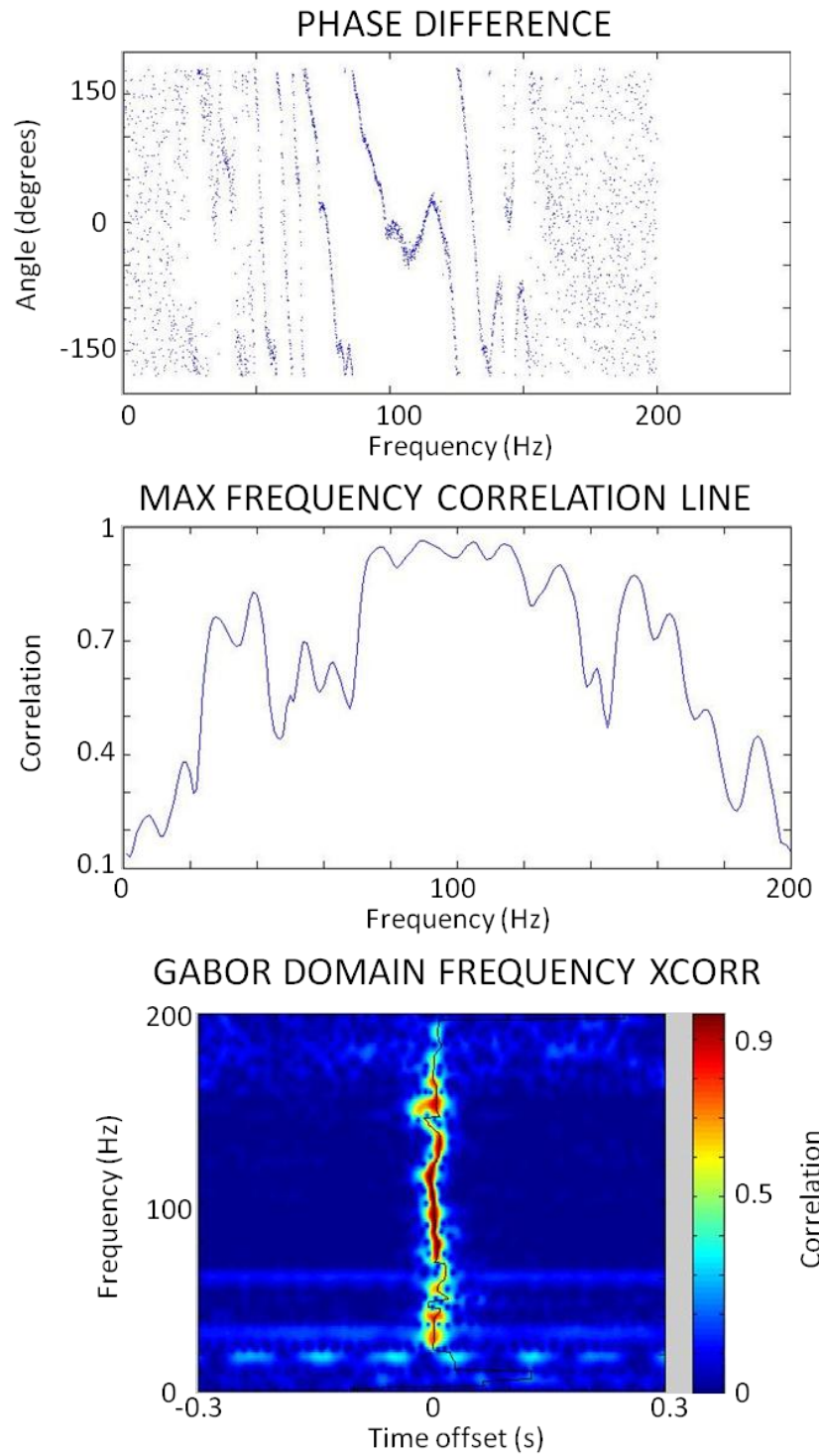
Figure 2.17: Correlation between the microphone and crossline geophone component.

To determine how each geophone component relates to the microphone, cross-correlation has been performed for data at all 13 test points. Displaying the maximum correlation value as a function of angle is a proxy for the similarity between microphone and geophone. In addition, plotting the time lag at which these maximum values occur, as a function of angle, is a proxy for phase similarity. The results of the max cross-correlation are in Figure 2.18, and the maximum correlation lag times are in Figure 2.19.

The results from the maximum cross-correlation are similar to the amplitude sensitivity charts. The inline component has a higher similarity to the microphone when it is detecting more air-noise, resulting in a bidirectional chart with lobes at 0° and 180°. Similarly, the crossline component shows higher similarities to the microphone at angles where it records more air-noise, resulting in bidirectional chart with lobes near 90° and 270°. The results from the vertical component are different from the unidirectional response from the amplitude sensitivity measurements. The cross-correlation chart shows a bidirectional response, with increased similarity to the microphone for sounds coming from 45° and 240°.

The maximum correlation lag offset is an indication of phase mismatch, with higher values indicating a larger phase mismatch between microphone and geophone records. Knowing this, this type of plot should show an orthogonal image compared to the maximum correlation chart. The inline component almost responds as expected, there is one lobe at 90°, indicating a large amount of phase mismatch to the microphone component. The expected lobe at 270° is missing

Maximum cross correlation value

Vertical component

Inline component

Crossline component
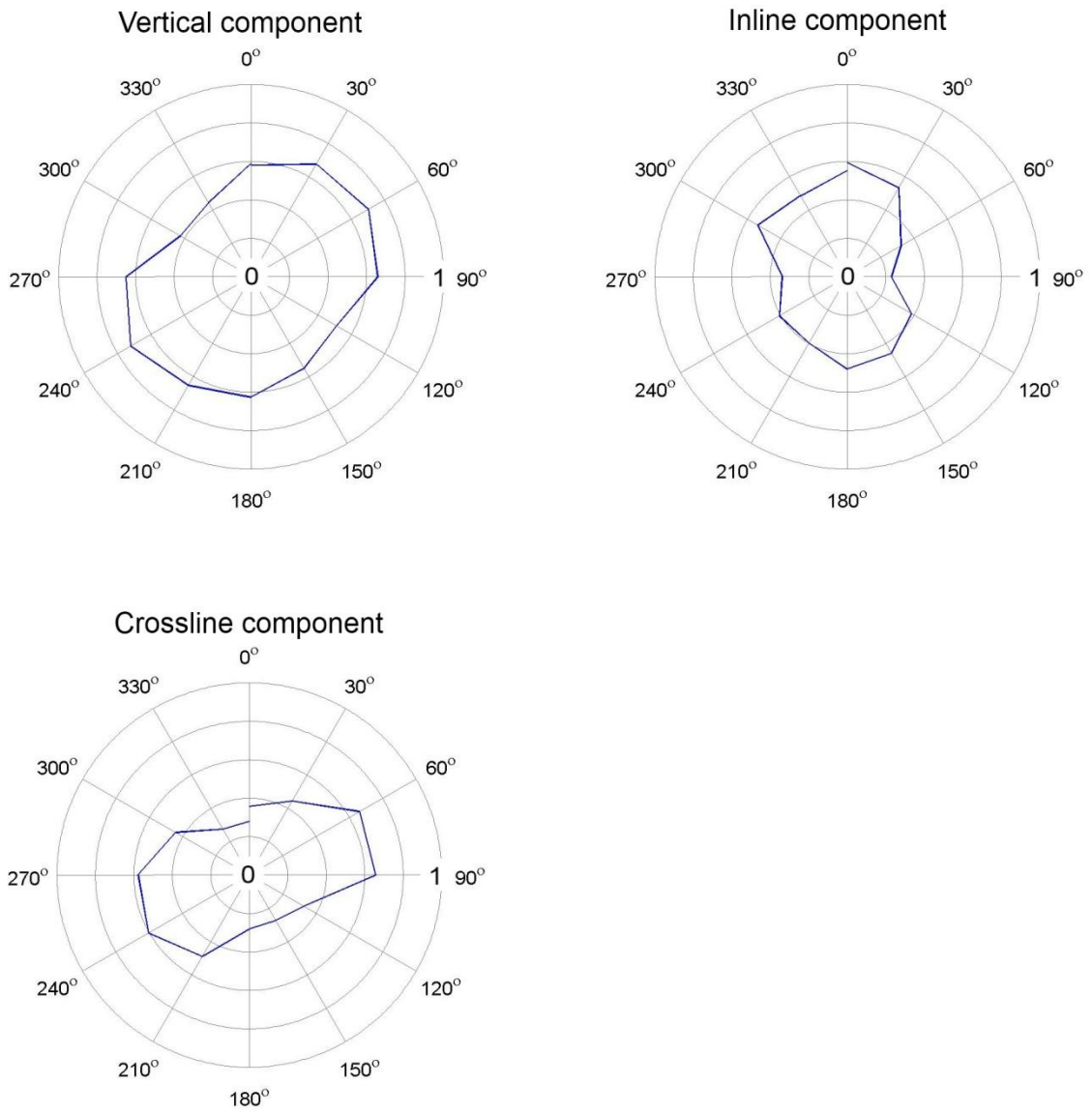
Figure 2.18: Maximum cross-correlation value of each geophone record and the microphone record. Values further from the center indicate higher correlations, and higher similarities.

Maximimum correlation lag offset

Vertical component

Inline component

Crossline component
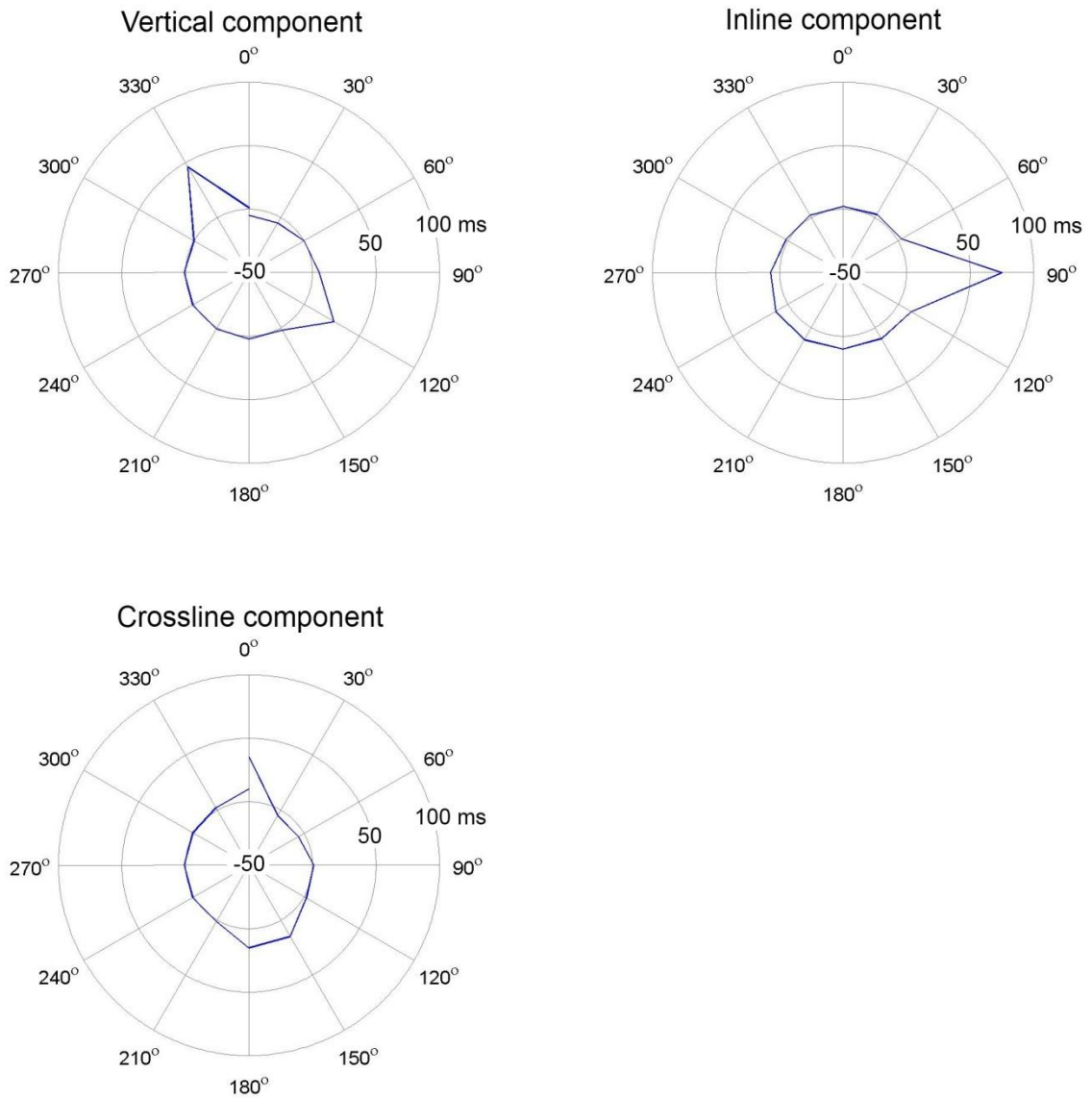
Figure 2.19: Maximum correlation lag offset for each geophone component, after cross-correlation with the microphone. Values further from the first ring indicate positive lag offsets, and values lower than the first ring indicate negative lag offsets. A bigger lag offset indicates larger phase mismatch between that component and microphone.

however. The crossline component responds as expected, with lobes at 0° and 180°, indicating high phase mismatch to sounds coming from those angles. The vertical component continues to show results contrasting with its earlier unidirectional sensitivity. There are lobes at 120° and 330°, indicating increased phase mismatch to sounds coming from those directions.

The final piece of information to come from the microphone-geophone transfer function is the amplitude relationship. The frequency-band correlation is an indication of similarity between two signals in the time-frequency domain, but it does not give any information about amplitude. A quick way to compare amplitudes in the time-frequency domain is to multiply two Gabor spectra together. This has been performed for the first test at 0°, position 1V (Figure 2.20). Stronger values indicate frequencies where both the geophone and microphone are strong, but not necessarily how strong the geophone is compared to the microphone. All charts show relatively strong responses between 70 Hz and 100 Hz, with the inline component being the strongest. This could be caused by an increase in geophone/microphone response to the sound sweep, or by an increase in subwoofer output. What is important is the comparison between geophone channels. The inline component shows a stronger response than the crossline component. For this test position, the inline component is pointing toward the subwoofer, thus it should have a stronger response.
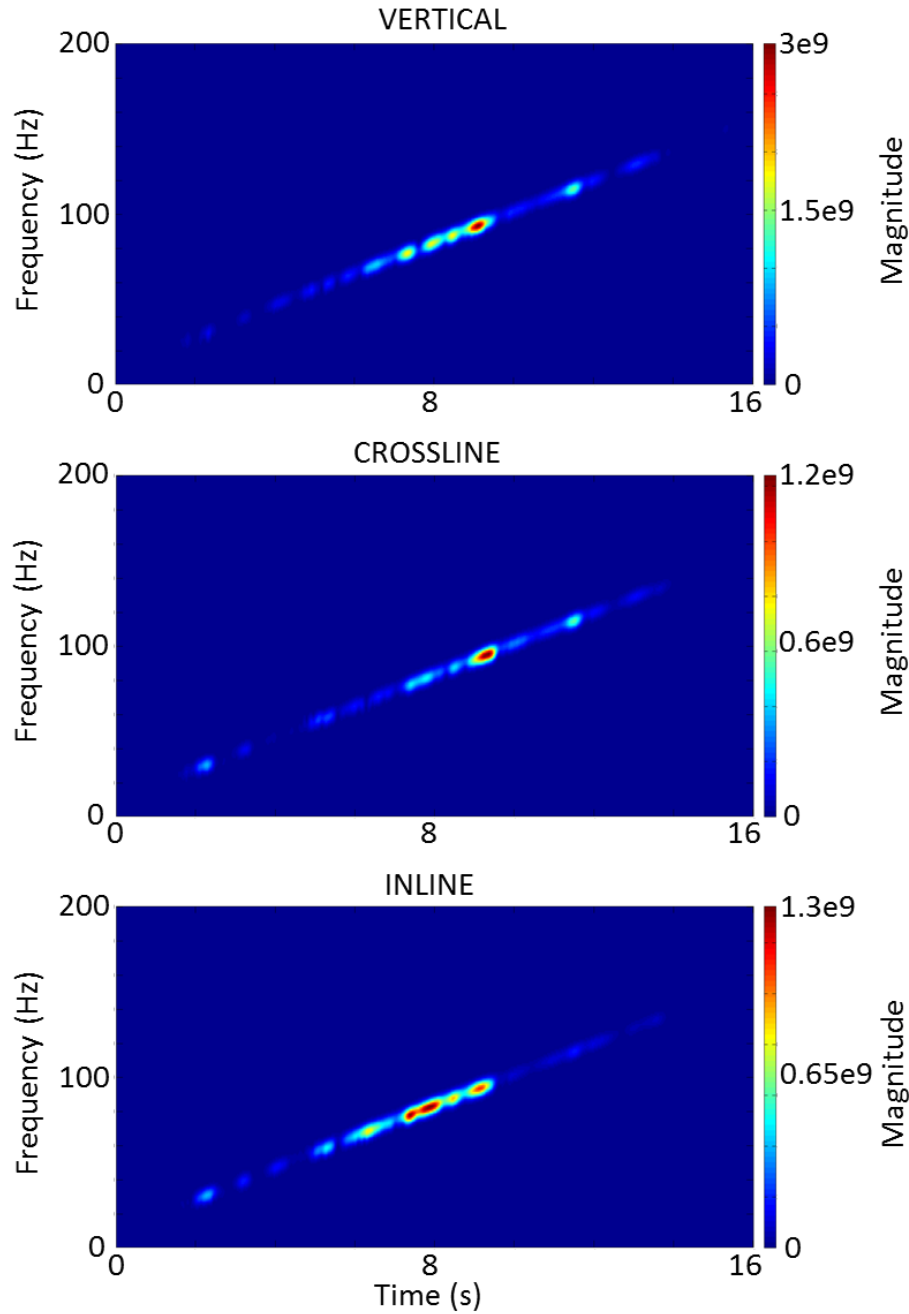
Figure 2.20: Gabor spectra multiplication of each geophone component with the microphone. The results show where both geophone and microphone responses are strong. The vertical component has the largest response. The inline response is stronger than the crossline response due to the incoming direction of the sound sweep.

54

2.5: Conclusions

The data acquired here, and subsequent analysis, forms the framework for the noise-cancellation filter design. A few conclusions about air-noise in seismic records can be made from these characterization studies. First, geophones are directionally sensitive to sound. In a multicomponent geophone, each component has its own directional sensitivity. The inline geophone component is more sensitive to sound coming from inline noise source (0° and 180°), and the crossline geophone is more sensitive to sounds from crossline sources (90° and 270°). For this particular geophone, the vertical geophone also shows directional sensitivity, showing an increased response to noise coming from behind the geophone (180°) and less to noises coming from the front (0°). The relation between microphone and geophone records is also not simple. While the two records may be highly similar in the time-frequency domain, there could be a frequency-dependent phase shift between them. This means that filtering air-noise from a geophone using the microphone signal must be done, at least partially, in the frequency domain. This will introduce problems when creating a filter that works in real-time.

CHAPTER 3:   FIELD EXPERIMENT

The previous study explored the effects of air-noise on the geophone case, mimicking the process direct interaction of air-noise would have as it struck a geophone in the field. There are other methods in which a geophone is affected by air-noise and can only be characterized in the field, like air-to-ground interactions and distance dependent amplitude response.

3.1: Experimental setup

A walk-away seismic experiment was performed to determine the effect of air-noise on geophones during a seismic survey. A 3-C geophone plus microphone was placed beside a road at the University of Houston Coastal Center. The Coastal Center, a remote facility in La Marque, Texas, is approximately four km² in size, and is used for atmospheric monitoring and contains producing oil wells. It has large, open areas and long, isolated roads, ideally suited for seismic experiments. The experiment consisted of one 3-C geophone, piezoelectric microphone, and vibroseis truck. The 3-C geophone is the same 14 Hz unit used in the noise characterization tests. The prototype microphone was also the same unit, but was outfitted in a vibration damping material. To reduce motion-induced noise, the microphone was wrapped in polyester fiber. This fiber is composed of small corkscrew shaped strings. These spiral strings act like tiny springs supporting the microphone, isolating it from vibrations. The 4-C geophone with microphone padding can be seen in Figure 3.1.

The geophone and microphone (4-C geophone) were placed along a dirt road inside the facility, and the shot line continued down the road. The first shot point was 2.5 m behind the 4-C geophone and shots were taken every 5 m, to 702.5 m in front of the 4-C geophone (Figure 3.2). Each shot consisted of a single sweep from the vibroseis truck, from 15 to 150 Hz over 12 s. Sixteen seconds of uncorrelated data were recorded for each shot, so that analysis could take place on the raw data.

Figure 3.1: The "pillow-top" vibration isolation system. The piezo microphone is placed inside a felt pocket, surrounded by polyester fibers. These springy fibers dampen vibrations that affect the microphone. Shown attached atop a 3-C geophone.

Figure 3.2: Survey location and schematic. Satellite imagery of the northern portion

of the UH Coastal Center, near La Marque, Texas. The blue circle shows the

approximate 4-C prototype geophone position, defined as 0 m. The red line indicates

the shot line, from -2.5 m to 702.5 m shot at a 5 m interval.

Imagery source (Google Maps, 2012)

The test site had little cultural noise; i.e. noise created from non-natural sources such as traffic, construction or other human activities. There was, however, a large amount of environmental noise, or natural background noise, mostly from wind. The nearest roads were located approximately 400 and 1000 meters away, behind a large stand of trees. Audible noise from the roads was occasionally discernible, but any vehicle-induced ground vibrations were undetectable. The dirt road on which the experiment took place carried sparse traffic. Shooting was halted when traffic passed to ensure clean data were acquired. Winds on the day of the survey ranged from 15 to 25 km/hr. This caused discernible noise in both the seismic and acoustic records.

After the survey, all shot records were combined in a common receiver gather, to simulate a 700 m, 4-C geophone line. This process allows the experimentation of noise cancellation along a full seismic record without needing to make 140 4-C geophones.

3.2: Geophone data analysis

Before analyzing the air-noise data, it is best to define from theory what to expect. While expectations about transient air-noise response cannot be determined beforehand, vibrator-induced air-wave is easily characterized. The majority of the air-wave energy transmits directly through the air. When travelling across a spread of geophones, this is seen as a linear event, originating at the shot location, travelling around 345 m/s (dependent on temperature and pressure). The air-wave will interact with the ground, creating ground-roll and compressional waves. The conversion to compressional waves occurs across a wide range of frequencies, and depends on many factors, such as the acoustic impedance of the weathering layer. The ground-roll conversion only occurs at a single frequency, which depends on the weathering layer thickness. Any air-wave-induced ground-roll will be seen as a monofrequency wave-train following any air-noise arrival. The reverse of these processes occur as well, ground motion will convert to air motion. Ground roll will couple to monofrequency air-wave, and compressional waves will convert to air-wave as well. In short, in the seismic record, the linear air-wave should be easily seen, which should be followed by a monofrequency wave-train.

59

The acoustic record will also show the direct air-wave arrival, and the monofrequency wave train following it. Microphones may also record the energy from other compressional seismic-wave arrivals, but recorded evidence of this process has yet to be published for seismic experiments.

The raw data were correlated in MATLAB for initial analysis. The correlated geophone gathers can be seen in Figure 3.3, Figure 3.4, and Figure 3.5. Even with the high levels of wind noise, and only single vertical fold, the geophone collected good data. Using only 500 ms AGC, reflectors can be seen deeper than 1000 ms on the vertical component. The crossline component detected reflectors down to 650 ms, but the inline component only detected the shallowest reflectors, below 400 ms. The head-wave response is very strong on the vertical and crossline components, but weaker on the inline component. There appears to be only a single visible refracting layer with a velocity of 1750 m/s. This refracting layer is also very shallow, evidenced by the lack of a visible direct arrival at near offsets. The weaker recordings by the inline component, compared to the crossline component, are of interest. Typically, the inline component should see a strong head-wave response while the crossline component is weaker. The nearby road could cause this. The high-velocity, well-compacted roadbed may bend incoming arrivals toward the crossline direction.

The air-wave response from the geophone is much more atypical. According to the sensitivity diagrams for the 3-C geophone, the vertical and inline components should show a strong response to air-wave, while the crossline component response
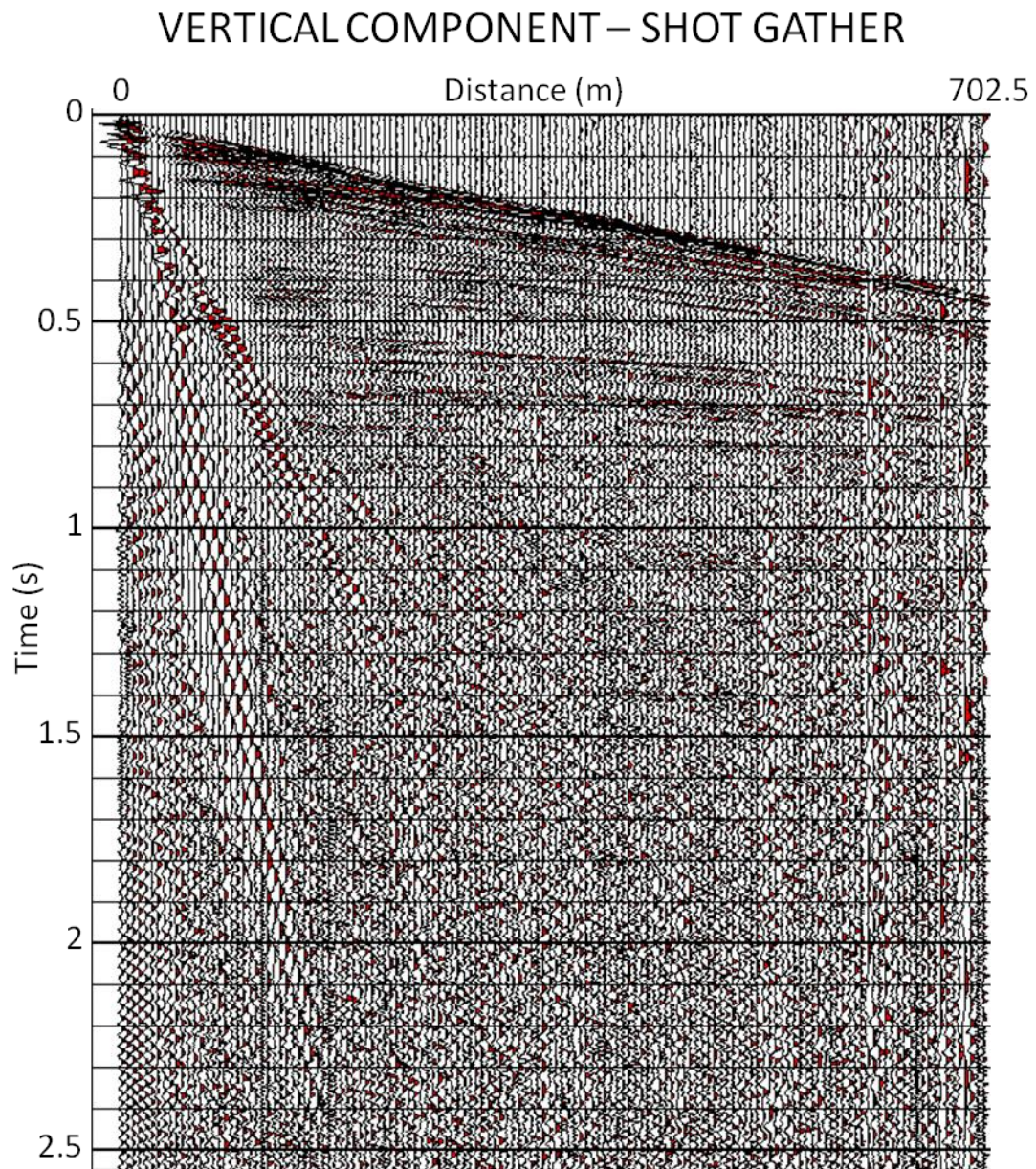
Figure 3.3: Vertical component correlated shot gather. Displayed using 500 ms AGC, showing the first 2.5 s of the record. Note the very weak air-wave.
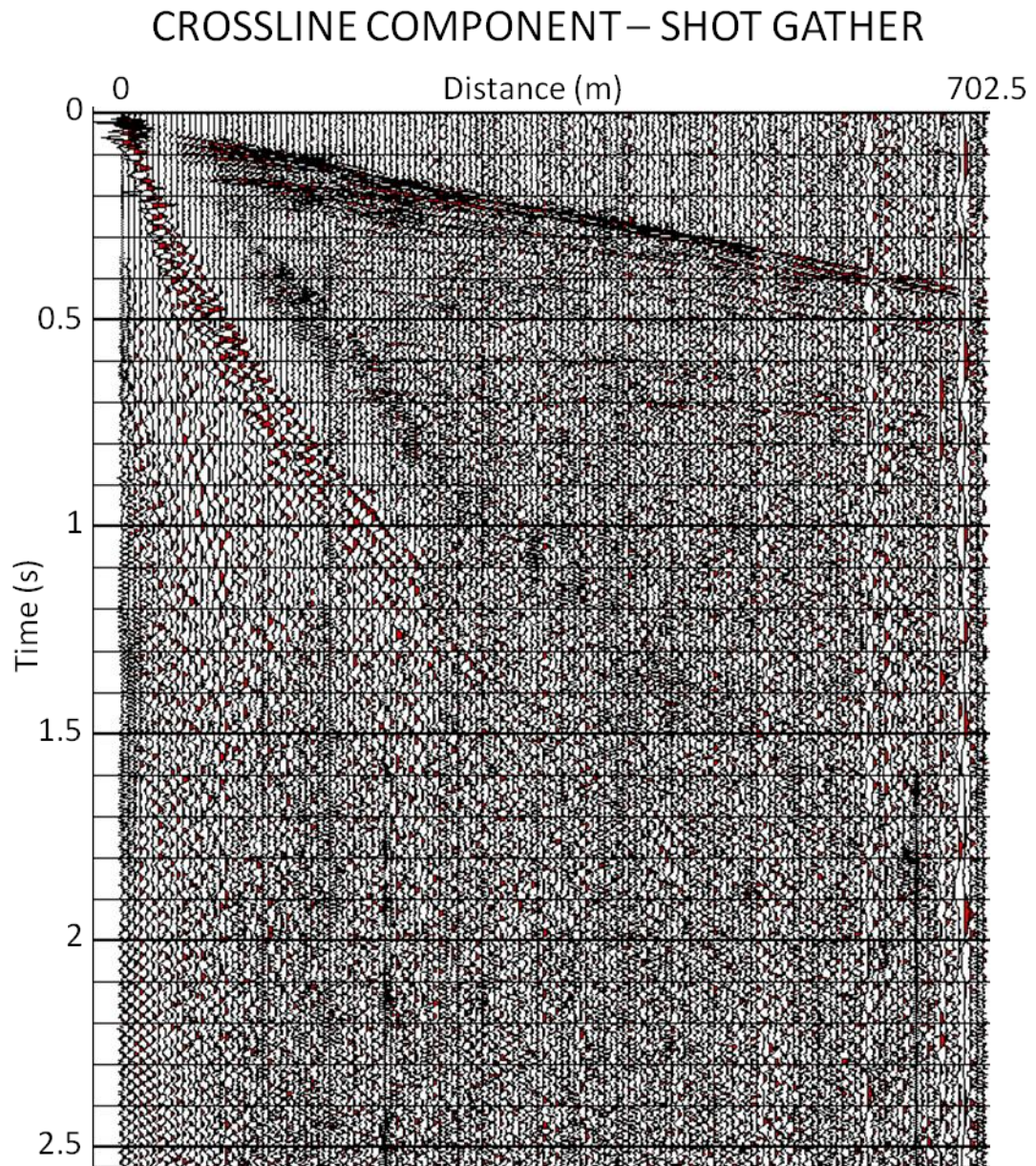
Figure 3.4: Crossline component correlated shot gather. Displayed using 500 ms AGC, showing the first 2.5 s of the record.

INLINE COMPONENT – SHOT GATHER
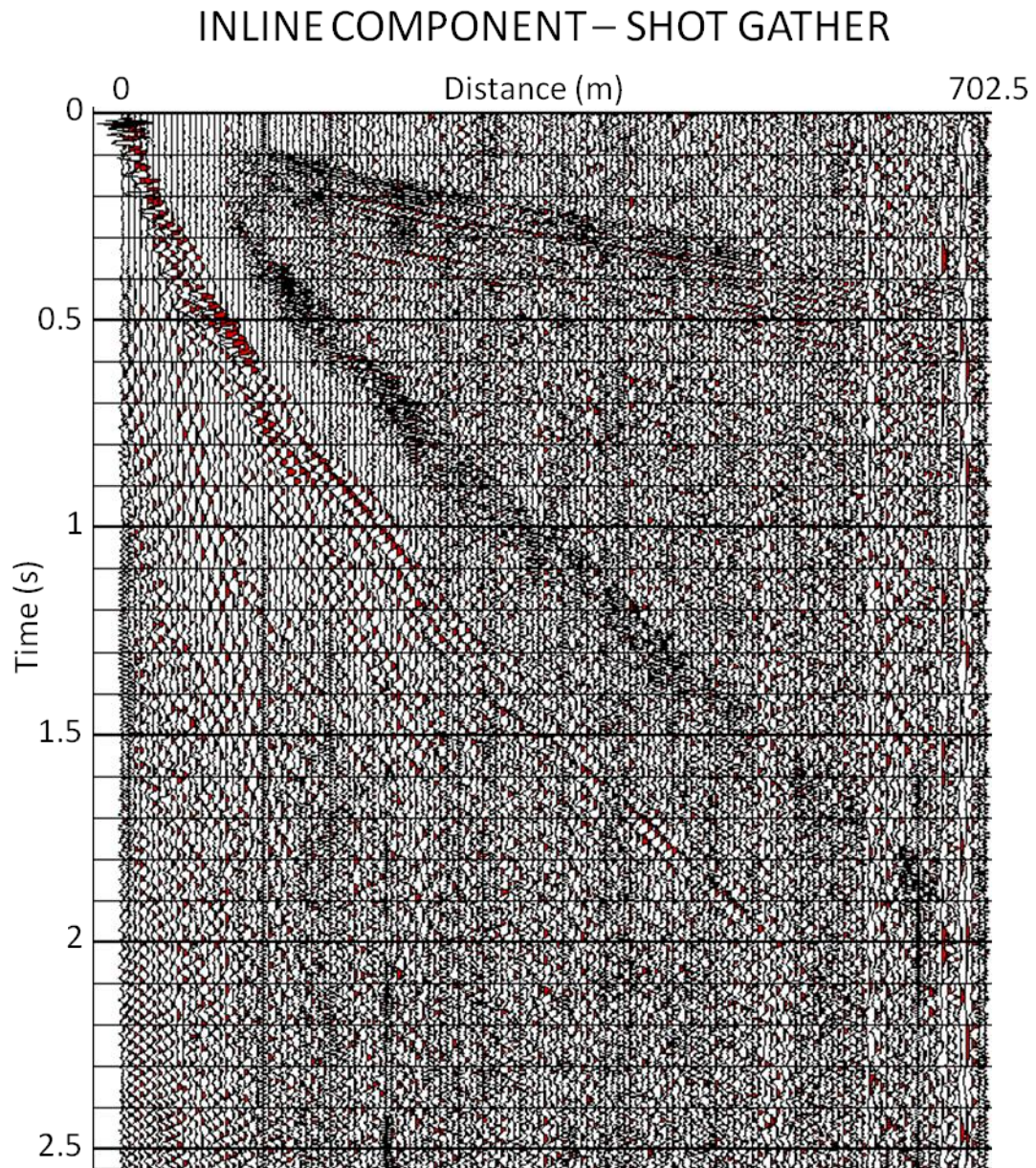
Figure 3.5: Inline component correlated shot gather. Displayed using 500 ms AGC, showing the first 2.5 s of the record. Note the strong air-wave. There is also shear-wave refractions located beneath the air-wave.

should be weaker. The data are contrary to this estimation. While there is a strong response from the inline component, and a relatively weaker response from the crossline component, the air-wave is nearly absent in the vertical record. This is particularly strange since previous surveys in this same location, using vertical 1-C geophones, showed strong air-wave presence.

The laboratory experiments in the previous chapter were used to characterize air-noise coming from differing directions, but not from differing distances. The air-blast recorded during this seismic survey is a useful marker for determining a geophone's response to sounds at a distance. As the shot point moves away from the geophone the air-wave arrival becomes weaker, as do all seismic arrivals. A typical seismic arrival, which propagates in three dimensions (e.g. arrival from a reflector) will decay at about $1/R$, where R is the total travel distance. The air-wave from the seismic source also propagates in three dimensions, which means it should also decay at $1/R$. However, the air-wave interacts with the ground surface. At the air-to-ground interface some air-wave energy will be absorbed or converted to ground motion. This increases the air-wave energy fall off, meaning the air-wave amplitude decay will be higher than $1/R$.

To calculate the air-wave decay, each geophone record was processed to isolate the air-wave. This was accomplished using top and bottom surgical mutes in Gedco's Vista Seismic Data Processing suite. After the air-wave was isolated, the peak amplitude at each shot distance was recorded. Plotting these maxima against distance shows the air-wave amplitude decay for each geophone.   For each

geophone component, the amplitudes from the first 50 m were discarded because they are affected by near offset effects. All data past 500 m was also discarded because the air-wave response was obscured by background noise. A power trend line was fit to the data from each geophone component to determine the amplitude decay. The data for each component, with trend lines, are in Figure 3.6. None of the air-wave arrivals had a decay rate of 1/R. The vertical component decayed at 1/R^1.8, while the inline components decayed at 1/R^1.4, and the crossline component decayed at 1/R^1.1. This indicated that each geophone element behaves differently to the same air-wave that passes the geophone.

Figure 3.6: Geophone amplitude decay comparison for the air-wave arrival. The vertical component amplitude decays much faster than the horizontal components.

3.3: Microphone data analysis

The microphone, as it should, shows a large air-wave presence across the entire spread (Figure 3.7). In its entirety the air-wave lasts for 200 ms in the near field and 150 ms in the far field. The record shows the constant presence of electrical cross-talk with the pilot channel. This is evidenced by the persistent high amplitude event between 0 and 75 ms. This crosstalk occurs because the microphone was not specifically designed to connect with this recording system. An optimized design would eliminate this effect. The peak crosstalk magnitude on the microphone is $1.3*10^{11}$, compared to $2.5*10^{15}$ for the auto-correlated pilot trace, giving a crosstalk ratio of 19000:1 or -86dB from pilot to microphone.

The air-wave amplitude decay was analyzed in the same manner as the geophone. The air-wave was isolated in the microphone record using surgical mutes, and the maximum amplitude at each shot point was recorded. The first 50 m of data were discarded to ignore near-field effects, but the rest of the data (out to 702.5 m) were used for analysis because the air-wave remained strong across the entire shot spread. A plot of the data with a power trend line is shown in Figure 3.8. Like the geophone, the microphone amplitude does not decay at 1/R; it decays at 1/R^1.4. The difference in amplitude decay between the microphone and each geophone component is important and must be taken into consideration when designing an air-wave filter.
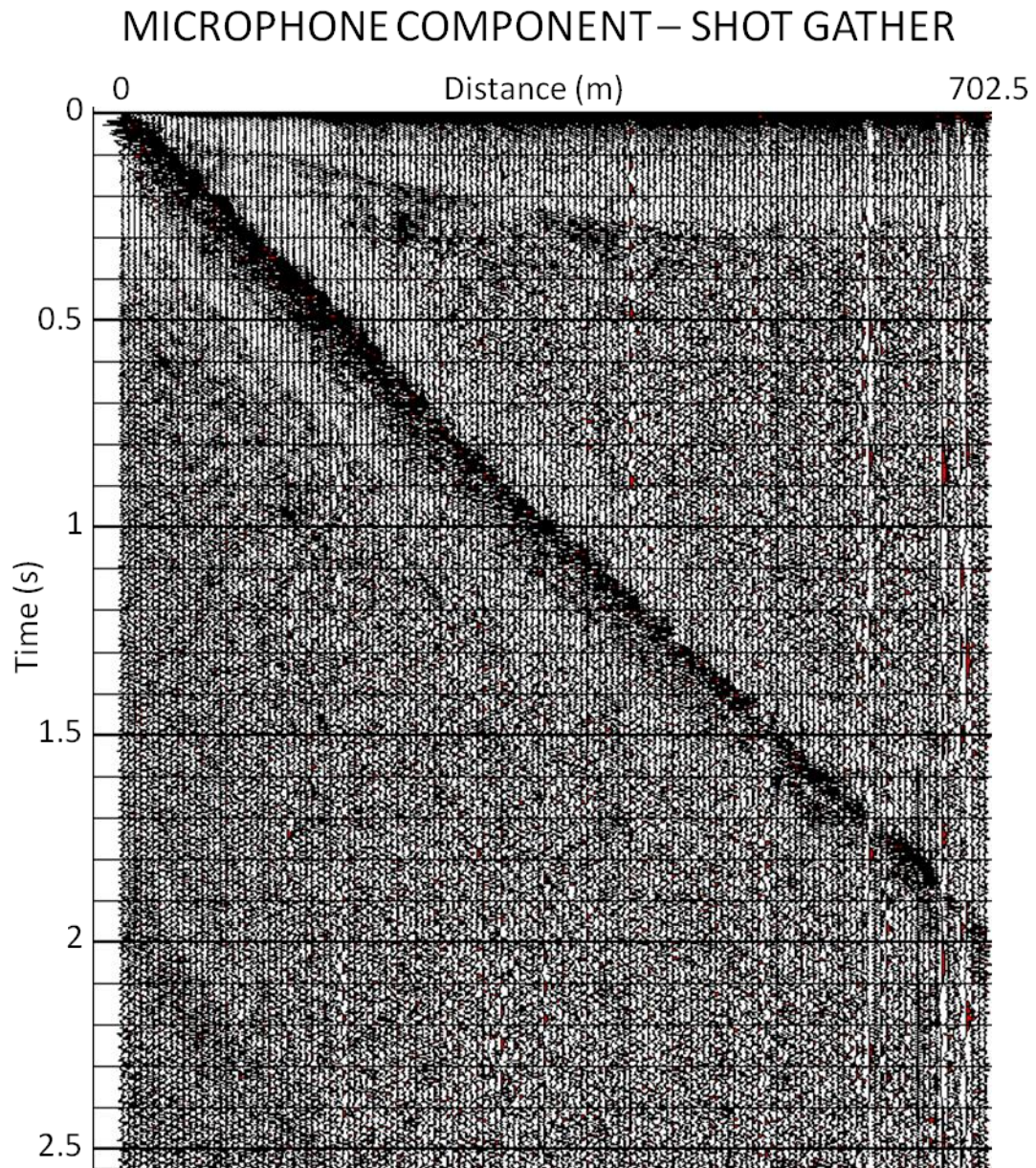
Figure 3.7: Microphone component correlated shot gather. Displayed using 500 ms AGC, showing the first 2.5 s of the record. Note the head-wave and reflections present in the record.

MICROPHONE COMPONENT AMPLITUDE DECAY

$$y = 7.9414x^{-1.396}$$
$$R^2 = 0.8024$$
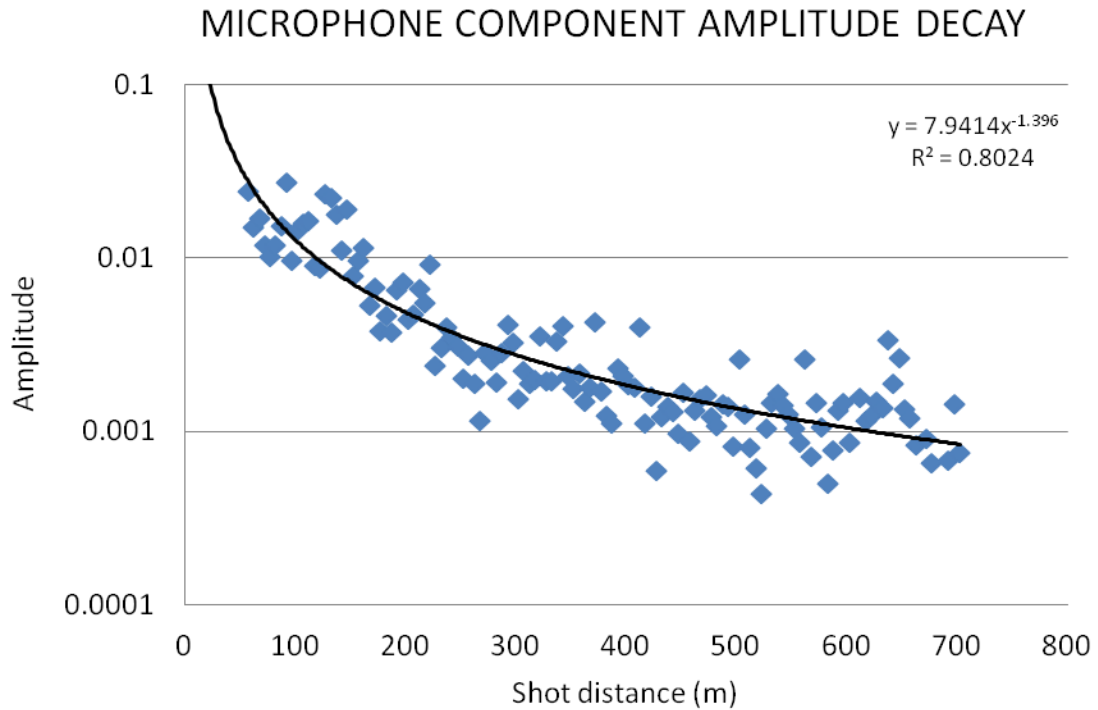
Figure 3.8: Microphone recorded air-wave amplitude decay. The microphone decay rate is similar to the horizontal geophone components.

There are other visible events in the microphone record, consisting of a series of monofrequency arrivals, which coincide with the head wave, and uppermost reflections. One of three things could cause these peculiar events: electrical crosstalk with the adjacent inline geophone component, physical motion of the microphone converting to spurious recorded voltage, or it could be the record of ground-to-air converted seismic energy. If these events were caused by electrical crosstalk, it should have a similar crosstalk ratio when compared to the pilot-channel crosstalk. The peak microphone head-wave response is $2.2*10^{10}$ whereas the inline geophone component only has a peak magnitude of $1.1*10^{10}$. This gives

69

an inline-to-microphone crosstalk ratio of 1:2 or +6 dB. This is much too large for electrical crosstalk. In fact, it would suggest microphone-to-inline crosstalk since the microphone magnitude is greater. Even the vertical geophone component, with the strongest head wave response, has a peak magnitude of $1.6*10^{11}$. This gives a vertical-to-microphone crosstalk ratio of 1.45:1 or -3 dB. Therefore, these events are most likely not caused by crosstalk.

The microphone is constructed of two piezoelectric discs glued on opposite sides of a ring. Each piezo-element is inherently susceptible to noise induced by motion of the element. However, the elements are mounted in opposing directions. This means, a motion that induces a positive voltage on one element produces a negative voltage on the other element. When wired in series these voltages effectively cancel out. This process is not perfect, so small voltage anomalies may arise when the microphone is moved, shaken, or vibrated. To reduce excess motion of the microphone, it was decoupled from the geophone. This was achieved by wrapping the microphone loosely with polyester fiber called poly-fill. When used in small amounts, it is acoustically transparent. The poly-fill fibers consist of small spirals of polyester, which act as a spring, absorbing vibration. If, after decoupling, the microphone were still moved by vibrations of the geophone, a visible response should be seen in the microphone record for each seismic event in the geophone record. The only events that correlate between microphone and geophone are the head-wave and uppermost reflections. Furthermore, any mechanical coupling recorded by the microphone should have similar frequency content when compared

to the geophone record. The head-wave and reflections recorded by the microphone are almost exclusively monofrequency, near 130 Hz. These factors strongly suggest that these events are not caused by mechanical vibration.

If the seismic waves recorded by the microphone were caused by ground-to-air interactions, how did this energy couple across the interface? This question is beyond the scope of this thesis, and additional experimentation and analysis are required for any full explanation. However, basic analysis may be used to rule out two conversion methods, and analyze a third possible method.

Since the weathering layer velocity is typically much lower than the refracting near-surface layer, most seismic waves will be travelling nearly vertical within the weathering layer. Thus, the normal-incidence, energy transmission equation may be used to calculate the ground-to-air energy coupling

$$T' = \frac{4 * V_2\rho_2 * V_1\rho_1}{(V_2\rho_2 + V_1\rho_1)^2}.$$

Given a weathering layer velocity of 245 m/s and density of 1200 Kg/m^3, and air velocity of 345 m/s and density of 1.2 Kg/m^3, T' would be 0.006. One important factor to consider when describing the conversion process is the frequency content of the recorded waveforms. Again, the microphone recorded head-wave and reflections consist mainly of 130 Hz acoustic waves. This suggests the ground-to-air conversion process acts as a filter when passing energy. A transmission coefficient of 0.006 is very small and would apply to waves of all frequencies, producing low-amplitude, broadband response on the microphone.

71

The conversion of ground-roll to air-wave occurs at only one frequency, which would explain the monofrequency microphone response (Press and Ewing, 1951). However, all microphone-recorded seismic data were from compressional events, so some form of compressional-to-Rayleigh wave conversion would have to occur before the final conversion to air-wave. This 3-stage conversion process is unlikely, and there is no evidence of any converted Rayleigh waves in the seismograms, suggesting this is not the cause of the microphone-recorded seismic events. Other near-surface models, viscoelastic, poroelastic, and others may induce ground-to-air conversion. The conversion mechanisms allowed by these models may help explain the microphone-recorded seismic events, but more experimentation would be required before conclusions can be made.

A simple method of ground-to-air conversion is presented here that may explain the microphone-recorded seismic events, and their monofrequency composition. As seismic waves travel through the unconsolidated weathering layer, they may affect the pore space. The compressional waves would cause the pore space to expand and contract. These volume oscillations would create pressure waves in the pore space. At the surface, the pressure waves would alternately draw in and expel air, from the atmosphere into the pore space, in a fashion similar to blowing air across the mouth of a soda bottle. This process of creating sound from the vibration of air at the opening of a cavity is called Helmholtz resonance. Helmholtz resonators create sound at a singular frequency based on many factors, such as cavity size, opening size and shape, and the velocity of sound in air.

A simplified near-surface may be mathematically modeled as a Helmholtz resonator. The weathering, layer is extremely low velocity. Any upward travelling waves will refract nearly vertically when entering the weathering layer. This allows the pore space to be simplified to a series of vertically oriented circular pores. The resonant frequency of these pores can be calculated using the equation for a Helmholtz resonator

$$F = \frac{V_{air}}{2\pi} \sqrt{\frac{A}{V * L_e}} \, ,$$

where F is the resonant frequency, V_{air} is the velocity of sound in air, A is the area of the open port, and V is the main cavity volume. L_e is the effective port length, calculated using

$$L_e = L + 1.5R \, ,$$

where L is the port length and R is the radius of the circular port. For the weathering layer the vertical pore is the port, so R is the radius of the pore and L is the length (i.e. weathering layer thickness). Since there is no independent main cavity, the entire resonant volume is contained within the pore. Thus, the area and volume of the pore can be calculated using:

$$A = \pi R^2 \; and \; V = \pi R^2 L \, .$$

Substituting into the original equation gives

$$F = \frac{V_{air}}{2\pi} \sqrt{\frac{\pi R^2}{\pi R^2 L * (L + 1.5R)}},$$

which simplifies to:

$$F = \frac{V_{air}}{2\pi} \sqrt{\frac{1}{L^2 + 1.5RL}}.$$

The pore radius is typically very small, 1 mm or less. For a suitably thick weathering layer, greater than 10 cm, the $1.5RL$ term becomes insignificant. This allows a further simplification

$$for\ R \ll L \qquad F = \frac{V_{air}}{2\pi L}.$$

Typical changes in air velocity will only produce a 5% variation in resonant frequency. This means that the resonant pore space only depends on the thickness of the weathering layer. Using 345 m/s for the air velocity, and 130 Hz for the resonant frequency, the calculated pore length, and weathering layer thickness, is 42 cm. This thickness is suitable for the UH Coastal Center because the water table in the area is very high, evidenced by the presence of standing water in roadside ditches less than a meter deep. The simplified Helmholtz equation presents an additional use for microphone recordings of seismic surveys, determining weathering layer thickness. This is especially useful for areas with weathering layers that are too thin to be seen in seismic records, like the UH Coastal Center.

3.4:   4-C geophone prototype

The need for a field-ready prototype was realized during the field experiment at the UH Coastal Center.   It would require a studier mounting area for the microphone, which would also provide more protection than the "pillow-top" system could provide. The requirements for this design are protection, vibration isolation, and acoustic permeability. The case must protect the microphone from impacts, possibly being tough enough to be stomped on during the planting of the geophone, and must also protect the microphone from water. The case must also allow the microphone to be mounted in such a way that it is isolated from vibrations. Lastly, the case must not significantly block the passage of sound, as this would affect the filter designed for use with the microphone.

After a few design iterations, a final 4-C geophone prototype was determined. The case is constructed of a steel and Lexan frame. Two Lexan squares are used as top and bottom plates, to protect the microphone from impacts. Two steel strips are placed on the top and bottom of the Lexan plates for added impact protection and increased rigidity. The entire microphone case is wrapped in a Gore-tex backed nylon.   This Gore-tex makes the case waterproof, and the nylon protects the microphone from pebbles, and sharp objects. The microphone is mounted in the center of the case using thin silicone sheets. These sheets are glued to the perimeter of the microphone, making sure not to cover up the pressure capsule area, and are secured to four posts using washers. The silicone is very thin and elastic, creating a spring mounting system that works regardless of the microphone case orientation.

This mounting method mimics the spring mounting used in professional microphone stands. To ensure the case remains acoustically transparent, holes were drilled in the top and bottom Lexan plates. In addition, the sides of the case are only surrounded by fabric, which should allow ample sound through. This case design creates a rugged field-ready microphone for use in the prototype 4C-geophone. Another benefit of this design is that it can be made for remarkably little money. Even when utilizing expensive materials, such as the waterproof nylon and silicone sheets, the entire microphone setup costs less than $20. A cross-sectional diagram can be seen in Figure 3.9, and pictures of the final 4-C geophone prototype are in Figure 3.10, and Figure 3.11.
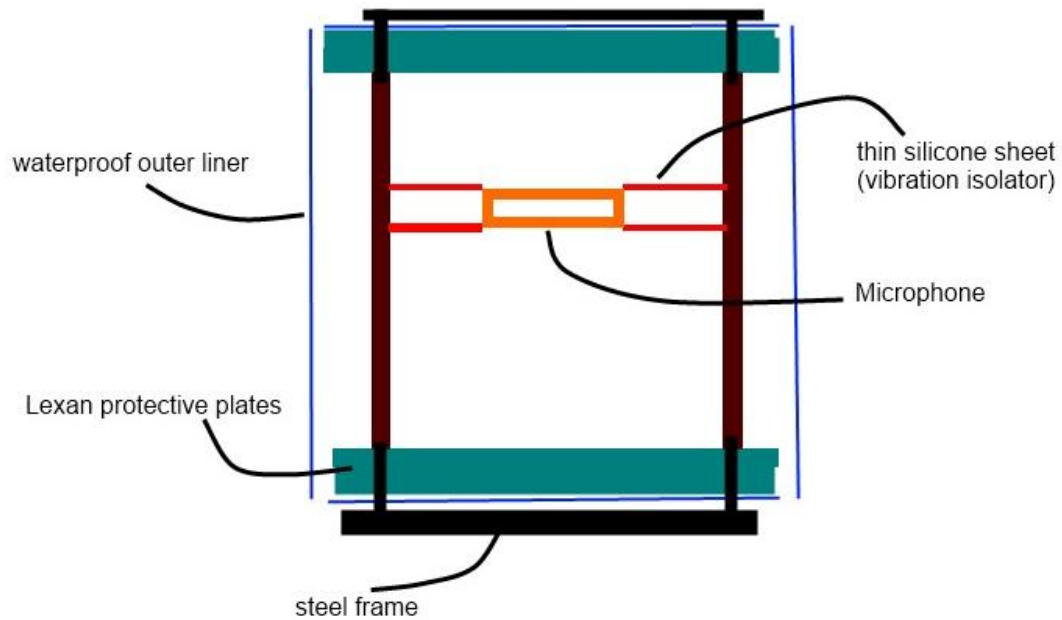
Figure 3.9: A simplified diagram of the microphone case. The diagram shows a cross-section running through the middle of the microphone and case.

Figure 3.10: The finished microphone case. The steel plates on top allow the microphone to be stomped on, while the blue nylon keeps the microphone dry.

Figure 3.11: The finished prototype 4-C geophone, sitting atop a 3-C geophone in the field.

3.5: Conclusion

The presence of head-waves and reflections in the microphone record is quite surprising. This phenomenon, thus far, has been unseen in published research. That is why extreme care was taken to consider other possible factors before suggesting these seismic events were recorded from ground-to-air converted energy. Electrical crosstalk was ruled out, due to the large amplitude of the events, relative to geophone records. Mechanical coupling is also very unlikely, due to the narrowband response of the events and care taken to decouple the microphone from ground motion. This leaves ground-to-air conversion as the explanation for these events. Helmholtz resonance of the near surface pores effectively explains the ground-to-air conversion causing the microphone-recorded seismic events. This resonance depends mainly on weathering-layer depth, which for the UH Coastal Center is defined by the water table. Calculating this depth from Helmholtz resonance agrees with field observations of a shallow water table, supporting this simplified conversion method. However, there are many other ways to convert seismic waves to atmospheric waves, and full testing of each method needs to be made before a full conclusion may be drawn.

The previous chapters covered the characterization of how noise affects geophones, and how microphones behave in the field. They are:

1. The geophone is directionally sensitive to noise

2. Each geophone component has a different directional sensitivity

3. The geophone-microphone amplitude transfer function is dependent on frequency and incident sound angle

4. The geophone-microphone phase transfer function is dependent on frequency and incident sound angle.

5. Each geophone component's amplitude decay curve differs from each other and the microphone.

The information gained from these characterizations helps define the structure and process of the air-noise filter.

4.1: Filter design

A geophone responds differently to sounds coming from differing directions. This means that the air-noise filter must be able to detect an incoming sound's direction. Furthermore, each geophone component responds differently to sounds coming from the same direction, so individual filters must be used for each geophone component.   The geophone's noise response not only varies with direction but distance as well. Thus, the filter must also determine the distance the

sound has travelled before hitting the geophone. Fortunately, a few behaviors of the geophone-microphone system may be exploited to greatly simplify the filtering process.

Because the sound phase varies between the microphone and geophone, their phases must be rectified before filtering. This solves the problem of determining any particular sound's direction. The filter can use the amplitude from the microphone with the phase from the geophone to create an effectively phase shifted microphone signal. This step not only accounts for the differing incoming sound directions, but the geophone-microphone phase transfer function as well. One weakness of this solution is that it will phase shift all data from the microphone, including background noise. For example, in windy environments, the wind noise will be phase shifted to match the geophone, possibly affecting geophone data. This factor can be controlled by housing the microphone in a protective case, which could block wind yet still pass sound.

The amplitude kernel is the relative air-noise response strength of the geophone compared to the microphone. It cannot be calculated during the filtering process because the filter cannot separate air-noise from seismic signal on the geophone component. Thus, it must be hard coded in the filter. An amplitude kernel is calculated by dividing the maximum Gabor amplitude from the geophone by the maximum from the microphone, for every frequency. This is performed using the equation,

$$A_{kernel}(f) = \frac{Max\left(DGT(G(f))\right)}{Max\left(DGT(M(f))\right)},$$

where A_{kernel} is the defined amplitude kernel, DGT represent the discrete Gabor transform of a signal, G is the geophone signal, and M is the microphone signal. The amplitude kernel for the filter has been calculated by averaging all amplitude kernels from each noise characterization test (Figure 4.1). This has the effect of removing any directionally dependent amplitude effects from the geophone responses. This is an unfortunate sacrifice, but is necessary to create the static kernel necessary for the filter. A result of this process is that the crossline and inline amplitude kernels are almost identical. In all cases, the kernel is set to one below 20 Hz. This reduces amplification of low frequency noise on the microphone, such as wind. Each kernel is only defined up to 400 Hz, because the noise characterization tests were performed at 1000 samples per second. Furthermore, the kernel above 150 Hz is small, and mostly defined by background noise during the characterization tests. Thus, the most important portion of the filter is between 20 Hz and 150 Hz, which includes most of the seismic band used during UH field surveys (15 Hz to 150 Hz).
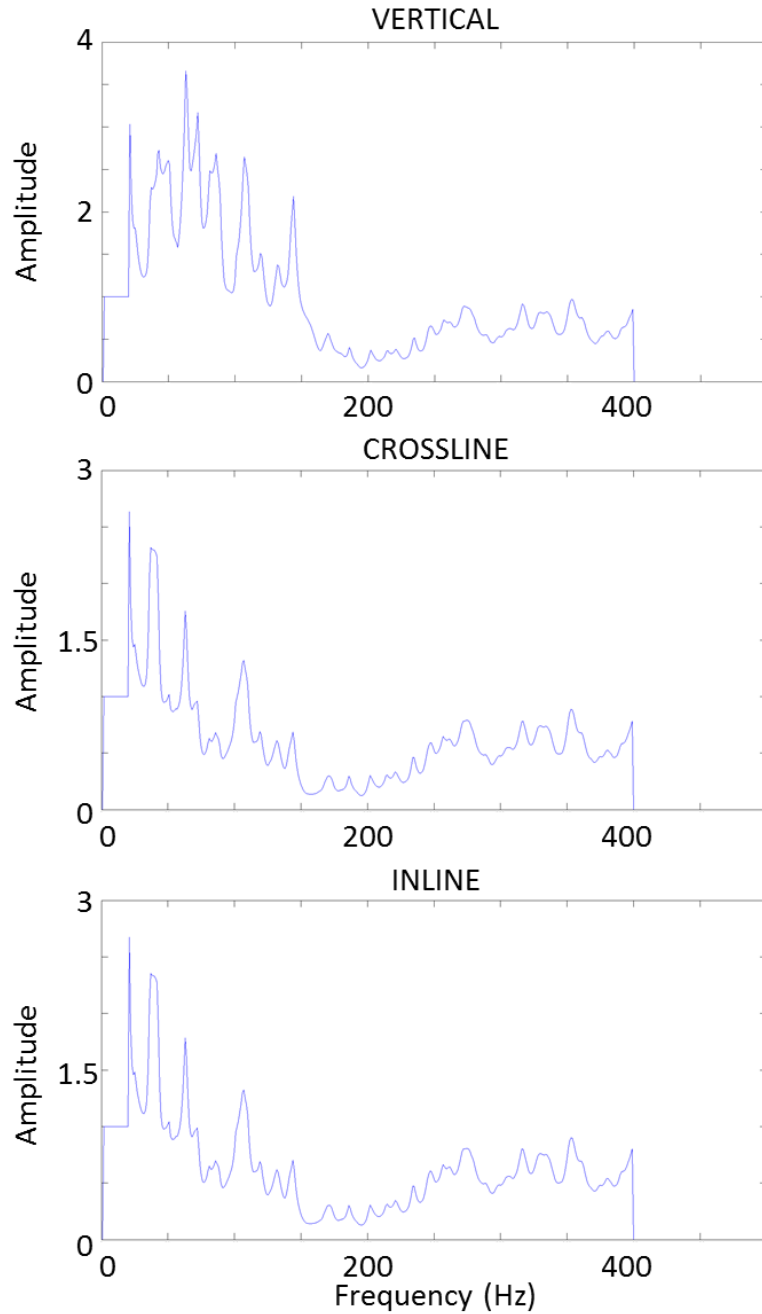
Figure 4.1: Amplitude kernels for each geophone component. The crossline and inline kernels are almost identical. This is the result of averaging kernels from multiple directions, removing directional dependency from kernel response.

82

The geophone and microphone respond differently to sounds from varying distances. This means that a filter designed to remove sounds coming from 20 m, might not work on sounds coming from 100 m. A method must be developed to rectify this distance effect. This is accomplished using the amplitude decay curves from the field survey. The microphone decay rate is 1/R^1.4, while the geophone decay rates are 1/R^1.8 for the vertical, 1/R^1.2 for the crossline, and 1/R^1.4 for the inline component. The Inline component decays at the same rate as the microphone, so no amplitude modulation is necessary. In addition, the crossline-component decay rate is close enough to the microphone rate that modulation should not be necessary either.

The vertical component decay rate is significantly different from the microphon. With the given rates, sounds at close range will be relatively louder on the geophone, but will die away quicker. To rectify this, the microphone data must be altered to mimic the 1/R^1.8 response before the filtering process occurs. Unfortunately, this process is not as simple as squaring the magnitude of the microphone data. Instead, the following equation is used:

$$M_{new} = M_{old} * \frac{S_{max}}{S_{cal}}.$$

The modification process must be able to discern far, loud sounds from close, quiet sounds. This requires the peak magnitude for an incoming sound, S_{max}, to be known. In addition, a calibration factor is required for the modification process. The calibration factor, S_{cal}, is unique to the microphone used in the system. It is the

peak amplitude, recorded by the microphone, of a vibroseis sweep 8 m away. Eight meters, was chosen as the calibration distance because it is the "crossover point" for the microphone-geophone amplitude relation. Sounds closer than 8 m away are relatively louder on the geophone, and sounds further than 8 m are relatively louder on the microphone. Thus, sounds closer than this distance must be magnified in microphone records while sounds further than this must be diminished. The peak incoming sound magnitude, divided by the calibration factor, effectively performs this transformation. When multiplied by the original microphone signal, M_{old}, a new microphone signal, M_{new}, is created with appropriately magnified or diminished sounds, based on the perceived sound's distance. This gives the microphone a pseudo 1/R^2 response, which is suitably matched to the geophone decay rate for the filter process to work effectively.

Each of the previous pieces fit together to make the complete air-noise filter. From start to finish, the filter works in the following way. An incoming sound is detected by the microphone and geophone, and is digitally sampled. The sample is triplicated for use on each geophone component. The sample bound for the vertical component is modified using a scaling factor determined by the maximum previous amplitude recorded by the microphone. Using the current time sample and the previous 127 samples, a frequency spectrum is calculated for the microphone, vertical, crossline, and inline components. The magnitude of the microphone spectrum, and the phase for each geophone component, are calculated. Using microphone magnitude and the three geophone phases, a new spectrum is created

called the noise estimate spectrum. These spectra mimic what the geophone air-noise response should be. The spectra are transformed back to the time domain, creating the noise estimate signal. The data point that corresponds to the current time sample is then subtracted from the corresponding geophone component. This removes the expected air-noise effect from the geophone creating "clean" geophone outputs. A diagram summarizing this process is in Figure 4.2, and the complete filtering program is located in Appendix A.

This program has been run on uncorrelated seismic data from the UH Coastal Center survey, to test its effectiveness and ability to run in real-time. The filter's effectiveness will be discussed in the next section, but a few statements can be made about its speed. It can process 16 s of uncorrelated data in 18 s. This is not true real-time processing, but the original program has not been optimized for speed and had significant overhead. The program runs on data already acquired, so it is merely simulating the real-time process of data acquisition. Each shot point is run separately in the program, and must be loaded from SEG Y files. Time samples are passed to the real-time filter, one at a time, simulating the live filtering process. After removing this overhead, and with minimal optimizations, this program should be able to run in real-time.
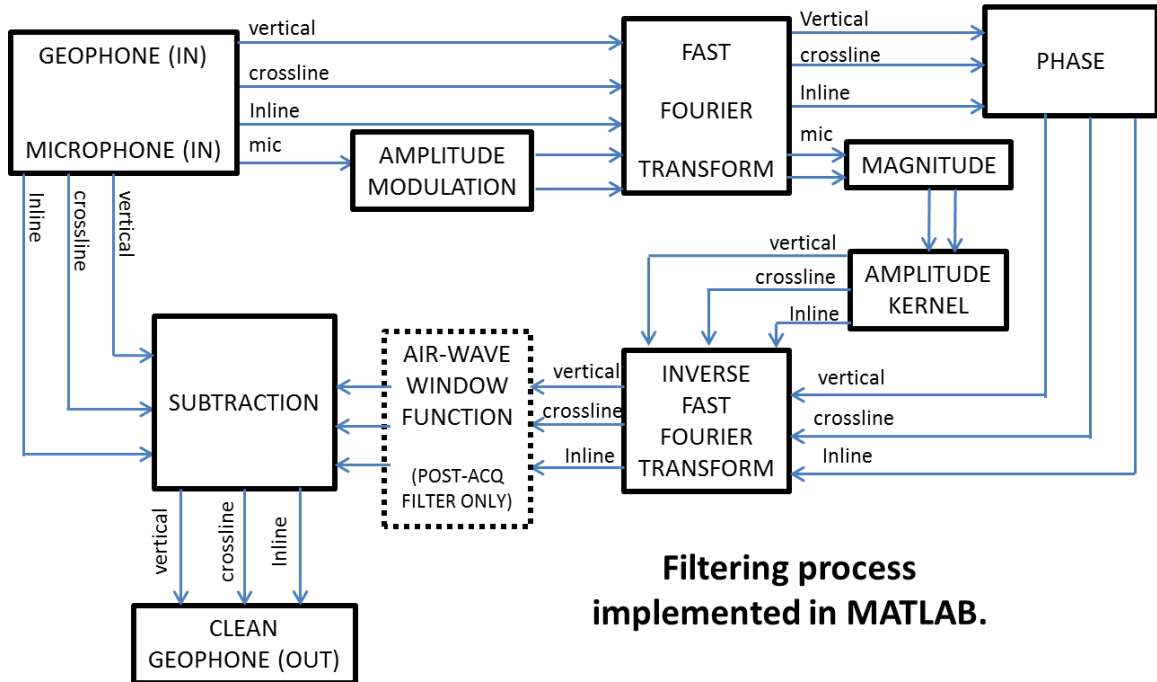
Figure 4.2: Filter process diagram. Data inputs are amplitude modulated for distance, then transformed to the frequency-domain. Three amplitude kernels are applied to the microphone spectrum to estimate the magnitude of noise for each geophone component. These noise-magnitude estimates are combined with the corresponding geophone phase to create noise-spectra estimates. Each noise spectrum is converted back to the time-domain, where the newly created noise signal is subtracted from the geophone signal. The post-acquisition filter includes an additional step; it applies a windowing function to the noise signal to isolate the air-noise for improved precision during air-noise removal.

4.2: Filter results

The data acquired at the UH Coastal Center has been processed through the real-time filter. Before discussing the results, a rubric should be created to evaluate the effectiveness of the filter. Primarily, the filter should remove a significant portion of the air-wave from the data. The filter should also not affect seismic information, such as the head-wave or reflections. Ground roll could possibly be affected, depending on how much ground-roll-coupled air-wave is present. The largest source of air-noise in the seismic records is the air-wave from the vibroseis truck. The filtering of this event will serve as the benchmark for the filter. The real-time filter results will be compared to other basic filtering methods, including a high-cut Ormsby filter, and FK-domain velocity filter. The high-cut Ormsby filter is a simple method of removing noise from seismograms, typically used for quality control checking in the field. The least restrictive filter that was able to remove the air-noise had high-cut corners at 90 Hz and 100 Hz. The next filter, a FK-domain velocity filter is typically used as a first attempt to remove noise during processing. To remove air-wave, a rejection zone is highlighted in the FK spectrum around events traveling 345 m/s. This method is only partially effective because air-wave is usually spatially aliased. Lastly, a post-processing version of the real-time filter will be shown. For each component, the air-wave in the noise-estimate signal is isolated, and the result is subtracted from the raw data. This filter shows how microphone data may be used to remove noise post-acquisition, and in the time domain.

4.2.1: Vertical component

The vertical component will be the first result shown, mostly because it is the most common in seismic data. This dataset has the weakest air-wave response, so any effect the filter has will be subtle. Comparison diagrams of the varying filter methods are shown in Figure 4.3 and Figure 4.4

Air-wave noise in the original vertical seismogram is very small, so filter comparison is fairly limited. The most visible presence of air-wave occurs between 1 s and 1.5 s, in the middle of the spread. This is the area of focus for the comparative discussion. The noise estimate shows a small amount of air-wave, but there is also seismic data included in the noise estimate. This is partly from the presence of seismic data in the microphone record, which is the result of ground-to-air conversion. While this is good for the prospect of seismic exploration using microphones, it is not beneficial for air-noise filtering. It can be argued that since there is a true air response to seismic events, the air pressure created is affecting the geophone as well, and that it should be removed to retrieve true ground response to the seismic events. The filtering process, however, is not perfect and seismic event amplitudes may be affected more than just the intended removal of air effects. Thus, it is best to leave the seismic arrival amplitudes as close to their original form as possible. There is also the presence of ground-roll in the noise estimate. This is an error on the part of the filter. The survey site had a large amount of background noise, mostly from wind, which was picked up by the

microphone. This noise has been phase shifted to match the geophone, creating a false noise estimate by the filter. Fortunately, this false noise is an order of magnitude smaller than their corresponding signals in the original seismogram.

The real-time filter removes what little air-wave is present in the original seismogram. Ground-roll, and other seismic effects, are only minimally affected by the noise removal process. The windowed post-processing filter produces results very similar to the real-time filter. The air-wave is effectively removed, but any effects the false noise estimates had in the real-time filter are gone due to the windowing process. The high-cut filter is also effective at removing air-wave. It has the added benefit of removing other high-frequency noise making the reflections at 0.5 s and 0.6 s more visible. However, the filter not only removes high-frequency noise, but data as well. A loss of detail can be seen in the head wave between 0.1 s and 0.2 s. The FK-domain filter is the only filter that is unsuccessful in removing the air-wave. The minor presence of air-wave is present between 1 s and 1.5 s. This filter also affects a linear event, most likely an S-wave refraction, that is present between 1 s and 1.6 s on the left side of the seismogram. Because there is so little air-wave present in the seismogram, a definitive best filter cannot be chosen.
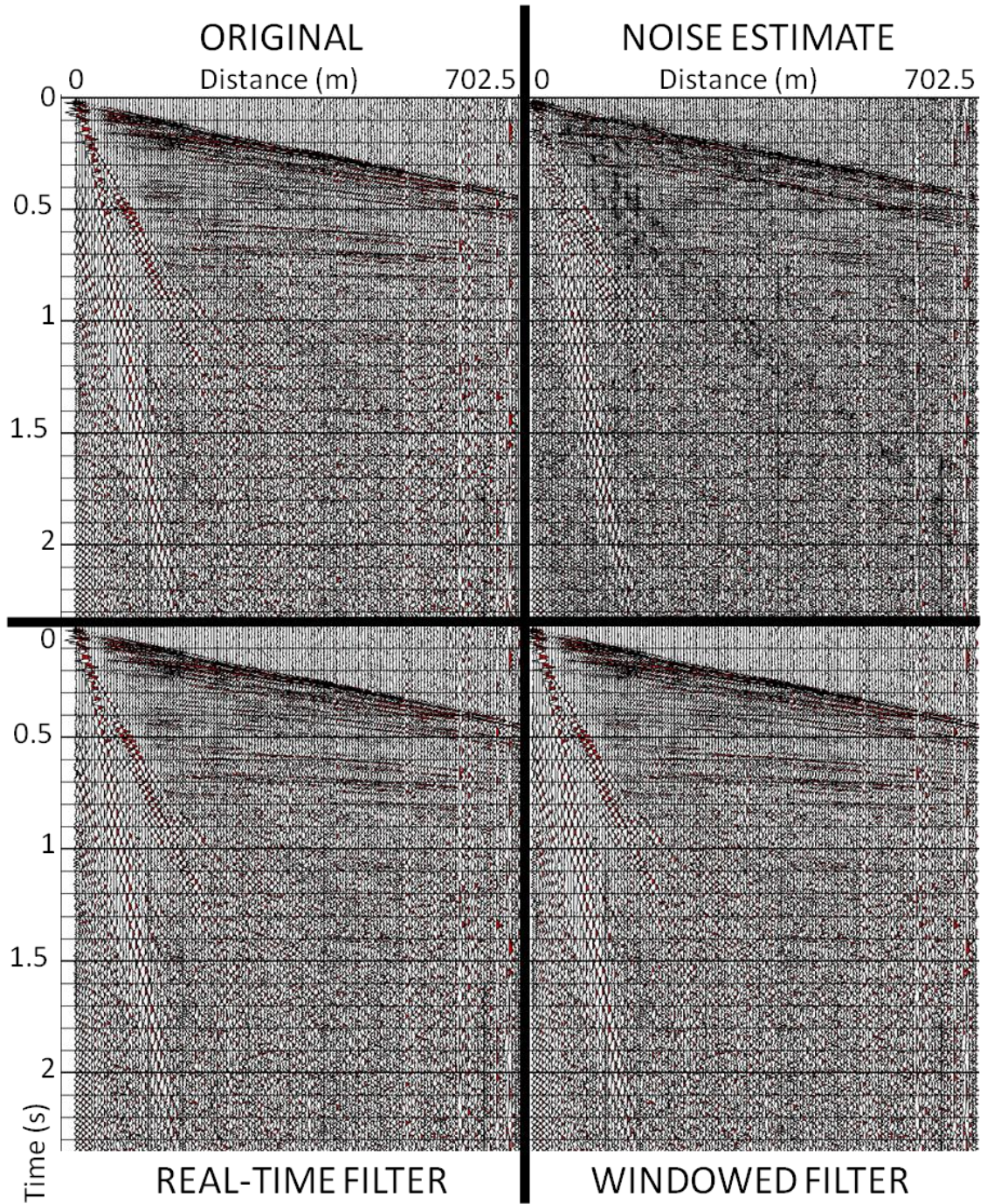
Figure 4.3: Vertical component: comparison of the real-time and windowed post-processing filters, to the original vertical seismogram and the filter-produced noise estimate.
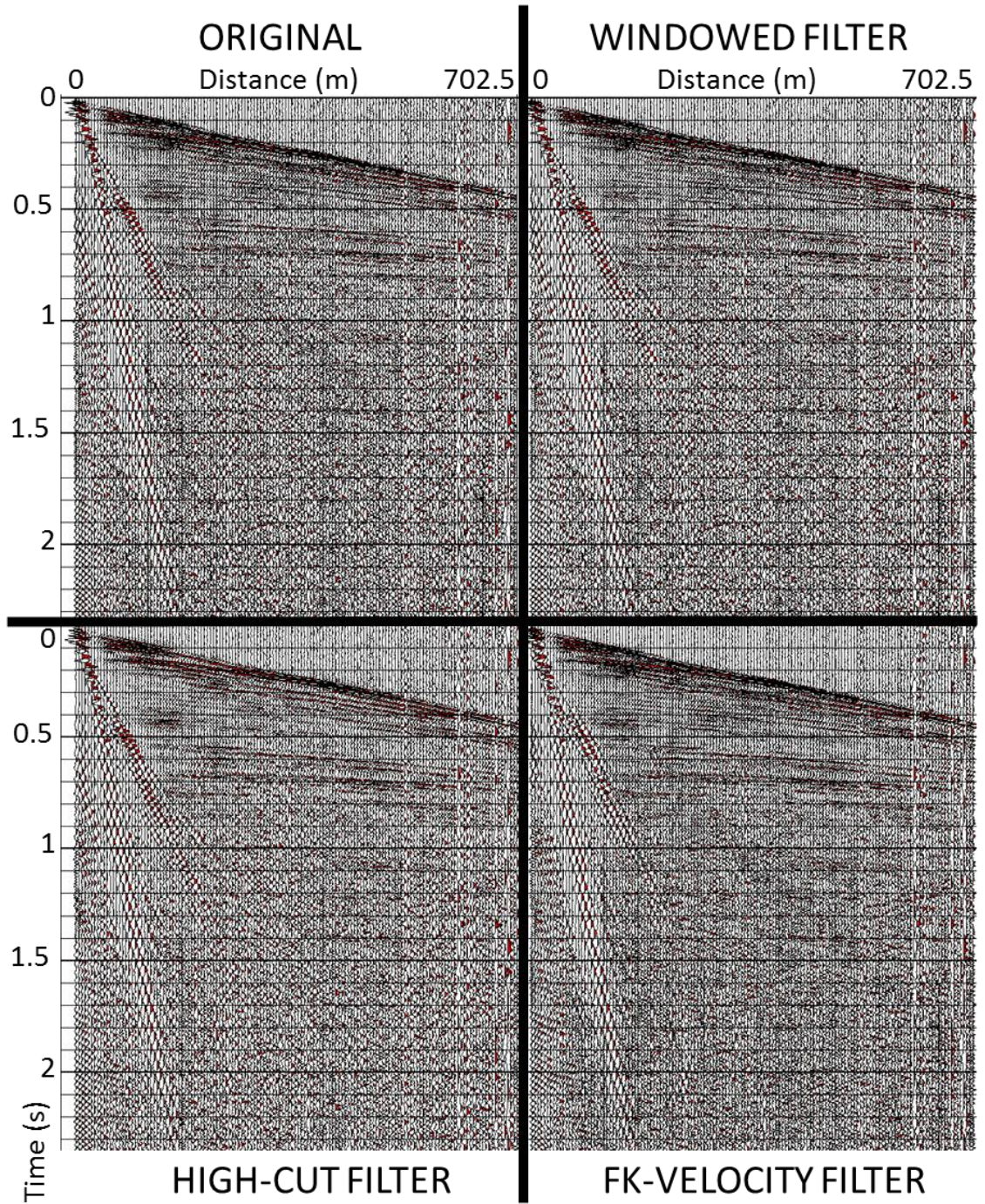
Figure 4.4: Vertical component: comparison of the high-cut and FK-domain velocity filters, to the original vertical seismogram and the windowed post-processing filter.

4.2.2: Crossline component

The crossline component (Figure 4.5 and Figure 4.6) shows a stronger response to air-wave, which is easily visible from 0.3 s to 1.2 s. After 1.2 s, the air-wave is still visible, but at diminished amplitudes. The noise estimate from the real-time filter mirrors the response of the crossline component, visible air-wave out to 1.2 s, with diminished response after. The side effects explored in the vertical component are also at work here. The presence of seismic arrivals in the microphone record creates corresponding noise estimates, and ground-roll phase matching by the wind noise is also visible. The real-time filter removes most of the air-wave from the crossline component seismogram. The air-wave is now barely visible before 1.5 s, and completely removed after that. The real-time filter does not affect the ground-roll very much, but it does affect the head-wave and reflections. The real-time filter appears to be creating a ghost head-wave 120 ms after the original arrival. This could be due to artifacts created in the filter. These artifacts would need to be removed before a field ready filter can be produced. The windowed filter enjoys the benefits of the real-time filter without the spurious artifacts. The windowed post-processing filter removes most of the air-wave, to barely visible levels. This filter is much more accurate than the real-time filter; the head-wave, reflections, and ground roll are all unaffected due to the windowing process. The high-cut filter is also effective at removing the air-wave. It does, however, greatly affect the head wave and near-surface reflections. This is most prevalent between 0.1 s and 0.3 s. For a near-surface, engineering-scale seismic
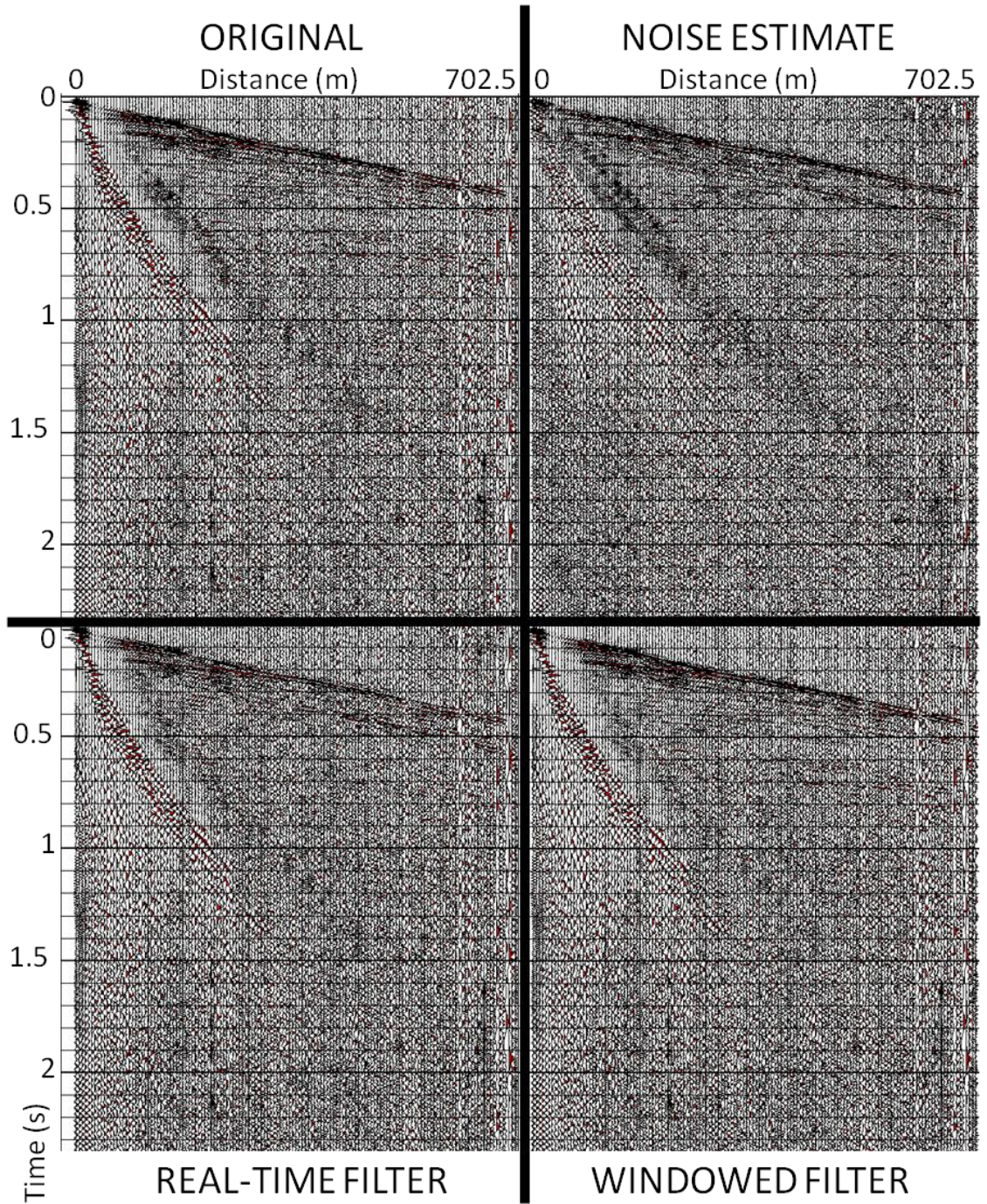
Figure 4.5: Crossline component: comparison of the real-time and windowed post-processing filters, to the original crossline seismogram and the filter-produced noise estimate.
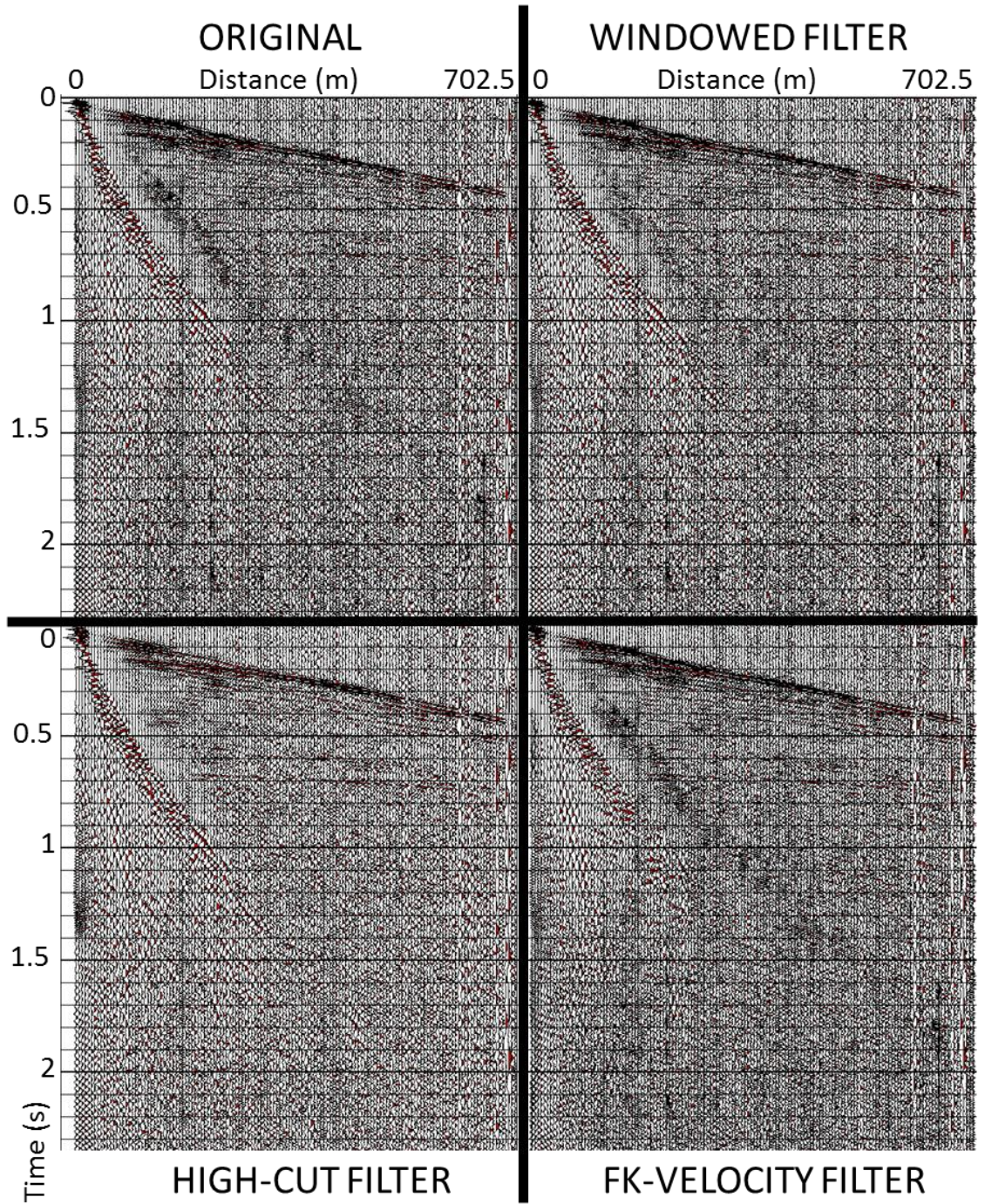
Figure 4.6: Crossline component: comparison of the high-cut and FK-domain velocity filters, to the original crossline seismogram and the windowed post-processing filter.

survey this could result in less accurate imaging of subsurface layers. The FK filter is again unsuccessful at removing air-wave. It only removes a minor portion of the air-wave. It also removes the S-wave refraction between 0.7 s and 1.2 s. The most effective filters for this geophone component are the windowed post-processing filter and the high-cut filter. The windowed filter, does not affect other seismic arrivals, like the high-cut filter does, making it the more precise filter.

4.2.3: Inline component

The inline geophone component (Figure 4.7 and Figure 4.8) has the strongest response to air-wave. This is to be expected. As sound travels, the air particles vibrate radially from their source. At the geophone location, this means the air-wave is vibrating along the inline direction of the geophone, which is easily visible across the entire spread. The air-wave noise estimate created by the real-time filter successfully mimics the inline component. The false ground-roll noise estimate is present, as well as the microphone-recorded seismic arrivals. The real-time filter removes most of the air-wave, but at the expense of the reflections and head-wave, which have been significantly reduced. The ground-roll remains largely unaffected in the filtering process. The windowed post-processing filter again shows the benefits of the real-time filter without the side effects. The air-wave is significantly reduced, and no other seismic information has been seemingly affected. The high-cut filter is also very effective at removing the air-wave, but again alters the
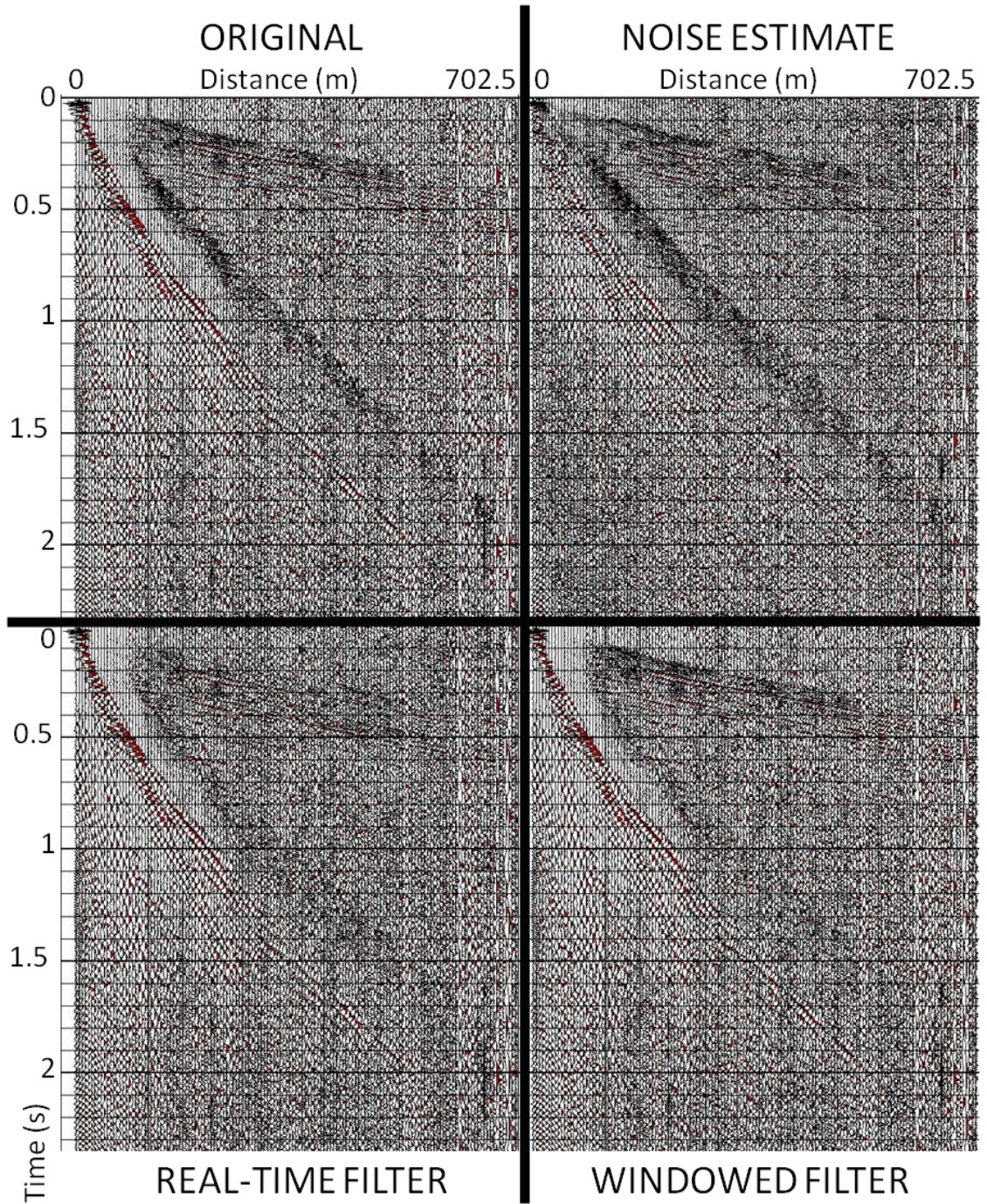
Figure 4.7: Inline component: comparison of the real-time and windowed post-processing filters, to the original inline seismogram and the filter-produced noise estimate.
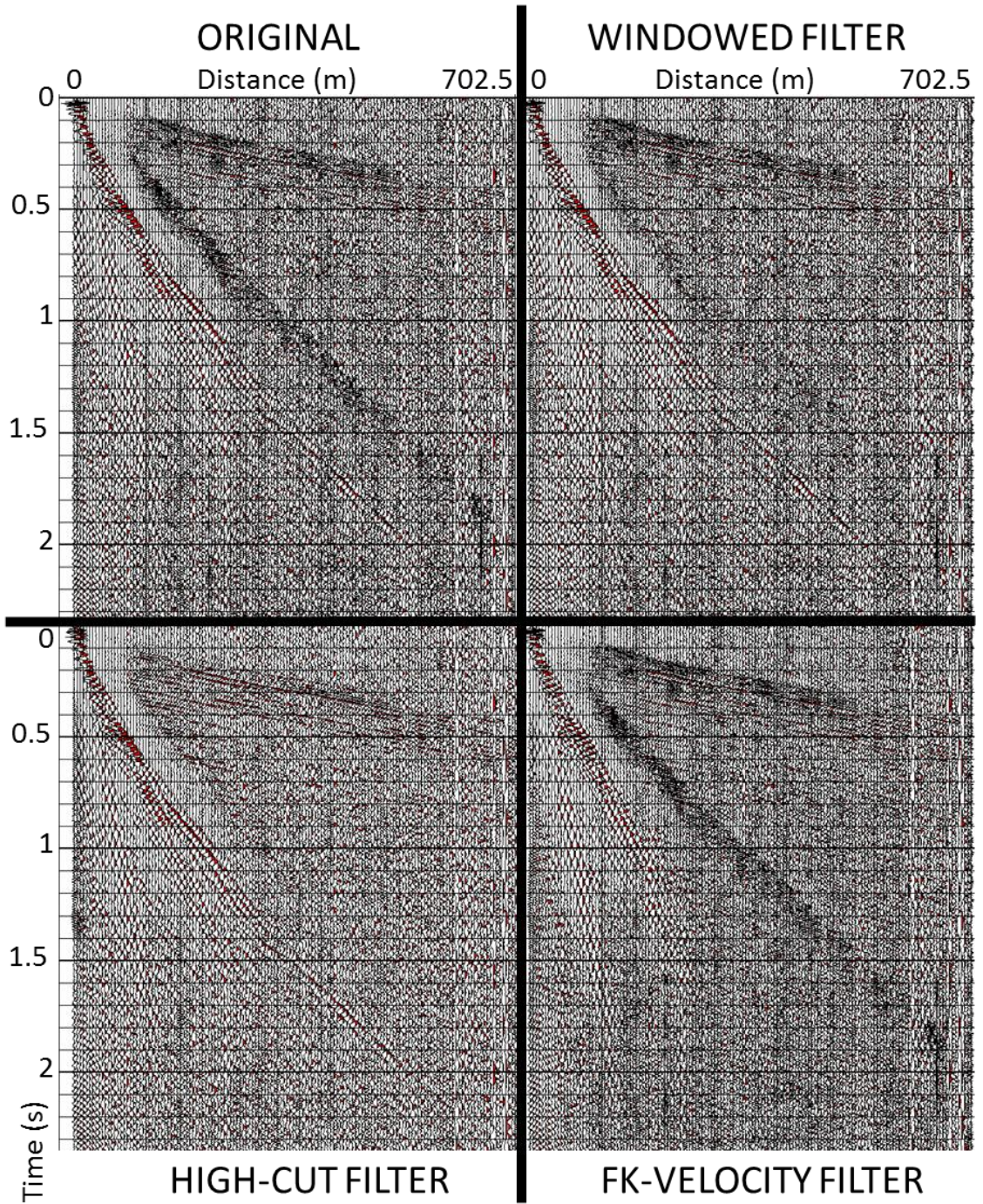
Figure 4.8: Inline component: comparison of the high-cut and FK-domain velocity filters, to the original inline seismogram and the windowed post-processing filter.

head-wave and reflections. A loss of high frequency content is seen across the entire head-wave, particularly between 0.15 s and 0.35 s on the left half of the seismogram. Lastly, the FK-domain filter remains largely ineffective at removing the air-wave. This filter also removes the S-wave refractions, seen between 0.8 s and 2.0 s. The conclusions for the inline geophone component are similar to those from the crossline component. The windowed post-processing filter and the high-cut filter remain the most effective at removing air-wave, but the windowed filter is more precise because it does not affect the surrounding seismic events.

4.3: Conclusion

A brief summary of each filter's effectiveness can be made. The real-time filter is an interesting prospect; it has the ability to remove air-noise before the seismograph records it. However, due to the complex relationship between microphone and geophone the filtering process is not always smooth. Overall, the real-time filter is effective at removing air-wave, but it also affects other seismic events. This is partly because these events are also recorded by the microphone, but also due to an inherent vulnerability in the design. This vulnerability, and the microphone recorded seismic events can be removed from any noise estimates using a windowing process around the air-wave. This can only happen as a post-processing step, removing the live-filtering abilities offered by the original design. The windowed, post-processing filter was very effective at removing air-wave from all geophone components, while keeping the remaining seismic events intact. The

high-cut filter is the simplest filter in use, and it remains a powerful tool for noise reduction. It also effectively removes air-wave, but it may not be appropriate for all seismic experiments. In near-surface studies, high-frequency data are important, and their removal by a high-cut filter reduces the precision of later measurements. The last filter used, the FK-domain velocity filter, was the only ineffective filter tested. It only marginally removed air-wave from the seismograms, yet had significant effects on other linear events with similar velocities to the air-wave.

In the absence of any microphones, the high-cut filter is recommended for removing the air-wave, but care should be taken in its application. The windowed post-processing filter is the best overall option as a filter. Not only is it effective, but it is very precise, removing only air-wave and not affecting seismic events.

CHAPTER 5:   DISCUSSION AND CONCLUSIONS

The original intent of this project was to create an air-noise filtering, 4-C geophone prototype. Initial results from the noise characterization study indicated a high degree of similarity between microphone and geophone recorded air-noise. The results from this experiment, combined with some observations from the field study, led to the development of a real-time air-noise filter. This filter is effective at removing air-wave from seismic records on all three components. However, the real-time filter cannot be recommended for field use, at this stage. Another result from the field survey shows a major flaw in the real-time filtering model, but at the same time opens great opportunities for microphones in seismic surveys. Real-time, air-wave filters are ineffective in some cases due to ground-to-air energy conversion. This conclusion was made because of the presence of head-waves and reflections in the microphone record, Figure 5.1.

The conversion of seismic-waves to air-waves, as seen in the microphone record, is not fully understood. One distinguishing trait of these seismic wave arrivals is they are dominated by a single frequency, near 130 Hz. A few conversion methods offer partial explanations, only covering the conversion process or the monofrequency nature of the conversion. Modeling the near surface as a Helmholtz resonator is the most complete explanation of the microphone-recorded seismic events. It offers a simplified, albeit incomplete, explanation of the conversion
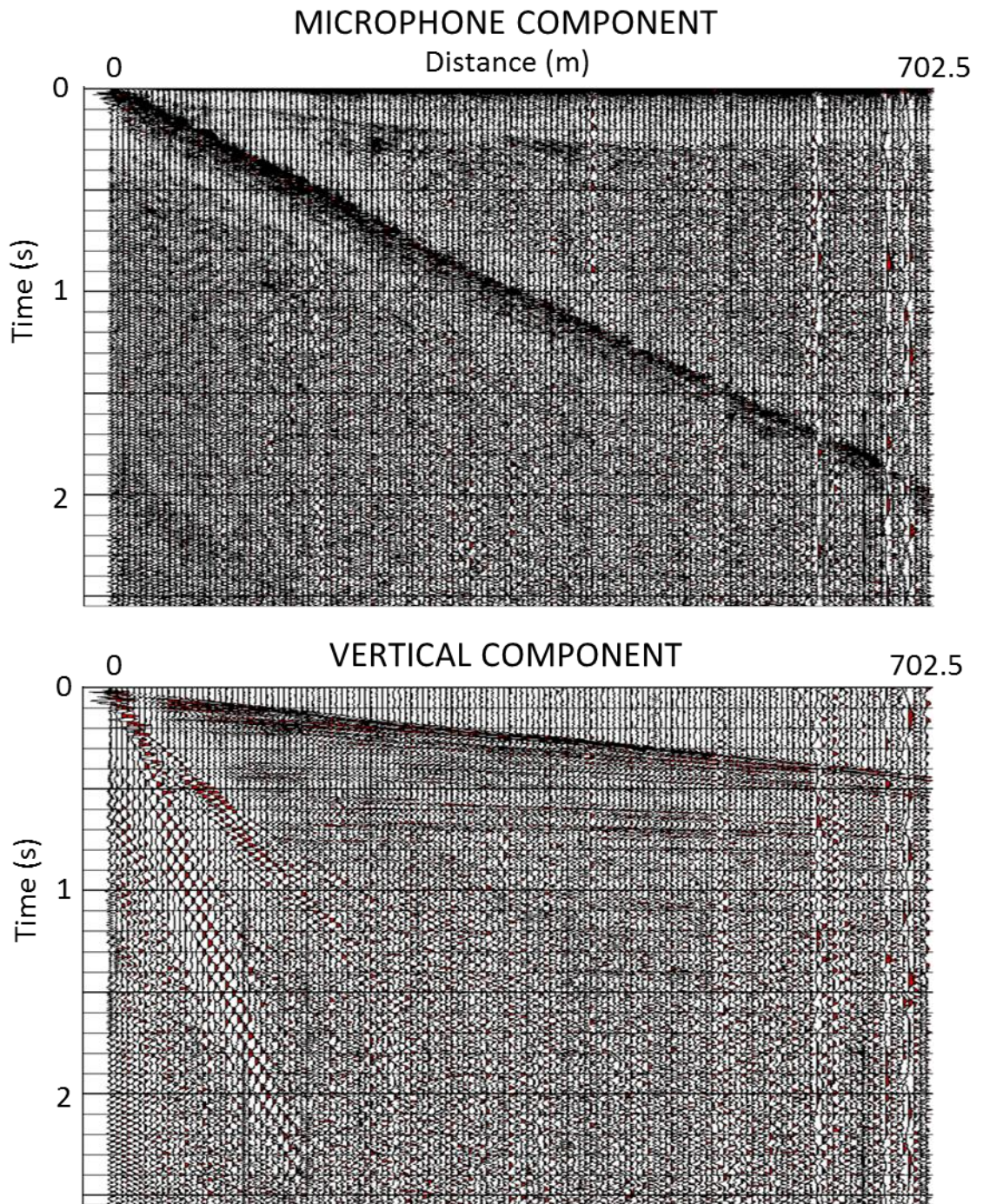
Figure 5.1: Microphone raw shot gather compared to the vertical raw shot gather, both with 500 ms AGC. The presence of reflectors and head-wave are seen in the microphone record.

process, but fully explains the bandpass filtering effect. Furthermore, using the near surface as a resonator allows for the calculation of the weathering layer depth. Simplifying the Helmholtz equation, for use with the simplified model, results in the following conversion from resonant-frequency to weathering-layer depth:

$$F = \frac{V_{air}}{2\pi L},$$

where V_{air} is the speed of sound in air, which is fairly constant, L is the depth of the weathering layer, and F is the resonant frequency of the weathering glayer. Using $V_{air} = 345$ m/s, $F = 130\ Hz$, and solving for the weathering layer gives a depth of 42 cm. This is in general agreement with field observations. At the UH Coastal Center the water table is very shallow, and defines the bottom of the weathering layer. Standing water was seen in roadside ditches near the survey site indicating a very shallow weathering layer.

This effect does not happen everywhere, as the weathering layer deepens the resonant frequency drops. When the weathering layer is 3 m thick the resonant frequency drops to 18 Hz, and a weathering layer 5 m thick would resonate at 11 Hz. This means that regions with relatively deep weathering layers might not necessarily couple to the atmosphere. In places like this, the real-time filter will work very well, and would be highly recommended for the removal of air-wave. Areas with shallow weathering layers are still able to utilize microphone records to remove air-noise, the process only need happen in a different manner. If microphone data are recorded during a seismic survey, they may easily be used to

remove air-wave from seismic records during processing. If the microphone records contain seismic information, the air-wave can be isolated using surgical mutes. After this point, the real-time filtering method can be applied using the modified microphone records to remove air-wave without affecting seismic arrivals. This is the process which is recommended for the UH Coastal Center, the results of which can be seen in Figure 5.2.

In conclusion, while this study may not have been a straightforward process in creating a real-time filter, it has been nonetheless educational. The recordings of seismic events by the microphone are unique and offer insight into air-ground interactions. In addition, the filter developed here could be used in real-time (near-surface conditions permitting), or as a processing step in any conditions.
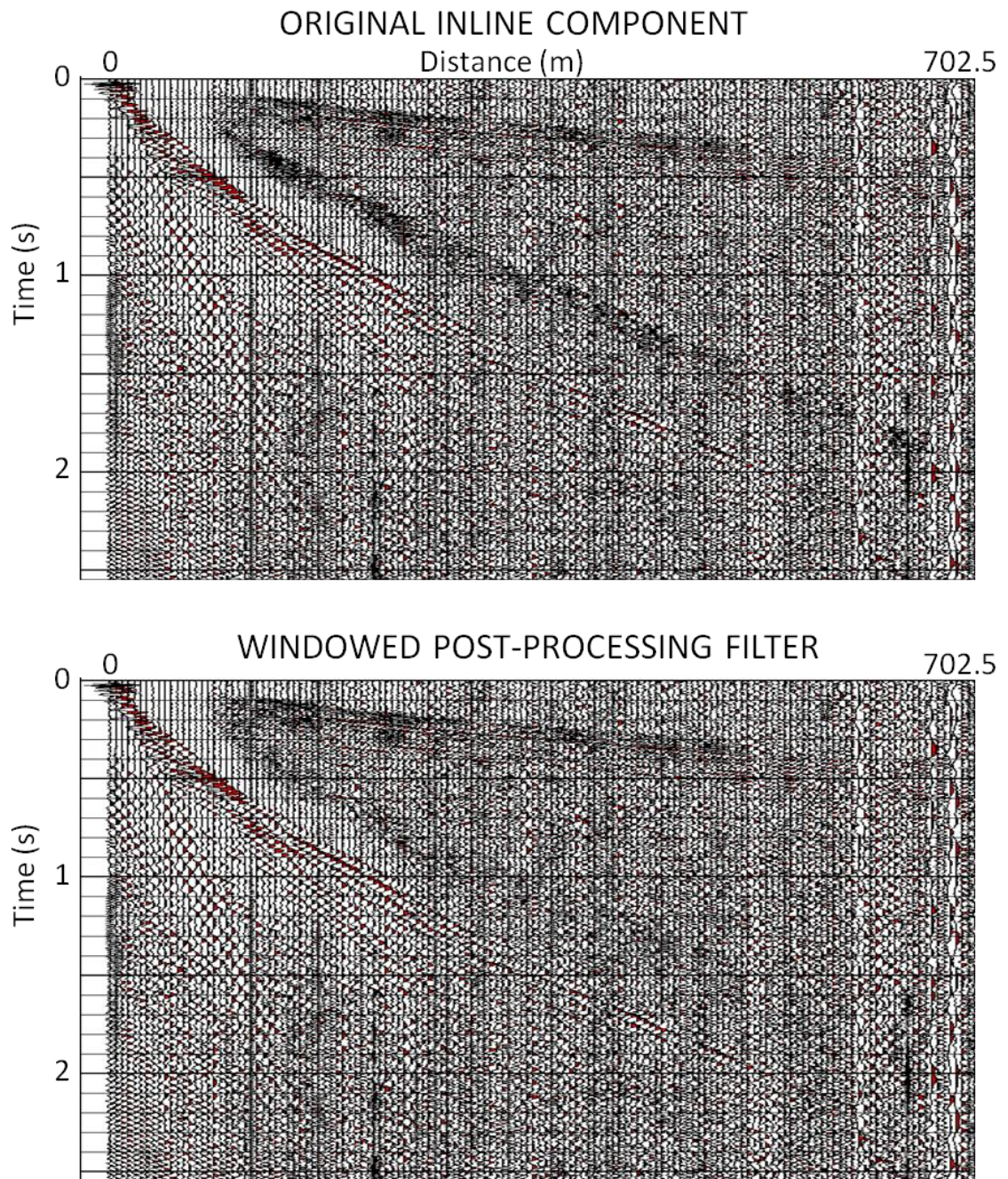
Figure 5.2: Inline component windowed post-processing filter results, both with 500 ms AGC. The filter removes most of the air-wave, without affecting any seismic arrivals.

APPENDIX A: REAL-TIME AIR-NOISE FILTER

This appendix includes the full MATLAB code for the real-time filter. It is reproduced exactly as it would in MATLAB. Program comments are colored green and are preceded by a %, logical constructs are blue, string declarations are pink, and main code is black. The program utilizes the Gabor transform from the Linear Time Frequency Analysis Toolbox (Søndergaard et al., 2011), and reads SEGY files using SegyMAT (Hansen, 2011).

```
Function [RAW,RAWC,NOISE,NOISEC,CLEAN,CLEANC]=
FilterRT(FF,LF,SL,LT,Vert,Xline,Inline,Mic,Pilot,FTL,ampK,ampFREQ,MULT);
%This program is a simulation of a real-time air noise filter. It uses a
%for loop to pass data point-by-point to the filtering algorithm. This
%filter method modifies the amplitude of a microphone and uses the phase
%from a geophone to create a frequency-domain noise estimate.  This is
%inverted back to the time domain to produce a time-domain noise estimate.
%The function is called using
%[RAW,RAWC,NOISE,NOISEC,CLEAN,CLEANC]=
%FilterRT(FF,LF,SL,LT,Vert,Xline,Inline,Mic,Pilot,FTL,ampK,ampFREQ,MULT)
%
%input variables
%FF - First File number
%LF - Last File number
%SL - Sweep length
%LT - listen time
%Vert - Vertical channel number
%Xline - Crossline channel number
%Inline - Inline channel number
%Mic - Microphone channel number
```

```
%Pilot - pilot channel number

%FTL - Fourier transform length

%ampK - amplitude filter kernel

%ampFREQ - amplitude kernel frequency axis locations

%MULT - final signal adjustment

%

%output variables

%RAW - uncorrelated data from the seismic record

%RAWC - correlated data from the seismic record

%NOISE - uncorrelated noise estimate for each geophone component

%NOISEC - correlated noise estimate for each geophone component

%CLEAN - uncorrelated noise free geophone record

%CLEANC - correlated noise free geophone record

%

%NOTES

%This program works for a single 3-C geophone and microphone combo. The

%input data (released as Data) can be attached to any channel. The output

%data (NOISE and CLEAN)is organized as such: Vertical-CH1, Crossline-CH2,

%Inline-CH3, Microphone-CH4.


%ABOUT THE FILTER

%The filter works by storing the most recent data samples in a buffer. This

%buffer is mirrored and a gaussian window is applied.  This action allows

%for th filter to work in real-time.  If the buffer was not mirrored the

%filter would work on the central sample, creating a delay of 1/2 the

%Fourier transform length. The microphone data is modified to mimic the

%geophone's amplitude decay (with respect to sound distance). an overview

%of this operation is available within the code. After the symmetric data

%buffer is created a FFT is performed, to convert to the frequency domain.

%In this domain the Microphone is multiplied by each geophones Filter

%Amplitude Kernel. The magnitude of the filtered microphone is used, along
```

```matlab
%with the phase from the geophone FFT's to create a frequency-domain noise
%estimate. After conversion back to the time-domain, the central sample of
%the noise estimate (which corresponds to the current time) is subtracted
%from the original data. This produces a single geophone signal-sample
%which should be free of air noise. After this the circular data buffers
%are rotated and the filter process is repeated for the next data sample.



    %pre allocate variables
NOISE=zeros(16000,3);
CLEAN=zeros(16000,3);
MAXr=zeros(LF-FF+1,1);
Mres=zeros(10,1);


TMPA=FF;
for n=1:LF-FF+1


TMPB=sprintf('%i.sgy',TMPA);
[Data,SegyTraceHeaders,SegyHeader]=ReadSegy(TMPB);
RAW(:,n,:)=Data(:,[Vert Xline Inline Mic Pilot]);
TMPA=TMPA+1;
dt=SegyHeader.time(2)-SegyHeader.time(1);
ts=length(RAW(:,1,1));
xaxisff=(1/dt)*linspace(0,1,2*FTL-1);
Akern=interp1(ampFREQ,ampK,xaxisff,'spline');



    %create circular data buffer for FFT
PastV=zeros(FTL,1);
PastX=zeros(FTL,1);
PastI=zeros(FTL,1);
```

```matlab
PastM=zeros(FTL,1);



    %for loop simulates real-time filtering of recorded data
for m=1:length(RAW(:,1,1));


    %pass stored data to live variable to mimic real-time filtering.
CdataV=RAW(m,n,1);

CdataX=RAW(m,n,2);

CdataI=RAW(m,n,3);

CdataM=RAW(m,n,4);



    %fill new value in data buffer
PastV(FTL)=CdataV;

PastX(FTL)=CdataX;

PastI(FTL)=CdataI;

PastM(FTL)=CdataM;




    %Store local peak amplitudes for distance estimation
    %local peak amplitudes are picked for each 1000 samples
    %they are stored in a buffer for 10000 samples
    %the maximum of the local peaks is used in a distance scaling factor
    %this factor adjusts the microphone's 1/r response to sound to mimic
    %the 1/r^2 response of the geophone. This is calibrated so that sounds
    %coming from 8 meters appear as the same ampltude on both Mic and Geop
M(2)=max(abs(PastM));
    if rem(m,1000)==0
Mres=circshift(Mres,[-1 0]);
```

```matlab
Mres(10)=0;

    end


    if M(2)>=Mres(10)

Mres(10)=M(2);

        if M(2)>=max(Mres)

M(1)=M(2);

        end

    end


    if M(2)<max(Mres)

M(1)=max(Mres);

    end


    if M(2)>MAXr(n)

MAXr(n)=M(2);


    end
    %creation of symmetric signal for real-time FFT
SymV=PastV;

SymX=PastX;

SymI=PastI;

    %microphone amplitudes are scaled by M(1)/8.5362e3 which is
    %[max(recent peak amplitudes)]/[peak amplitude of sound from 8m]
    %This adjusts the microphone to have a psuedo 1/r^2 response
    %This is only used on the Vertical geophone component
SymMV=PastM*(M(1)/8.5362e3);

    %The Inline and Xline components don't need affected mic inputs
SymM=PastM;
```

```
    %fill out symmetric signal

SymV(FTL+1:2*FTL-1)=fliplr(SymV(1:FTL-1));

SymX(FTL+1:2*FTL-1)=fliplr(SymX(1:FTL-1));

SymI(FTL+1:2*FTL-1)=fliplr(SymI(1:FTL-1));

SymM(FTL+1:2*FTL-1)=fliplr(SymM(1:FTL-1));

SymMV(FTL+1:2*FTL-1)=fliplr(SymMV(1:FTL-1));


    %calculate fft of current data buffer

VftS=fft(gausswin(2*FTL-1).*SymV);

XftS=fft(gausswin(2*FTL-1).*SymX);

IftS=fft(gausswin(2*FTL-1).*SymI);

MftS=fft(gausswin(2*FTL-1).*SymM);

MftSV=fft(gausswin(2*FTL-1).*SymMV);


    %calculate phase for each geophone FFT

VphS=angle(VftS);

XphS=angle(XftS);

IphS=angle(IftS);



    %apply amplitude filter kernel to microphone FFT

filtV=(abs(MftSV)).*(Akern(:,1));

filtX=(abs(MftS)).*(Akern(:,2));

filtI=(abs(MftS)).*(Akern(:,3));


  %filter Vertical geophone trace:

        %apply geophone phase to filtered microphone amplitude

        %to create Noise estimate FFT

RR=abs(filtV).*cos(VphS);

II=abs(filtV).*sin(VphS);

VftNEWS=complex(RR,II);
```

```
        %IFFT to create local-noise estimate time signal

TMP4=real(ifft(VftNEWS));

TMP6=TMP4(1:2*FTL-1);

NOISE(m,n,1)=TMP6(FTL);

        %subtract current-time noise estimate from geophone signal

CLEAN(m,n,1)=RAW(m,n,1)-MULT(1)*NOISE(m,n,1);


    %filter Crossline geophone trace

RR=abs(filtX).*cos(XphS);

II=abs(filtX).*sin(XphS);

XftNEWS=complex(RR,II);

TMP4=real(ifft(XftNEWS));

TMP6=TMP4(1:2*FTL-1);

NOISE(m,n,2)=TMP6(FTL);

CLEAN(m,n,2)=RAW(m,n,2)-MULT(2)*NOISE(m,n,2);


    %filter Inline geophone trace

RR=abs(filtI).*cos(IphS);

II=abs(filtI).*sin(IphS);

IftNEWS=complex(RR,II);

TMP4=real(ifft(IftNEWS));

TMP6=TMP4(1:2*FTL-1);

NOISE(m,n,3)=TMP6(FTL);

CLEAN(m,n,3)=RAW(m,n,3)-MULT(3)*NOISE(m,n,3);


 if rem(m,1000)==0

TMP8=sprintf('finished loop #%i',m);

disp(TMP8)

 end


    %advance data buffer 1 time sample
```

```matlab
PastV=circshift(PastV,[-1 0]);

PastX=circshift(PastX,[-1 0]);

PastI=circshift(PastI,[-1 0]);

PastM=circshift(PastM,[-1 0]);


end


%correlate data
    %Raw data
TMP2=xcorr(RAW(:,n,1),RAW(:,n,5),SL*(1/dt));

RAWC(:,n,1)=TMP2(SL*(1/dt)+1:SL*(1/dt)+1+LT*(1/dt));

TMP2=xcorr(RAW(:,n,2),RAW(:,n,5),SL*(1/dt));

RAWC(:,n,2)=TMP2(SL*(1/dt)+1:SL*(1/dt)+1+LT*(1/dt));

TMP2=xcorr(RAW(:,n,3),RAW(:,n,5),SL*(1/dt));

RAWC(:,n,3)=TMP2(SL*(1/dt)+1:SL*(1/dt)+1+LT*(1/dt));

TMP2=xcorr(RAW(:,n,4),RAW(:,n,5),SL*(1/dt));

RAWC(:,n,4)=TMP2(SL*(1/dt)+1:SL*(1/dt)+1+LT*(1/dt));

    for o=1:3
      %Noise estimate
TMP2=xcorr(NOISE(:,n,o),RAW(:,n,5),SL*(1/dt));

NOISEC(:,n,o)=TMP2(SL*(1/dt)+1:SL*(1/dt)+1+LT*(1/dt));

      %Clean signal
TMP2=xcorr(CLEAN(:,n,o),RAW(:,n,5),SL*(1/dt));

CLEANC(:,n,o)=TMP2(SL*(1/dt)+1:SL*(1/dt)+1+LT*(1/dt));

    end


TMP=sprintf('Completed file %i',TMPA-1);

disp(TMP)

fclose('all');

end
```

APPENDIX B: PATENTS

There are a few applicable patents relating to noise cancellation in seismic surveys. One such patent, U.S. Patent #4890264, granted in 1989 is now expired (Crews and Martinez, 1989). It describes a method of cancelling "non-uniformly distributed noise signals generated by wind, machinery, or surface wave propagation." Multiple sensors are used to detect wind, surface waves, and mechanical noise (e.g. pump jacks). The signal from these sensors is used in an adaptive filter to suppress noise contained in the geophone signal. While the sensors described are not specific, the authors recommend a horizontal geophone for surface wave detection and a microphone for wind detection, each collocated with a geophone. For mechanical vibration, the authors suggest a strong motion geophone be placed nearby, which would provide data for all geophones. A schematic diagram is shown in Figure B-1.

The benefits of this apparatus are its ability to suppress different types of noise including ground roll, spurious vibrations (that are well located), and wind. However, it greatly increases acquisition complexity, requiring two extra sensors per geophone and additional sensors located near noise sources. In addition, as described in the patent, the apparatus only suppresses wind noise; its ability to suppress other types of air-noise (e.g. air-blast/wave) is unknown.
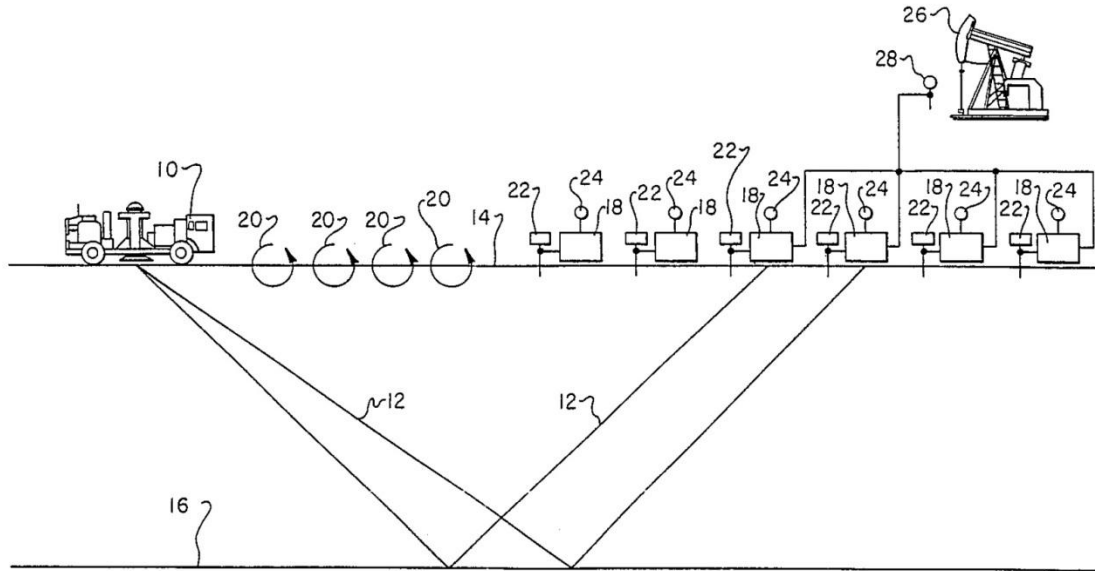
Figure B-1: Receiver-based noise cancellation system. Horizontal geophones (22) are used to record and cancel surface waves (20) from the vertical geophones (18). Microphones (24) are used to cancel wind noise. A strong motion geophone (28) is located near a mechanical noise source (26) to record and cancel ground noise on nearby geophones. (Crews and Martinez, 1989)

U.S. Patent #6381544, granted in April 2002, is still active (Sallas and Moerig, 2002). It describes a method of cancelling air-noise produced by a seismic source using microphones collocated at geophones and a speaker system collocated at the seismic source (Figure B-2).

During seismic acquisition the speaker will output a tone or sequence of tones. These tones are received by the microphone and geophone and are used to create a microphone-geophone transfer function.   The microphone signal is multiplied by the transfer function and then subtracted from the geophone signal,

suppressing source-induced air-noise. This method creates unnecessary acquisition complexity, requiring two surveys to be run at once. In addition, it is unable to suppress wind and other sources of air-noise.

Figure B-2: Source-based noise cancellation system. A speaker (16) located at a seismic source (12) plays a tone or series of tones during a seismic shot. This tone is received by a microphone (28) and is used to cancel source based air-noise from recorded geophone signal (26). (Sallas and Moerig, 2002)

REFERENCES

Alcudia, A. D., 2009, Microphone and geophone data analysis for noise characterization and seismic signal enhancement: M.Sc thesis, University of Calgary.

Bland, H. C., and E. V. Gallant, 2001, Wind noise abatement for 3-C geophones: CREWES Research Report, **13**.

Crews, G. A., and D. R. Martinez, 1989, Seismic exploration method and apparatus for cancelling non-uniformly distributed noise: United States Patent 4890264.

Dey, A. K., R. R. Stewart, L. R. Lines, and H. C. Bland, 2000, Noise suppression on geophone data using microphone measurements: CREWES Research Report, **12**.

Google, DigitalGlobe, Houston-Galveston Area Council, Texas General Land Office, Texas Orthoimagery Program, U.S. Geologic Survey, and USDA Farm Service Agency, 2012, UH Coastal Center: La Marque, Texas, **accessed 06/15/2012**, satellite imagery.

Hansen, T., 2011, SegyMAT: Revision 1.5, website: segymat.sourcefourge.net.

Hedlin, Michael A. H., and Richard Raspet, 2003, Infrasonic wind-noise reduction by barriers and spatial filters: The Journal of the Acoustical Society of America, **114**, 1379.

Hons, M. S., and R. R. Stewart, 2007, MEMS for the masses part 1: comparison to geophones in theory: CREWES Research Report, **19**.

Kromer, R. P, 2000, Infrasound sensor models and evaluation: Defense Center Information Center document.

Press, F., and M. Ewing, 1951, Ground roll coupling to atmospheric compressional waves: Geophysics, **16**, 416.

Sabatier, J. M., H. E. Bass, and L. N. Bolen, 1986a, Acoustically induced seismic waves: The Journal of the Acoustical Society of America, **80**, 646.

Sabatier, J. M., H. E. Bass, and L. N. Bolen, 1986b, The interaction of airborne sound with the porous ground: the theoretical formulation: The Journal of the Acoustical Society of America, **79**, 1345.

Sallas, J. J., and R. Moerig, 2002, Deterministic cancellation of air-coupled noise produced by surface seimic sources: United States Patent 6381544.

Shields, D. F., 2005, Low-frequency wind noise correlation in microphone arrays: The Journal of the Acoustical Society of America, **117**, 3489.

Søndergaard, P. L., B. Torrésani, and P. Balazs, 2011, The linear time frequency analysis toolbox: International Journal of Wavelets, Multiresolution and Information Processing, **10**, website: ltfat.sourceforge.net.

Stewart, R. R., 1998, Air-noise reduction on geophone data using microphone records: CREWES Research Report, **10**.

Withers, M. M., R. C. Aster, C. J. Young, and E. P. Chael, 1996, High-frequency analysis of seismic background noise as a function of wind speed and shallow depth: Bulletin of the Seismological Society of America, **86**, 1507.